NASA CR-112118

FINAL REPORT

INTEGRATED DYNAMIC ANALYSIS SIMULATION OF SPACE STATIONS WITH CONTROLLABLE SOLAR ARRAY

By

Joseph A. Heinrichs
Fairchild Industries, Inc.

Joseph J. Fee
Wolf Research and Development Corp.

Prepared Under Contract No. NAS1-10155

By

FAIRCHILD

Fairchild Industries
Germantown, Maryland 20767

For

NATIONAL AERONAUTICS AND SPACE ADMINISTRATION

September 1972

NASA CR-112118

FINAL REPORT

INTEGRATED DYNAMIC ANALYSIS SIMULATION OF SPACE STATIONS WITH CONTROLLABLE SOLAR ARRAY

By

Joseph A. Heinrichs
Fairchild Industries, Inc.

Joseph J. Fee
Wolf Research and Development Corp.

Prepared Under Contract No. NAS1-10155

By

Fairchild Industries
Germantown, Maryland 20767

For

NATIONAL AERONAUTICS AND SPACE ADMINISTRATION

September 1972

SUMMARY

A methodology is formulated and presented for the integrated structural dynamic analysis of space stations with controllable solar arrays and non-controllable appendages. The structural system flexibility characteristics are considered in the dynamic analysis by a synthesis technique whereby free-free space station modal coordinates and cantilever appendage coordinates are inertially coupled. A digital simulation of this analysis method is described and verified by comparison of interaction load solutions with other methods of solution. Motion equations are simulated for both the zero gravity and artificial gravity (spinning) orbital conditions. Closed loop controlling dynamics for both orientation control of the arrays and attitude control of the space station are provided in the simulation by various generic types of controlling systems. The capability of the simulation as a design tool is demonstrated by utilizing typical space station and solar array structural representations and a specific structural perturbing force. Response and interaction load solutions are presented for this structural configuration and indicate the importance of using an integrated type analysis for the predictions of structural interactions.

INTRODUCTION

The solar cell and battery system has been sucessfully used on many small spacecraft; however, space stations of the future will have power requirements which are much larger than those within the present design experience of solar cell systems. The solar cell arrays used on future space stations will therefore be relatively large and must be capable to tracking the sun in a manner which does not restrict the desired space station orientation. A potential problem area exists due to undesirable interactions between the flexible solar arrays and space station caused by required control and stabilization forces and external perturbations.

Spacecraft instabilities have been observed in the past when flexible appendages are part of the satellite structure. This past experience is summarized by Likins and Bouvier (Reference 1). Because of the requirements imposed upon large area solar arrays, a weight-efficient design rather than a stiffness design results, and the primary array modal frequencies fall within the control system bandwidth. A digital computer simulation for evaluating the dynamic interactions of large solar cell arrays and orbiting space stations is formulated which considers the dynamic characteristics of the array structure and the required systems for attitude and orientation control. The objective of this simulation is to provide an automated methodology of interaction loads analysis for use as a design tool. The capability of the simulation is demonstrated by obtaining interaction solutions for array structural concepts which will provide 100 KW of electrical power to future space stations.

The equations of motion for an orbiting space station with attached controllable arrays are generated and digitally programmed for solution by numerical techniques. In the development of the equations of motion a modal synthesis technique is employed whereby the elastic characteristics of the arrays are described by a finite set of orthogonal cantilever modes and are inertially coupled with the flexible characteristics of the space station described by free-free orthogonal coordinates.

Structural mode descriptions of the arrays are required as input to the simulation; therefore, a structural analysis of the elastic system with the appropriate boundary conditions is required prior to the performance of this simulation. The simulation input requirements specifically include a finite element dynamic model of the structure in terms of discrete mass and model geometry. Structural analyses of space station and solar array configurations have been performed and results are presented in this report. Provision is made for closed loop attitude control system dynamics of the space station and orientation control dynamics for the solar arrays. The latter control system provides the desired orientation of the arrays with the sun by controlling the rotation about the orbit-adjust and seasonal-adiust. Several generic types of control systems are mathematically modeled and are included as subprograms within the simulation. Outputs of the simulation include interaction forces and moments, magnitudes of all motion variables and control parameters as functions of time.

SYMBOLS

$[B],[G]$	-	force coefficient matrices defined by rigid body rotation rates.
C_i	-	direction cosine matrix for the i^{th} coordinate frame.
CG_{SYS}, CG_{SS}, CG_J	-	center of mass of the orbiting structural system, center of mass of space station, center of mass of J^{th} appendage, respectively.
$\bar{C}$	-	vector from space station reference point O_B to system center of mass.
$[D],[E]$	-	defined by Equation 17.
F_1, F_2, F_3, F_4	-	rigid body forcing terms
F_i	-	defined in Equation (8).
f	-	externally applied forces defined in Equation (25).
$\bar{F}_R$	-	externally applied force vector to the space station
$\bar{F}_{A_J}$	-	total interaction force vector produced by the flexible and rigid dynamics of the J^{th} controllable appendage.
$\bar{F}'_{A_J}$	-	transient interaction force vector produced by flexible dynamics of the J^{th} controllable appendage.
$\bar{F}_{FA_J}$	-	total interaction force vector produced by flexible and rigid dynamics of the J^{th} fixed appendage.
$\bar{F}''_{A_J}$	-	interaction force vector produced by the rigid dynamics of the J^{th} controllable appendage.
$\bar{F}'_{FA_J}$	-	transient interaction force vector produced by the flexible dynamics of the J^{th} fixed appendage.
g	-	structural damping coefficient.
$\bar{h}_J$	-	position vector for J^{th} appendage defined in Figure 2.
$\bar{I}_J$	-	rigid body inertia tensor of J^{th} appendage (3 x 3).

$[I]$	-	unity matrix.
J, j, i	-	indices.
$[J]$	-	$\sqrt{-1}\,[I]$
$\bar{\ell}_R$	-	vector from point of external force application to space station center of mass.
$\bar{L}_J$	-	angular momentum of J^{th} controllable appendage about its center of mass.
$\bar{L}_o$	-	angular momentum of space station about its center of mass.
L	-	vector of applied forces to discrete masses.
L'	-	defined by Equation (17).
LA, LB, LC, LD, LE	-	force coefficients defined by Equation (25).
$[M],[K]$	-	mass and stiffness matrices of a discretized elastic system.
m_i	-	i^{th} discrete mass in a discretized structure.
M_{eq_i}	-	generalized mass of i^{th} modal coordinate.
M_{i_J}	-	flexible discrete mass intertia tensor for the J^{th} appendage, a 3J x 3J matrix.
M_J	-	total mass of J^{th} appendage.
M_s	-	mass of space station
M_T	-	total structural system mass.
O_B, O_N	-	spacecraft reference point, Newtonian reference point, respectively.
Q	-	defined by Equation (17).
q	-	matrix of discrete coordinates defined by Equation (10).
$\bar{r}_i$, $\bar{U}_i$	-	position vectors defined in Figure 4.
$\bar{r}_o$	-	position vector defined in Figure 2.
$[R]$	-	inertial force coefficient matrix referenced to rigid body coordinates.

$\ddot{R}_{o_{1,2,3}}$ - space station translational accelerations along the 1,2,3 axes directions, respectively.

$\bar{R}_o$ - radius vector in ECI.

$\bar{r}_J'$ - $(\bar{r}_o - \bar{h}_J)$ force moment arm vector for J^{th} appendage.

$\bar{r}_J$ - vector from space station/controllable appendage interface to the center of mass of the J^{th} controllable appendage.

R_B - array of rigid body motion variables.

$[S]$ - inertial force coefficient matrix referenced to flexible space station coordinates.

$\bar{T}_{A_J}$ - total interaction torque vector produced by the flexible and rigid dynamics of the J^{th} controllable appendage about its constrained axes.

$\bar{T}_{FA_J}$ - total interaction torque vector produced by the flexible and rigid dynamics of the J^{th} fixed appendage.

$\bar{T}'_{FA_J}$ - interaction torque vector produced by the flexible dynamics of the J^{th} fixed appendage.

T_s - defined by Equation (29).

$\bar{T}_R$ - externally applied torque vector to the space station.

$\bar{T}_C$ - control torque vector produced by the attitude control system.

$\bar{T}_{C_J}$ - total interaction torque vector produced by the orientation control system about the unconstrained axes of the J^{th} controllable appendage.

V_i, M_i - modal force and moment coefficients in i^{th} mode, respectively.

W - defined by Equation (24).

X - defined by Equation (14).

X_I - vector in ECI coordinate frame.

X_S - vector in space station coordinate frame.

X_{A_J}	-	vector in the J^{th} controllable appendage coordinate frame.
Y	-	uncoupled generalized coordinate of the spinning structure.
$Z_i^{(1)}, Z_i^{(2)}$	-	coordinates defined by Equation (21).
$\dot{\alpha}$	-	angular rate of control gyro.
β_i	-	defined by Equation (39).
$\dot{\omega}_{O_{1,2,3}}$	-	space station rotational accelerations about the 1,2,3 axes directions, respectively.
$\dot{\omega}_{A_{J_{1,2}}}$	-	J^{th} controllable appendage rotational accelerations about the 1,2 axes directions, respectively.
ω	-	circular frequency.
ω_s	-	steady spin rate of space station.
ω_T	-	wobble rate.
$\omega_{i1}, \omega_{i2}, \omega_{i3}$	-	rotational rates about the i^{th} coordinate frame axes.
θ_o, θ_{A_J}	-	rotational coordinates of the space station and J^{th} controlled appendage.
Φ	-	modal deflection coefficients.
$\Phi_{s,J}$	-	matrix of space station modal deflection coefficients at the J^{th} appendage attachment location (3 x J)
$\Phi'_{s,J}$	-	matrix of space station modal slope coefficients at the J^{th} appendage attachment location (3 x J)
Φ_J	-	modal deflection coefficient matrix (3J x J)
ξ_c, ξ_s	-	generalized coordinates of cantilever appendage structure and space station structure respectively.
Λ	-	complex circular frequency

NOTATION

$\frac{d(\ )}{dt}_I$	-	implies differentiation with respect to an inertial reference
$[\ ]$	-	rectangular matrix
$\begin{bmatrix} \diagdown \end{bmatrix}$	-	diagonal matrix
$\{\ \}$	-	column matrix
$[\ ]^T$	-	designates the matrix transponse operation
$\sim$	-	vector operator in a 3-axis system defined by Equation (7).
$*$	-	designates the conjugate of a complex quantity.
$-$	-	designates a vector quantity in a 3 x 1 array.
$\sum_E^T$	-	an operator designating the matrix $[I \mid I \mid I \mid I]$ having dimensions of 3 x 3J

ANALYTICAL CONSIDERATIONS

In order to provide an automated methodology of predicting the dynamic interactions of solar arrays and space stations, an analysis must be initially formulated which considers all space station parameters affecting both rigid and flexible body dynamics. The analytical considerations which have been included in this study are the representive influencing parameters and their interactive paths depicted in Figure 1. These considerations should be basic to any structural analysis of an orbiting space station, especially if design criteria do not automatically minimize the possible couplings shown. Since weight minimization of orbiting structures is usually of prime importance, each of the parameters is a necessary consideration in structural dynamic analyses. The following describes the specific manner in which each of the important space station parameters are treated in this methodology.

The space station structural dynamics are described by rigid body and flexible body motion degrees of freedom, the latter being represented by generalized coordinates of the free-free structural vibration modes. The modal method of describing flexible motions is employed so that a system frequency range of interest can be chosen and model truncation employed. External perturbations such as docking forces and crew motions which can be independently described in time, are considered to specifically interact with the space station dynamics and result in total system motions. In addition, control forces and torques, as provided by the attitude control of the space station interact with the space station rigid and flexible dynamics. Attached to the space station are flexible appendages, such as solar cell arrays which are usually controllable about seasonal and orbital adjust axes. The rigid body characteristics of these controllable appendages are described by hinged motions relative to the space station body about the controllable axes and rigidly constrained about the other axis. The flexible dynamics of these appendages are considered in terms of orthogonal cantilever modes, the root constraint being at the appendage/space station interface. A modal synthesis technique is therefore inherent in the

analytic formulation and consists of the description of coupled motion terms of rigid body appendage and space station motions and the flexible dynamics of the appendages (or solar arrays) and free-free flexible dynamics of the space station structure. The use of orthogonal cantilever modal coordinates for the appendages allows for the provision of modal truncation.

Interactive with these flexible and rigid motions are the influence of controlling torques by a solar array orientation control system. This system produces torques about the unconstrained array axes so that sun orientation is maintained by a mathematically described control law. Guidance commands for an orbiting system at specified orbital parameters are automatically generated within the simulation.

The governing equations of the structural system and general types of applicable control laws are represented in the digital simulation. The simulation provides the real time solutions of structural motions and interaction loads which result from applied perturbations.

SPACE STATION-SOLAR ARRAY EQUATION FORMULATIONS

The following presents a summary of the motion equations contained in the digital simulation. These equations form the basis for the calculation of interaction loads which result from external perturbations during orbital operations. Two separate orbiting space station conditions have been considered in the analytical formulation. One condition represents the structural configuration in a zero "G" or operational mode with the arrays tracking the sun according to a designated control law. The other condition represents the structural configuration spinning at a constant rate about some designated spin vector for simulation of an artificial "G" environment. This condition will not require sun tracking arrays, but rather, solar arrays which are rigidly constrained to the space station. Detailed formulations of these equations are contained in Reference 2.

"Zero "G" Structural Condition

Because the solar arrays may have large angular motion with respect to the space station during simulation of structural perturbations, a linear analysis is inadequate. Therefore, a Newton-Euler representation of the rigid body dynamics is employed. The rigid body system consists of a central body or space station to which is attached fixed and controllable appendages -- the latter representing controlled solar arrays. Fixed appendage mass and inertia properties, in a rigid body sense, are considered as part of the central body. The rigid characteristics of the rotating arrays are represented as hinged bodies suitably constrained at the point of attachment in those directions in which motion is not controlled. In this study two arbitrarily located appendages have been designated as controlled, and up to four appendages are considered uncontrollable. Therefore, the rigid body system of structures comprises a three-hinged body system of connected structures. Vector equations of motion are defined and formulated with reference to the central body and attached appendage system depicted in Figure 2. The equation sets are chosen

to be defined in terms of a system force equation, a space station moment equation, and a hinged body moment equation for each controllable appendage.

System Force Equation (three-body rigid system)

$$M_T \frac{d}{dt^2} (\bar{R}_o + \bar{C}) \Big|_I = \sum_J^2 \bar{F}_{A_J}' + \sum_J^4 \bar{F}_{FA_J}' + \bar{F}_R \tag{1}$$

Space Station Moment Equation

$$\frac{d}{dt} (\bar{L}_o) \Big|_I = (-\bar{\ell}_R) \times \bar{F}_R + \sum_J^2 \left(\bar{T}_{A_J} - \bar{T}_{C_J} \right) + \sum_J^4 \bar{T}_{FA_J}' + \bar{T}_C + \bar{T}_R \tag{2}$$

$$+ \sum_J^2 \bar{r}_J' \times \bar{F}_{A_J} + \sum_J^4 \bar{r}_J' \times \bar{F}_{FA'_J}$$

Jth Hinged Body Moment Equation

$$\frac{d}{dt} (\bar{L}_J) \Big|_I = \bar{T}_{C_J} - \bar{r}_J \times \bar{F}_{A_J}'' \tag{3}$$

The right hand side of the above equations include all external interaction forces and torques applied to the respective rigid body. All motion variables, both rigid body and flexible body, are coupled with the appropriate inertial coupling terms. For example, in the above system force equation, flexible body dynamics are treated as external forces while in the flexible body dynamics equation, the rigid body dynamics are considered as external perturbations. The vector Equations (1 - 3) are formulated into a set of matrix equations for the facilitation of digital computations. The system force and space station moment equations are formulated with respect to the space station reference axes and the hinged body equations are formulated with respect to the solar array reference axes. The transformation to the solar array reference system requires the use and computation of specific direction cosine matrices.

The principle coordinate frames and direction cosine identities utilized are as follows:

$$\{X_S\} = [C_o]^T \{X_I\} \tag{4}$$

$$\{X_{A_1}\} = [C_1]^T \{X_S\} \tag{5}$$

$$\{X_{A_2}\} = [C_2]^T \{X_S\} \tag{6}$$

These direction cosine matrices are calculated in terms of Euler angles and are updated in time in the simulation by the following equation:

$$\dot{C}_i = C_i \begin{bmatrix} 0 & -\omega_{i3} & \omega_{i2} \\ \omega_{i3} & 0 & -\omega_{i1} \\ -\omega_{i2} & \omega_{i1} & 0 \end{bmatrix} = C_i \tilde{\omega}_i \tag{7}$$

The equations representing all considered rigid body motion variables are shown in Figure 3. Submatrices A_i represent linear and time-dependent coefficients of the appropriate motion variables. The right hand side of this equation is representative of the applied forces, control forces, and all non-linear terms. Detailed descriptions of these equation coefficients are given in Reference 2.

Flexibilities of the attached appendages are described by generalized coordinates associated with a set of orthogonal vibration modes for each structure cantilevered from the space station. This modal synthesis method of coupling rigid body and flexible body motions is adapted from the formulations developed by Likins (Reference 3). Space station flexibility is described by generalized coordinates associated with a set of vibration modes representing a freely translating and rotating structure. Coupled motion equations of the complete rigid body and flexible body structural system are represented in the digital simulation and the numerical solution of these equations are used to predict the structural interactions. The flexibility

equations for the attached appendages are formulated with reference to the elastic system depicted in Figure 4. It is assumed that the particle masses have negligible inertias and elastic deflections are small so that linear structural analysis is valid. The force on the i^{th} mass of a flexible appendage is given by the following.

$$\bar{F}_i = m_i \frac{d^2}{dt^2} (\bar{R}_o + \bar{h}_J + \bar{r}_i + \bar{U}_i) \Big|_I \tag{8}$$

Substitution in Equation (8) of the appropriate direction cosine matrices and consideration of the properties resulting from elastic deformation of controllable appendages, produce the following equations.

$$[M] \ddot{q} + [K] q = -[G] q - [B] \dot{q} + \{L\} \tag{9}$$

where

$$q = \left[U_1^1 \; U_2^1 \; U_3^1 \; U_1^2 \; U_2^2 \; U_3^2 \; \text{---} \; U_1^N \; U_2^N \; U_3^N \right]^T \tag{10}$$

The matrices designated by $[B]$ and $[G]$ in Equation (9) represent force coefficients which are dependent upon rotation rates; i.e., they are analogous to centrifugal and coriolis type force coefficients. The matrix designated by $\{L\}$ contains the time varying inertial loads produced by all rigid body and flexible coordinates of the space station. $\{L\}$ can be further defined by the following equation.

$$\{L\} = \left[R \;\vdots\; S \right] \left[\begin{array}{c} \ddot{R}_B \\ \hline \ddot{\xi}_s \end{array} \right] \tag{11}$$

Following the method of Reference 3, it is convenient to transform Equation (9) into orthogonal coordinates, representing cantilever modes of vibration. This permits the system of uncoupled equations to be truncated on the basis of some chosen engineering criterion. The transformed equations then become

$$[I]\{\ddot{\xi}_c\} + [g\omega]\{\dot{\xi}_c\} + [\omega^2]\{\xi_c\} = [\Phi]^T [G][\Phi]\{\xi_c\} - [\Phi]^T [B][\Phi]\{\dot{\xi}_c\} + [\Phi]^T \{L\} \tag{12}$$

The modal damping matrix is inserted in Equation (12) in the classical manner. The assumption made in going from Equation (9) to Equation (12) is that the motion dependent matrices which are functions of rigid body rotation rates, are small and have a negligible effect. Without this assumption the simulation would be required to be performed in discrete coupled coordinates with resulting manipulations of large order matrices.

The motion equations considered for the fixed appendages are similar to that given by Equation (12) with the exception that the motion dependent matrices $[G]$ and $[B]$ are assumed negligible. This assumption implies small space station flexible and rigid rotation rates (however the total rotation rates of controllable appendages are still maintained in the analytical considerations).

The flexible space station equations are formulated as a truncated set of free-free modal coordinates of the following form.

$$\left[I\right]\left\{\ddot{\xi}_s\right\} + \left[g\omega\right]\left\{\dot{\xi}_s\right\} + \left[\omega^2\right]\left\{\xi_s\right\} = \left[\Phi\right]^T \left\{F\right\} \tag{13}$$

The columns of the modal deflection matrix on the right hand side of Equation (13) produce generalized forces to the free-free modes. The column vector of time dependent forces include those which are discretely applied as external forces or attitude control forces. In addition, the force vector includes the inertial force interactions produced by all attached appendages.

Equations (1 - 3), (12) and (13) form a second order differential matrix equation. This equation is represented in its final form by the following:

$$\left[M\right]\left\{\ddot{X}\right\} + \left[C\right]\left\{\dot{X}\right\} + \left[K\right]\left\{X\right\} = \left\{P\right\} \tag{14}$$

Partitioning of this equation logically leads to four variable subgroups, such that the solution vector takes the following form:

$$\left\{X\right\} = \left[\left\{R_o\right\}^T, \left\{\theta_o\right\}^T, \left\{\theta_{A_1}\right\}^T, \left\{\theta_{A_2}\right\}^T, \left\{\xi_s\right\}^T, \left\{\xi_c\right\}_1^T \ldots \left\{\xi_c\right\}_J^T\right] \tag{15}$$

The left hand side of Equation (14) is constructed in the simulation from computed direction cosines, input rigid body inertia tensors, center of gravity and appendage attachment locations in the space station coordinate frame, and modal properties of flexible appendages and the space station. The latter includes deflection coefficients, frequencies, damping coefficients, and discrete masses, for a chosen number of orthogonal modes for each flexible structure. It is noted that the coefficient matrix of $\left\{\dot{X}\right\}$ in Equation (14) results from the terms produced by $[\Phi]^T \left[B\right] [\Phi]$ and the inclusion of structural damping only; the coefficient matrix of $\left\{X\right\}$ results from the terms produced by $[\Phi]^T \left[G\right][\Phi]$ and the inclusion of the generalized stiffnesses of respective flexible modes. The primary coupling terms associated with each structure of the three body hinged system is therefore the inertial coupling matrix $\left[M\right]$. A representative matrix subset of the inertial coupling matrix would be that given in Figure 3. The right hand side of Equation 14 is comprised of the externally applied forces, control forces and non-linear terms containing the motion variables. A detailed description of each of the matrix subsets of Equation (14) is given in Reference 2. A simultaneous solution of the combined system equations is provided by using a numerical integration algorithm (References 2, 4), with a specified integration time interval. Time dependent terms in the $\left[M\right]$ matrix are updated at each interval or can be updated at multiples of this interval.

The simulation computes interaction loads at the connection point of each flexible appendage from the time solution of the motion equations. The detailed formulations for the interaction loads in terms of vector forces and torques are given in Figure 5. These interaction loads account for all rigid body inertial forces and torques applied to the appendages and the elastic body force contributions. The direction cosine matrices included in these equations produce the interaction load description in the space station coordinate system.

Artificial "G" Structural Condition

Equation formulations contained in the simulation for a flexible space station with rigidly attached flexible appendages also consider the influence of a steady spin rate of the structural system upon perturbed motion. The rigid body motion equations are of the same form as Equations (1) and (2), and the hinged body equations are omitted since all appendages are considered to be constrained to the space station.

In order to account for the possible effect of large magnitude spin rate upon the flexible coordinates described by cantilever modes of the appendages or the free-free modes of the space station, the following formulation of flexibility equations is utilized

$$[M] \{\ddot{q}\} + [B] \{\dot{q}\} + [K'] \{q\} = \{L'\} \tag{16}$$

where q has the same definition as is given in Equation (10). The matrices $[B]$ and $[K']$ incorporate the force coefficients defined by the steady spin rate and a detailed description of these matrices are presented in Reference 5. The above second order matrix equation is reduced to the following first order state equation for purposes of defining generalized coordinates.

$$[D] \{\dot{Q}\} + [E] \{Q\} = \{L'\} \tag{17}$$

where

$$D = \left[\begin{array}{c|c} [0] & -[M] \\ \hline [M] & [B] \end{array}\right], \quad \left[E\right] = \left[\begin{array}{c|c} [M] & [0] \\ \hline [0] & [K] \end{array}\right], \quad \left\{Q\right\} = \left[\begin{array}{c} \dot{q} \\ \hline q \end{array}\right], \quad \left[L'\right] = \left[\begin{array}{c} \{0\} \\ \hline \{L\} \end{array}\right]$$

The reduced order motion equations given by Equation (17) in terms of coupled discrete coordinates can be uncoupled by the transformation so that

$$\{Q\} = [\Phi] \{Y\} \tag{18}$$

The transformation matrix consists of deflection coefficients of the complex eigenvectors and their conjugates pairs, and corresponding eigenvalues are complex with imaginary parts only and also exist in conjugate pairs. An automated procedure for producing the transformation eigenvectors from discrete coordinate matrices is

given by Gupta (Reference 6). Substitution of Equation (18) into Equation (17) and premultiplication by $[\Phi^*]^T$ results in the following.

$$\{\dot{Y}\} = -[\Lambda]\{Y\} + \{\bar{L}\} \tag{19}$$

where Λ is the matrix of the complex eigenvalues, and $\{\bar{L}\} = [\Phi^*]^T \{L'\}$

Equation (19) can be written as:

$$\begin{bmatrix} \dot{\bar{Y}} \\ \dot{\bar{Y}}^* \end{bmatrix} = -\begin{bmatrix} \bar{\Lambda} & 0 \\ 0 & \bar{\Lambda}^* \end{bmatrix} \begin{bmatrix} \bar{Y} \\ \bar{Y}^* \end{bmatrix} + \begin{Bmatrix} \bar{L} \end{Bmatrix} \tag{20}$$

where $\bar{Y} = [\, Y_1 \quad Y_2 - - - Y_N \,]^T$

$$\bar{Y} = [\, Y_1^* \quad Y_2^* - - - Y_N^* \,]^T$$

$$\bar{\Lambda} = \begin{bmatrix} \Lambda_1 & & & 0 \\ & \Lambda_2 & & \\ & & \ddots & \\ 0 & & & \Lambda_N \end{bmatrix} \qquad \bar{\Lambda}^* = \begin{bmatrix} \Lambda_1^* & & & 0 \\ & \Lambda_{2^*} & & \\ & & \ddots & \\ 0 & & & \Lambda_{N^*} \end{bmatrix}$$

Multiplying both sides of Equation (20) by the following

$$1/2 \begin{bmatrix} [I] & [I] \\ [J] & [-J] \end{bmatrix}$$

and letting $Z_i^{(1)} = (1/2)\ (Y_i + Y_i^*)$ (21)

$$Z_i^{(2)} = (1/2)\ \sqrt{-1}\ (Y_i - Y_i^*)$$

The following modal equations result.

$$\begin{bmatrix} \dot{\bar{Z}}^{(1)} \\ \dot{\bar{Z}}^{(2)} \end{bmatrix} = \begin{bmatrix} 0 & |\bar{\Lambda}| \\ -|\bar{\Lambda}| & 0 \end{bmatrix} \begin{bmatrix} \bar{Z}^{(1)} \\ \bar{Z}^{(2)} \end{bmatrix} + \begin{bmatrix} V \end{bmatrix} \begin{Bmatrix} \bar{L} \end{Bmatrix} \tag{22}$$

where

$$[V] = 1/2 \begin{bmatrix} [I] & [I] \\ [J] & -[J] \end{bmatrix} [D]^{-1} [\Phi^*]^T$$

When N modes are retained as a truncated set, the following definitions apply.

$$\bar{Z}^{(1)} = \begin{bmatrix} Z_1^{(1)} \\ \cdot \\ \cdot \\ \cdot \\ Z_N^{(1)} \end{bmatrix} \qquad \bar{Z}^{(2)} = \begin{bmatrix} Z_1^{(2)} \\ \cdot \\ \cdot \\ \cdot \\ Z_N^{(2)} \end{bmatrix}$$

Modal damping may be introduced into Equation (22) by the coefficient "g" in the classical manner.

$$\begin{bmatrix} \dot{\bar{Z}}^{(1)} \\ \dot{\bar{Z}}^{(2)} \end{bmatrix} + \begin{bmatrix} 0 & -|\bar{\Lambda}| \\ |\bar{\Lambda}| & g|\bar{\Lambda}| \end{bmatrix} \begin{bmatrix} \bar{Z}^{(1)} \\ \bar{Z}^{(2)} \end{bmatrix} = [V] \{\bar{L}\} \tag{23}$$

In terms of the new coordinates, $\bar{Z}$, Equation (18) is written as

$$\{Q\} = [\Phi]\{Y\} = [\Phi] \begin{bmatrix} [I] & [J] \\ [I] & -[J] \end{bmatrix} \begin{bmatrix} \bar{Z}^{(1)} \\ \bar{Z}^{(2)} \end{bmatrix} \tag{24}$$

Equations (23) and (24) are implemented in the simulation for describing appendage and space station flexibility. These equations are combined with the rigid body force and space station moment equations in the same manner as that utilized for the total system equations representing the zero "G" condition. A simultaneous solution of the rigid body and generalized coordinate variables is provided by the digital simulation. Interaction forces and torques are computed by equations similar to that given in Figure 5. A complete and detailed set of matrix equations representing the artificial "G" or spinning condition is given in Reference 2.

The transient interaction forces and torques at any solution time are dependent upon the number of finite modes utilized, and the steady-state portion of force and torque is exactly represented. To demonstrate a step forcing function with a finite number of cantilever appendage modes and an expected solution with an infinite mode usage, Table 2 is presented. Contained are the numerical values of interaction force coefficients, modal mass and modal participation factors for the first six modes of a five slug mass uniform beam, 10 feet in length, and a designated fundamental cantilever frequency of 2Hz. Modal participation is defined as that contribution of steady state moment and/or force provided by that mode in its statically deflected shape. The use of an infinite number of modes gives 100% modal participation in exactly defining the static loads. The accumulated percentage with number of modes utilized is shown in Figure 16. The numerical values presented are derived from the tabularized data given in Reference 14. Table 3 presents the initial forces and torques produced by both the analytical solution and the digital simulation for a finite number of utilized modes and the solution which would be given by an infinite number of modes. A comparison of numerical values shows significant differences do exist with the finite mode approximation and that interaction loads at zero time will always have an initial finite value rather than zero. This initial force value is also seen to be dependent upon structural position since in the results given in Figure 14, for shear force at the quarter span, an unobservable initial value is indicated. The above numerical data and comparisons show that the modal synthesis method represents an approximation of the transient response interaction forces, and the magnitude of the approximation can be evaluated in terms of the number of modes utilized in the solution. In addition, the percentage accumulation of modal participation factor can be a measure of this approximation. It is generally concluded that in most engineering applications, the synthesization method is a satisfactory method if a sufficient choice and number of modes are utilized.

To further substantiate the structural dynamics methodology and simulation verification, a simple arrangement of uniform beams in a planar "T"

where

$$[V] = 1/2 \begin{bmatrix} [I] & [I] \\ [J] & [-J] \end{bmatrix} [D]^{-1} [\Phi^*]^T$$

When N modes are retained as a truncated set, the following definitions apply.

$$\bar{Z}^{(1)} = \begin{bmatrix} Z_1^{(1)} \\ \cdot \\ \cdot \\ \cdot \\ Z_N^{(1)} \end{bmatrix} \qquad \bar{Z}^{(2)} = \begin{bmatrix} Z_1^{(2)} \\ \cdot \\ \cdot \\ \cdot \\ Z_N^{(2)} \end{bmatrix}$$

Modal damping may be introduced into Equation (22) by the coefficient "g" in the classical manner.

$$\begin{bmatrix} \dot{\bar{Z}}^{(1)} \\ \dot{\bar{Z}}^{(2)} \end{bmatrix} + \begin{bmatrix} 0 & -|\bar{\Lambda}| \\ |\bar{\Lambda}| & g|\bar{\Lambda}| \end{bmatrix} \begin{bmatrix} \bar{Z}^{(1)} \\ \bar{Z}^{(2)} \end{bmatrix} = [V] \left\{ \bar{L} \right\} \tag{23}$$

In terms of the new coordinates, $\bar{Z}$, Equation (18) is written as

$$\{Q\} = [\Phi] \{Y\} = [\Phi] \begin{bmatrix} [I] & [J] \\ [I] & [J] \end{bmatrix} \begin{bmatrix} \bar{Z}^{(1)} \\ \bar{Z}^{(2)} \end{bmatrix} \tag{24}$$

Equations (23) and (24) are implemented in the simulation for describing appendage and space station flexibility. These equations are combined with the rigid body force and space station moment equations in the same manner as that utilized for the total system equations representing the zero "G" condition. A simultaneous solution of the rigid body and generalized coordinate variables is provided by the digital simulation. Interaction forces and torques are computed by equations similar to that given in Figure 5. A complete and detailed set of matrix equations representing the artificial "G" or spinning condition is given in Reference 2.

DIGITAL SIMULATION PROGRAM

Structural Representation

The digital simulation program is designed to accept rigid body and flexible body structural data in a general format. The structural configuration may consist of a flexible central body (space station) with two attached controllable flexible appendages (solar arrays) and four attached non-controllable flexible appendages. For the case of a spinning space station, only four non-controlled appendages can be considered. Required rigid body input data consists of the inertia tensors for the central body and all considered flexible appendages, the attachment locations of the appendages in the coordinate axis of the central body, and direction cosine matrices relating the rigid body axes of the appendages with the central body axes.

Flexible dynamics are input in terms of a discrete mass matrix corresponding to a derived structural finite element model and modal data such as mass, frequency, and deflection coefficients. As stated previously, the flexible dynamics of the space station are represented by free-free modes and the flexible dynamics of the solar arrays and appendages are represented by cantilever modes. A total of 60 modes can be represented in the program. All modal descriptions are referenced to each respective structural coordinate reference frame. Modal deflections for the flexible appendages can be described by three translations and those for the central body or space station can be described by three translations and three rotations. Modal descriptions, as required for input to the simulation, are obtainable from the results of most finite element structural analysis computer programs, such as those described in References 7 and 8.

For the representation of spinning structures, both the coriolis force coefficient and "effective" stiffness matrices (Reference 5), in addition to the mass matrix of the discretized structure,are required as input. In addition the modal representations in the complex domain, resulting from orthogonalization and subsequent modal truncation are required input. Transformation of the discrete coordinates to

sets of orthogonal coordinates for both the spinning cantilever appendage structures and the spinning "free-free" space station structure can be obtained by the method given in Reference 6.

Perturbation of the structural system is produced by the application of defined force and/or torque histories applied at a specified node point of the central body. In addition, perturbation may be obtained by the non-zero initialization of appendage and central body motion variables so that attitude and orientation controlling forces and torques are non-zero at the initiation of the simulation. Output data from the simulation includes the time solutions of all motion variables and their time derivatives, and the time solutions of appendage-central body interaction forces and torques. In the case where control systems are active, controlling torques are also given. A typical list of simulation output parameters for a specific simulation real time value are shown in Figure 6.

A subprogram of the simulation calculates internal structural loads in the elements of the structural model. A loads transformation matrix relating internal loads to the rigid body and generalized coordinate variables must be initially derived and used as input. The general matrix equation represented in this subprogram is given by the following.

$$\left\{ \text{LOADS} \right\} = \left[\text{LA} \right] \left\{ \ddot{X} \right\} + \left[\text{LB} \right] \left\{ \dot{X} \right\} + \left[\text{LC} \right] \left\{ X \right\} + \left[\text{LD} \right] \left\{ f \right\} + \left\{ \text{LE} \right\} \quad (25)$$

Matrices LA, LB, LC, LD, and LE are user supplied and all or a portion of the matrix input capability is optional. $\{ X \}$, $\{ \dot{X} \}$, and $\{ \ddot{X} \}$ are the motion variables and their time derivatives and $\{ f \}$ is a force matrix (time variant) which includes external forces, interaction forces and control forces. It is seen that both the modal acceleration and modal displacement methods of internal load evaluation (Reference 9) can be considered by this general matrix equation.

The simulation can be viewed as being completely general when considering the structural dynamics of arbitrary configurations as defined by precalculated rigid body and flexible body structural parameters. Influences of attitude and orientation control system dynamics are incorporated in the simulation by the inclusion of specific mathematical control system representations. These representations are subroutines

and provide optional closed loop control dynamics. Other types of control systems can be easily included in the simulations as optionally coded subroutines by the user. Those which are presently included are described.

Control System Representations

Control system definitions which are contained in the simulation program for orientation control of the solar arrays and attitude control of the space station are representative of the following generic types.

- o Continuous Array Drive System
- o Non-Linear Array Drive System
- o Control Moment Gyro Attitude Control System
- o Reaction Jet Attitude Control System
- o Wobble Damper

Produced torques and forces from these systems to the solar arrays and space station contribute to the reactive rigid body and flexible body dynamics of these structures. The first four systems are incorporated for use only in simulations of a space station and solar array configuration while in a zero "G" or non-spinning condition. It is assumed that orientation control of solar arrays is not a requirement of a spinning condition, and therefore the arrays would be rigidly constrained to the space station in this operational mode. The attitude control of a spinning space station configuration is provided by a simple wobble damper model. The solar array orientation control systems (OCS) provide the controlling torques for the plane of the solar array to be maintained normal to the sun line to a desired degree of angular accuracy. A continuous-type drive system employs either a DC torque motor or a variable frequency synchronous motor as its drive element and is continuously correcting for solar array errors with the sun line during the specified orbit. A block diagram of the continuous drive system is given in Figure 7. Attitude of the space station is generated by the use of Lyddane's method (Reference 10) and appropriately defined orbital constants. Array guidance commands as well as error angle and angular rate feedback are computed relative to space station rigid body and flexible body degrees of freedom. The difference between the commanded array angle and actual array angle

are used to generate the angle error signal. Array angular rate is multiplied by the back EMF coefficient and added (negatively) to the filtered error signal. This gives the effective drive signal for the motor which is modeled as a first order lag. Numerical values of drive systems constants have been generated for specific 100 kw array structural configurations and are given in Reference 2. These values are contained in the simulation as default values and may be easily changed by user option to complement other structural configurations.

The non-linear drive OCS is similar to the continuous drive system with the exception that the control logic of the non-linear OCS is operated in an on-off manner. When the array error exceeds some preselected threshold value, the motor is turned on until the array is driven to a null position at which point the motor is switched off. The specific representation of the non-linear OCS model contained in the simulation is that presented by the block diagram in Figure 8. Because of the on-off manner of the non-linear OCS, inherent friction in the drive mechanism requires consideration and is represented by an input variable of friction torque in the simulation. It is programmed so that the driving torque on the array is zero if the motor torque is less than a designated friction torque value when the array is not moving relative to the space station. When the array is rotating and the motor torque is less than a friction torque value, the torque on the array is the friction torque minus the motor torque and when motor torque is greater than the friction torque the torque applied to the arrays is the difference between these respective torques. Numerical values for the non-linear drive system constants have been generated for a specific 100 Kw array structural configuration and they are given in Reference 2. These values are contained in the simulation as default values and may be easily changed by user option to complement other desired structural configurations.

The guidance and control systems which are mathematically modelled are the control moment gyro (CMG) and reaction jet systems. One CMG control system that is simulated is that designed by the Defense Electronics Division (DED) of the General Electric Company (Reference 11) in support of the space station studies performed by the North American Rockwell Corporation (Reference 12). A complete description of this system is presented in Reference 2. Reference 11 specifies that this control

Figure 13 presents a comparison of the shear histories obtained by using the simulation with one cantilever mode and one free-free mode in Equations (32) and (33), respectively. An Adams numerical integration method is used to obtain the solution of the motion histories given by the above motion equations for the free-free beam and both the modal acceleration and model displacement methods are used for the shear force evaluations. Numerical coefficients of the motion equation are derived from the tabulations given in Reference 14. Comparison of the shear force history produced by the simulation with the fundamental cantilever mode is seen to be in excellent agreement with that produced by one free-free mode. Minor differences in force magnitude are observable between the two methods of force calculation. Simulation results for this forced response condition are also compared with the results obtained by the NASTRAN Direct Transient Response Method (Reference 7). These histories are presented in Figure 14 and results reflect the use of the first five cantilever modes for each of two flexible appendages (beams). The free-free uniform beam used in NASTRAN is represented by 40 discrete masses, each having two structural degrees of freedom (one translational and one rotational). No modal damping is considered in the presented response solutions. In general, good agreement exists between the frequency content and magnitude of shear history obtained by the two methods. Higher frequency transients, however, exist in the NASTRAN solution which are due to the inherent representation of all beam modes.

The above comparisons indicate that the modal synthesis method is adequate for the determination of dynamic response solutions. It is also indicated that a sufficient number of modal coordinates must be used to accurately describe the basic parameters of the given response condition. For a complex structural arrangement, this might necessitate an iteration in the number of modes used for obtaining an accurate response solution.

are used to generate the angle error signal. Array angular rate is multiplied by the back EMF coefficient and added (negatively) to the filtered error signal. This gives the effective drive signal for the motor which is modeled as a first order lag. Numerical values of drive systems constants have been generated for specific 100 kw array structural configurations and are given in Reference 2. These values are contained in the simulation as default values and may be easily changed by user option to complement other structural configurations.

The non-linear drive OCS is similar to the continuous drive system with the exception that the control logic of the non-linear OCS is operated in an on-off manner. When the array error exceeds some preselected threshold value, the motor is turned on until the array is driven to a null position at which point the motor is switched off. The specific representation of the non-linear OCS model contained in the simulation is that presented by the block diagram in Figure 8. Because of the on-off manner of the non-linear OCS, inherent friction in the drive mechanism requires consideration and is represented by an input variable of friction torque in the simulation. It is programmed so that the driving torque on the array is zero if the motor torque is less than a designated friction torque value when the array is not moving relative to the space station. When the array is rotating and the motor torque is less than a friction torque value, the torque on the array is the friction torque minus the motor torque and when motor torque is greater than the friction torque the torque applied to the arrays is the difference between these respective torques. Numerical values for the non-linear drive system constants have been generated for a specific 100 Kw array structural configuration and they are given in Reference 2. These values are contained in the simulation as default values and may be easily changed by user option to complement other desired structural configurations.

The guidance and control systems which are mathematically modelled are the control moment gyro (CMG) and reaction jet systems. One CMG control system that is simulated is that designed by the Defense Electronics Division (DED) of the General Electric Company (Reference 11) in support of the space station studies performed by the North American Rockwell Corporation (Reference 12). A complete description of this system is presented in Reference 2. Reference 11 specifies that this control

Figure 13 presents a comparison of the shear histories obtained by using the simulation with one cantilever mode and one free-free mode in Equations (32) and (33), respectively. An Adams numerical integration method is used to obtain the solution of the motion histories given by the above motion equations for the free-free beam and both the modal acceleration and model displacement methods are used for the shear force evaluations. Numerical coefficients of the motion equation are derived from the tabulations given in Reference 14. Comparison of the shear force history produced by the simulation with the fundamental cantilever mode is seen to be in excellent agreement with that produced by one free-free mode. Minor differences in force magnitude are observable between the two methods of force calculation. Simulation results for this forced response condition are also compared with the results obtained by the NASTRAN Direct Transient Response Method (Reference 7). These histories are presented in Figure 14 and results reflect the use of the first five cantilever modes for each of two flexible appendages (beams). The free-free uniform beam used in NASTRAN is represented by 40 discrete masses, each having two structural degrees of freedom (one translational and one rotational). No modal damping is considered in the presented response solutions. In general, good agreement exists between the frequency content and magnitude of shear history obtained by the two methods. Higher frequency transients, however, exist in the NASTRAN solution which are due to the inherent representation of all beam modes.

The above comparisons indicate that the modal synthesis method is adequate for the determination of dynamic response solutions. It is also indicated that a sufficient number of modal coordinates must be used to accurately describe the basic parameters of the given response condition. For a complex structural arrangement, this might necessitate an iteration in the number of modes used for obtaining an accurate response solution.

are used to generate the angle error signal. Array angular rate is multiplied by the back EMF coefficient and added (negatively) to the filtered error signal. This gives the effective drive signal for the motor which is modeled as a first order lag. Numerical values of drive systems constants have been generated for specific 100 kw array structural configurations and are given in Reference 2. These values are contained in the simulation as default values and may be easily changed by user option to complement other structural configurations.

The non-linear drive OCS is similar to the continuous drive system with the exception that the control logic of the non-linear OCS is operated in an on-off manner. When the array error exceeds some preselected threshold value, the motor is turned on until the array is driven to a null position at which point the motor is switched off. The specific representation of the non-linear OCS model contained in the simulation is that presented by the block diagram in Figure 8. Because of the on-off manner of the non-linear OCS, inherent friction in the drive mechanism requires consideration and is represented by an input variable of friction torque in the simulation. It is programmed so that the driving torque on the array is zero if the motor torque is less than a designated friction torque value when the array is not moving relative to the space station. When the array is rotating and the motor torque is less than a friction torque value, the torque on the array is the friction torque minus the motor torque and when motor torque is greater than the friction torque the torque applied to the arrays is the difference between these respective torques. Numerical values for the non-linear drive system constants have been generated for a specific 100 Kw array structural configuration and they are given in Reference 2. These values are contained in the simulation as default values and may be easily changed by user option to complement other desired structural configurations.

The guidance and control systems which are mathematically modelled are the control moment gyro (CMG) and reaction jet systems. One CMG control system that is simulated is that designed by the Defense Electronics Division (DED) of the General Electric Company (Reference 11) in support of the space station studies performed by the North American Rockwell Corporation (Reference 12). A complete description of this system is presented in Reference 2. Reference 11 specifies that this control

system has a natural frequency of 1.414 Hz and a damping ratio of 0.707; however, it was found that during the performance of various digital simulations, considering the space station as a rigid body, that a relatively small numerical integration interval (Δt = .005 second) was required to stabilize solutions to motion equations when the CMG was chosen as the active control system, thus indicating higher frequencies of inner control loops. Because of the small integration time required for stability of solution with the CMG of Reference 11, a simpler and equivalent system for the control of relatively large structural motions is also included in the simulation to represent CMG controlling torques. This simplified system produces a more efficient computer simulation time to real time ratio when the CMG is chosen as the active control. It is programmed in the simulation as represented by the diagram shown in Figure 9, and is comprised of a lead-lag compensator, a constant multiplying of the moment of inertia properties of the orbiting structure and an output torque limiter. The time constants of the lead-lag compensator, the constant multiplying spacecraft inertia and the limiting torque are allowed to be input quantities to the control subroutine. This simplified representation allows a certain degree of flexibility when analyzing general space station configurations. The space station attitude is obtained from parameters calculated by Lyddane's method, the angles being comprised of rigid plus flexible spacecraft body structural motions. Since space station structural flexibility is considered in the feedback control loop, the positions of angle sensors and angular rate sensors within the structural system are specified by user input. In like manner, the position of the control torque is specified so that torques produced by the control system can be considered as input generalized torques to modal degrees of freedom.

The reaction jet control system (RCS) is used as an alternate to the CMG for controlling the attitude of the space station. A description of this system, as used for the control of the space station, when considered as a rigid body, is given in Reference 2. The method of simulating space station motions and their effect upon dynamic interaction is designed to account for space station flexibility. Therefore the reaction jet control system is configured to consist of six individual constant-thrust-magnitude thrusters at user specified structural locations to control the three angular rigid body motions. Location of each thruster, thrust magnitude and direction,

are user options. The typical applied torque to the rigid body is given by

$$T_C = K \cdot 1 (\theta_\varepsilon - \theta_{DB}) \tag{26}$$

where

T_C = output torque of the reaction jets at any given time for which the computed error is θ_ε.

K = torque capability of the reaction jets

1( ) = unit step function having the value zero for negative or zero arguments and the value unity for positive arguments.

θ_ε = computed equivalent attitude/rate error of the space station determined by

$$\theta_\varepsilon = K_1 (K_2 \theta_o - \omega_o) \tag{27}$$

where K_1 and K_2 are input constants.

θ_{DB} = deadband threshold level for equivalent attitude/rate error which determines when the reaction jets are active.

As previously mentioned, a simple wobble damper control representation is included for control of the spinning structural configuration. It consists of a single degree-of-freedom control moment gyro with its gimbal axis along the nominal spin axis and its momentum vector normal to that axis. With reference to Figure 10, the structural system is considered to be spinning about the X axis. The control moment gyro is torqued so that its momentum vector $\bar{h}$ always lags the wobble rate ω_T by 90°. A correction torque is applied to the space station which is equal to the following.

$$T_C = -(\omega_S + \dot{\alpha}) \times \bar{h} \tag{28}$$

An increase in the nominal spin rate also occurs in the correction wobble torque and is given as $\bar{T}_S = -\bar{\omega}_T \times \bar{h}$ (29)

The magnitude of parameters associated with the wobble damper are user option.

SIMULATION WITH SIMPLE STRUCTURAL CONFIGURATIONS

In order to verify the program, simple structural configurations are utilized and perturbed by classical forcing functions. A comparison of solution results with other methods of analysis then provides a measure of the adequacy of the employed modal synthesis techniques. Uniform beams are represented as flexible appendages and attached to both finite and zero mass central bodies. The attachment of two flexible cantilevers to a zero mass central body is analogous to a free-free beam system representation when the axes of each cantilever lie along one line. Therefore, comparisons of modal solutions from both perturbation of the two appendage system and its equivalent free-free system provides a desired measure of simulation adequacy and accuracy. Initially the adequacy of the modal syntheses method is compared by transforming the coordinates of the coupled appendages into a set of coordinates representing the free-free modes of the composite structure. Reference is made to Figure 11 depicting the rigid body and modal coordinates of the cantilever beams and the represented free-free beam structure for planar translational motion. Equilibrium equations are derived for the two connected cantilevers when fixed in inertial space so as to facilitate the coordinate transformations; these equations are derived in Reference 13 and are summarized below

$$M_J \ddot{R}_o(t) + \sum_{i=1}^{J} V_i \left(\frac{L}{2}\right) \ddot{\xi}_{c_i}(t) = 0 \tag{30}$$

$$M_{eq_i} \ddot{\xi}_{c_i}(t) + M_{eq_i} \omega_i^2 \xi_{c_i}(t) + V_i \left(\frac{L}{2}\right) \ddot{R}_o(t) = 0 \tag{31}$$

Equations (30) and (31) give the coordinate description for the system in terms of one rigid body coordinate R_o and the generalized coordinates of the cantilevers. A transformation of the coordinates given in Equations (30) and (31) to orthogonal coordinates then provides a basis of comparison between the derived orthogonal coordinates and the orthogonal coordinates of a free-free beam. The tables given in Reference 14 are utilized to obtain the invariant modal data for both free-free and cantilever beams.

Values of cantilever beam mass (5.0 slugs), frequency (12.566 rad/sec) and length (10 feet) were assigned for purposes of making numerical comparisons. Evaluation of the modal force coefficients of Equations (30) and (31) are based upon a 25-point discretized mass representation of the cantilever beam. The resulting frequencies obtained by a coordinate transformation analysis utilizing the method of Reference 6 (at zero spin rate) are listed in Table 1. These frequencies, together with corresponding free-free beam frequencies have been normalized with respect to the frequency of the fundamental free-free beam mode. The rate of convergence provided by the modal synthesis method is demonstrated by the successive number of cantilever modes utilized in Equations (30) and (31) and the subsequent transformations. Similarly, the degree of correlation and convergence in the modal amplitude domain is given by the comparisons of mode shapes in Figure 12. The comparisons show the cantilever beam description of the free-free beam modal properties is an excellent synthesis method when a sufficient number of cantilever coordinates is used.

Since the primary purpose of the simulation is to obtain interaction loads between the space station and solar array, a comparison of load histories for the cantilever and free-free beams subjected to a unit step force input at mid-span as shown in Figure 11. Shear force histories at the one-quarter beam span are chosen for these comparisons.

The motion equations for the cantilever beam which are utilized for this perturbation condition are

$$\begin{aligned} M_J \ddot{R}_o + \sum_{i=1}^{J} V_i \left(\frac{L}{2}\right) \ddot{\xi}_{c_i} &= f_{o/2} \\ M_{eq_i} \ddot{\xi}_{c_i} + M_{eq_i} \omega_i^2 \xi_{c_i} + V_i \left(\frac{L}{2}\right) \ddot{R}_o &= 0 \end{aligned} \tag{32}$$

Similarly, the motion equations utilized for the free-free beam are

$$\begin{aligned} 2 M_J \ddot{R}_o &= f_o \\ M_{eq_i} \ddot{\xi}_{s_i} + M_{eq_i} \omega_i^2 \xi_{s_i} &= \Phi_{s_i}(\mathfrak{L}) f_o \end{aligned} \tag{33}$$

Figure 13 presents a comparison of the shear histories obtained by using the simulation with one cantilever mode and one free-free mode in Equations (32) and (33), respectively. An Adams numerical integration method is used to obtain the solution of the motion histories given by the above motion equations for the free-free beam and both the modal acceleration and model displacement methods are used for the shear force evaluations. Numerical coefficients of the motion equation are derived from the tabulations given in Reference 14. Comparison of the shear force history produced by the simulation with the fundamental cantilever mode is seen to be in excellent agreement with that produced by one free-free mode. Minor differences in force magnitude are observable between the two methods of force calculation. Simulation results for this forced response condition are also compared with the results obtained by the NASTRAN Direct Transient Response Method (Reference 7). These histories are presented in Figure 14 and results reflect the use of the first five cantilever modes for each of two flexible appendages (beams). The free-free uniform beam used in NASTRAN is represented by 40 discrete masses, each having two structural degrees of freedom (one translational and one rotational). No modal damping is considered in the presented response solutions. In general, good agreement exists between the frequency content and magnitude of shear history obtained by the two methods. Higher frequency transients, however, exist in the NASTRAN solution which are due to the inherent representation of all beam modes.

The above comparisons indicate that the modal synthesis method is adequate for the determination of dynamic response solutions. It is also indicated that a sufficient number of modal coordinates must be used to accurately describe the basic parameters of the given response condition. For a complex structural arrangement, this might necessitate an iteration in the number of modes used for obtaining an accurate response solution.

Additional qualifications of the modal synthesization method are indicated by the numerical analysis results provided below. The analysis is presented to show that the numerical solutions can be very dependent upon the number of cantilever modes used to represent the flexible appendage. Again, a uniform cantilever beam having the same numerical properties as previously described and constrained to rigid body translation in one plane is utilized. A rigid center mass between the two cantilevers is utilized and assigned a mass of five slugs. The motion equations for this structural system are the same as Equations (32) and (33) except that a center body mass M_S must be added to the total mass of the appendages M_J. Simultaneous solution of Equations (32) and(33) for the coordinate accelerations at zero simulation time for an applied step force on the center body yields the following.

$$\ddot{\xi}_{c_i}(t=0) = \frac{V_i f_o}{M_{eq_i} Q} \tag{34}$$

$$\ddot{R}_o(t=0) = f_o/Q \tag{35}$$

$$Q = \left[(M_S + M_J) - \sum_{i=1}^{J} \left(\frac{V_i^2}{M_{eq_i}} \right) \right] \tag{36}$$

From the free body diagram shown in Figure 15, the interaction forces and torques are

$$F_{FA_1} = f_o - M_S \ddot{X} = M_J \ddot{X} + \sum_{i=1}^{J} V_i \ddot{\xi}_{c_i} \tag{37}$$

$$T_{FA_1} = M_J \frac{L}{2} \ddot{X} + \sum_{i=1}^{J} \beta_i L V_i \ddot{\xi}_{c_i} \tag{38}$$

where $\beta_i L$ is defined as the ratio of modal moment and modal shear coefficients of the i^{th} mode.

$$\beta_i L = \frac{M_i}{V_i} \tag{39}$$

The transient interaction forces and torques at any solution time are dependent upon the number of finite modes utilized, and the steady-state portion of force and torque is exactly represented. To demonstrate a step forcing function with a finite number of cantilever appendage modes and an expected solution with an infinite mode usage, Table 2 is presented. Contained are the numerical values of interaction force coefficients, modal mass and modal participation factors for the first six modes of a five slug mass uniform beam, 10 feet in length, and a designated fundamental cantilever frequency of 2Hz. Modal participation is defined as that contribution of steady state moment and/or force provided by that mode in its statically deflected shape. The use of an infinite number of modes gives 100% modal participation in exactly defining the static loads. The accumulated percentage with number of modes utilized is shown in Figure 16. The numerical values presented are derived from the tabularized data given in Reference 14. Table 3 presents the initial forces and torques produced by both the analytical solution and the digital simulation for a finite number of utilized modes and the solution which would be given by an infinite number of modes. A comparison of numerical values shows significant differences do exist with the finite mode approximation and that interaction loads at zero time will always have an initial finite value rather than zero. This initial force value is also seen to be dependent upon structural position since in the results given in Figure 14, for shear force at the quarter span, an unobservable initial value is indicated. The above numerical data and comparisons show that the modal synthesis method represents an approximation of the transient response interaction forces, and the magnitude of the approximation can be evaluated in terms of the number of modes utilized in the solution. In addition, the percentage accumulation of modal participation factor can be a measure of this approximation. It is generally concluded that in most engineering applications, the synthesization method is a satisfactory method if a sufficient choice and number of modes are utilized.

To further substantiate the structural dynamics methodology and simulation verification, a simple arrangement of uniform beams in a planar "T"

orientation is analyzed. This arrangement is representative of a flexible space station and two flexible appendages (solar arrays) as depicted in Figure 17. Stiffness and mass properties of each beam are chosen so that the center member has an uncoupled fundamental free-free axial mode frequency of 1 Hz and each of the appendage beams have an uncoupled fundamental cantilever bending frequency of 1 Hz. The structural system is perturbed by a unit step force as shown. Several methods of obtaining interaction moment solutions of the formulated problem are used and compared with the simulation. These solutions are presented in Figure 18. Modal solutions of the structural arrangement considered as a system were obtained by the transient response solution method provided in Reference 7. One rigid body translational degree of freedom and the first four elastic modes are used. The results for both the modal displacement and modal acceleration methods of load calculation are shown. A solution of interaction moment produced by a coupled system response, as given by the direct transient response method of NASTRAN, is also presented. The finite element model of the "T" beam is represented by a total of 79 discrete mass points and complete description of this modal and system mode results are given in Reference 2. The interaction moment of the "T" beam given by the simulation reflects the use of the first 10 free-free axial deflection modes of the center body and the first two cantilever modes of the appendages. Modal input for these substructures were obtained by the NASTRAN program. The results obtained by all of the methods compare very well and show the adequacy of the methodology.

Solutions to a simple problem are also presented for a spinning body representing the artificial "G" condition and an independent method. This problem was formulated for the purpose of providing a verification of the simulation. The configuration consists of the rotating mass appendage, shown in Figure 19, elastically attached to a spinning and infinitely large central mass. The central mass is allowed perturbed translational motion only. Motion equations for the appendage mass are derived on the basis of being attached to an infinite mass foundation undergoing accelerated motion and are given below.

$$\begin{bmatrix} M_1 & \\ & M_1 \end{bmatrix} \begin{Bmatrix} \ddot{U}_1 \\ \ddot{U}_2 \end{Bmatrix} + \begin{bmatrix} 0 & -2M_1\,\omega_s \\ 2M_1\,\omega_s & 0 \end{bmatrix} \begin{Bmatrix} \dot{U}_1 \\ \dot{U}_2 \end{Bmatrix}$$

$$+ \begin{bmatrix} AE/r_1 - M_1\,\omega_s^2 & \\ 0 & \dfrac{12EI}{r_1^3} - M_1\,\omega_s^2 \end{bmatrix} \begin{Bmatrix} U_1 \\ U_2 \end{Bmatrix} = \begin{Bmatrix} 0 \\ -M_1\ddot{R}_{o_2} \end{Bmatrix} \quad (40)$$

Solutions to these equations are obtained by use of a digital program and interaction loads are given in Figure 19. A solution to this problem was also obtained by the artificial "G" simulation using a large magnitude mass for the central body. Orthogonal coordinates were initially defined by the method of Reference 6 for input to the simulation. A step force is applied to the central mass to duplicate the value of "$\ddot{R}_{o_2}$" used in the formulation. Resulting interactions loads obtained by the simulation duplicated those obtained by simultaneous solution of Equation (40).

SIMULATION WITH SPACE STATION-SOLAR ARRAY CONFIGURATIONS

The applications of the simulation with various space station and solar array configurations is performed to demonstrate the effect of system parameters upon interaction loads and system response. Present design concepts of the solar array and space station are utilized and consist of a modular-type space station and a rollup solar array. The results of independent configuration studies of these type of structural systems are given in References 12 and 15. Figures 20 and 21 present configuration details of the space station and solar array concepts, respectively. Geometrical sizes of the 1/2 array wing section shown in Figure 21 correspond to an electrical power output of 10 watts per square foot. In a zero "G" configuration, each wing is comprised of a series of 10 flexible substrates deployed with an extendible center boom. Each strip is attached to the inner boom assembly by a linear spring and tensioned to 12 pounds. A guy wire is provided between the outboard end of the extendible boom and the extremity of the inner boom as a tension carrying member. Pertinent stiffness and mass data for the array components are given in Table 4. During a proposed artificial "G" mode of operation only, the two substrate strips on each side of the center boom are deployed. A complete array configuration in an artificial "G" environment is shown in Reference 2.

The space station configuration is comprised of a series of modules which can be assembled in "cruciform" and "bar bell" arrangements. These modules can be considered as part of the total station structural system or as attached flexible appendages to that system. A power boom is also part of the space station and provides the structural support for the solar arrays. Detailed stiffness properties of the space station modules and power boom are shown in Figure 22. Mass properties of these structures are taken to be uniform.

Structural Analyses

Analysis of the space station was required to be performed to obtain the basic structural mode parameters for input to the simulation. Finite element models of both the solar array and space station structures were derived for this purpose. The automated method of finite element structural analysis given by Reference 4 was used for these modal definitions. The finite element models are depicted in Figures 23 and 24 and utilize discrete mass and stiffness data based upon the properties contained in Table 4 and Figures 20 and 22. For the space station, each discrete point is allowed three translational degrees-of-freedom and one rotational degree-of-freedom corresponding to module torsion. Shear flexibility is considered because of the relatively small length to diameter ratio (3) of each module. A complete set of free-free modal data for the configuration as obtained by NASTRAN is given in Reference 2 and a partial list is included in Table 5. It is to be noted that joint flexibility has not been considered in these analyses. The analysis predicts the lowest space station frequency to be 1.57 Hz and this fundamental mode is described by core module torsion with the appendages acting as rigid bodies. (See Figure 25). In addition to the modal analysis of the space station, modal extraction was performed for the cantilever attached module and the core-power boom structure alone, as a free-body, for subsequent use in the simulation. Detail results are presented in Reference 2 and a tabular summary of modal data are given in Table 5.

The vibration properties of the solar array are obtained with only the inherent tension load providing stiffness to each membrane strip. The effect of the compression load upon bending stiffness of the central boom is accounted for in the stiffness matrix. However, the beam columning has only a small effect upon the array frequencies for the configuration investigated. It is to be noted that the beam columning effects should be a necessary consideration in rollup array configuration design analyses since the structural system frequency cannot be simply increased by increasing membrane tension forces without considering frequency reduction effects produced by beam columning. Descriptions of the membrane and boom sfiffness properties are depicted in Figures 22 and 26. Initial structural models which were

analysed and presented in Reference 2 utilized the membrane analogy for the specification of the out-of-plane stiffness matrix (Figure 26). However, subsequent modal extraction produced sets of membrane twisting modes which were self-equilibrating and produced only small constraint forces at the root of the array. Therefore, length 1_2 of the membrane element (Figure 26) was set equal to zero for purposes of defining the stiffness. In this case, the matrix reduces to a 2 x 2.

The inplane stiffness descriptions of tensioned membrane substrates have been found to be non-linear and dependent upon rollup mechanism and structural design details. For example, vibration testing of the blanket array described in Reference 16 exhibited the non-linearity of membrane buckling. Due to the lack of analysis and supporting test data the inplane stiffness properties were assumed to be the same as the out-of-plane properties.

For purposes of optimizing computer execution time, in the modal extraction analysis, summetry properties of the array are utilized. Specifically, four different boundary conditions are considered for the extendible boom nodes shown in Figure 24 to produce the following modal deflection characteristics:

- Out-of-Plane Symmetric Bending
- Out-of-Plane Antisymmetric Bending
- In-plane Symmetric Bending
- In-plane Antisymmetric Bending

For example, the out-of-plane symmetric bending motion is obtained by rigidly constraining the nodes along the boom in the "Y" translation, "X" translation and rotation about the "X" axis. Modal properties from the rollup array are characterized by sets of almost numerically equal frequency modes representing individual but similar modal motions of each array membrane strip. This is readily observable by the detailed tabular listings of modal data presented in Reference 2. Most of these modes represent internal structural loads that are self-equilibrating; i.e., they do not represent a significant load reaction to space station/array interface. Also, they will not be perturbed by accelerated motions at the interface since the resulting

Simulations

Simulations are performed with several space station and array structural configurations fixed in inertial space. Results from these simulations are described and interpreted in the following paragraphs. The configurations utilized in the simulations consist of the Zero "G" space station shown in Figure 20, the core module and power boom combination, a cantilever space station module, a cantilever solar array and a cantilever uniform beam representing basic solar array modal properties. In all simulations the plane of the solar array is positioned in the space station "X-Z" plane and the axis of symmetry is normal to the space station X axis. The uniform beam structure is utilized to perform response analysis with NASTRAN and to provide comparisons with simulation results. A symmetrical triangular force pulse shape is used as an externally applied force history to excite structural motions and this shape was chosen to be representative of a docking force. The direction of force application is designated by the "X", "Y" or "Z" subscript and is referenced to space station axes.

Several simulation solutions were obtained with the space station configuration consisting of the core and power boom with the two attached uniform beams, and inoperative control systems. Solutions for the same condition were also obtained by the "Direct Transient Response Method" of NASTRAN. The beam fundamental mode and mass distribution properties were chosen so as to approximately represent the corresponding properties of the rollup array. Figure 30 presents simulation and NASTRAN interaction load solutions for this structural combination forced by the triangular pulse. Each of the appendage and core boom structures was discretized into ten masses for NASTRAN analysis purposes. It is observed that a high frequency transient, representing the core boom frequency, exists in the simulation solution, but not in the NASTRAN solution. The reasons for this difference in wave form is attributed to the finite number of core-power boom and beam modes used in the simulation analysis. The NASTRAN solution, which is performed in discrete coordinates, does not represent modal truncation,

analysed and presented in Reference 2 utilized the membrane analogy for the specification of the out-of-plane stiffness matrix (Figure 26). However, subsequent modal extraction produced sets of membrane twisting modes which were self-equilibrating and produced only small constraint forces at the root of the array. Therefore, length 1_2 of the membrane element (Figure 26) was set equal to zero for purposes of defining the stiffness. In this case, the matrix reduces to a 2 x 2.

The inplane stiffness descriptions of tensioned membrane substrates have been found to be non-linear and dependent upon rollup mechanism and structural design details. For example, vibration testing of the blanket array described in Reference 16 exhibited the non-linearity of membrane buckling. Due to the lack of analysis and supporting test data the inplane stiffness properties were assumed to be the same as the out-of-plane properties.

For purposes of optimizing computer execution time, in the modal extraction analysis, summetry properties of the array are utilized. Specifically, four different boundary conditions are considered for the extendible boom nodes shown in Figure 24 to produce the following modal deflection characteristics:

- Out-of-Plane Symmetric Bending
- Out-of-Plane Antisymmetric Bending
- In-plane Symmetric Bending
- In-plane Antisymmetric Bending

For example, the out-of-plane symmetric bending motion is obtained by rigidly constraining the nodes along the boom in the "Y" translation, "X" translation and rotation about the "X" axis. Modal properties from the rollup array are characterized by sets of almost numerically equal frequency modes representing individual but similar modal motions of each array membrane strip. This is readily observable by the detailed tabular listings of modal data presented in Reference 2. Most of these modes represent internal structural loads that are self-equilibrating; i.e., they do not represent a significant load reaction to space station/array interface. Also, they will not be perturbed by accelerated motions at the interface since the resulting

generalized forces are small. Therefore, a criterion was established for the specific modes which would contribute to significant interaction loads. This criterion was to select modes which contain the highest modal participation of interaction load. The modes selected by this criterion are listed in Table 6 in terms of mode number from the lowest frequency, frequency and the numerical evaluated modal participation factors. It is noted that the participation factors are described for each type of constraint produced by the boundary conditions. For example, a symmetric out-of-plane mode requires both a root moment and force constraint while an out-of-plane antisymmetric modes requires only a moment constraint. The resulting array fundamental frequencies produced are less than 0.1 Hz, with the exception of the fundamental inplane symmetric mode which is greater than 1 Hz. These primary cantilever modes, will probably lie within the control system frequency bandwidth of space station control system. The frequency and generalized mass modal parameters together with the modal deflections at each mass point are required as input to the digital simulation. Examples of the modal deflection results in a vector format are shown in Figure 27 and 28 and correspond to the significant modes of out-of-plane symmetric and inplane antisymmetric motions. Reference 2 also presents analysis results of a fold-out array which is sized to meet the same power requirements as the presented rollup array. The design is based upon a fold-out array concept presented in Reference 18. Although the stiffness of a fold-out panel array might be thought to be inherently greater than the rollup array structure, weight minimization in the design resulted in significantly lower structural frequencies than shown in Table 6. For example, a fundamental out-of-plane symmetric mode frequency of 0.034 Hz resulted. A weight comparison between the two arrays in 2930 lbs. per wing panel of the rollup array and 6100 lbs. for the fold-out panel array. The fold-out panel array modal characteristics are not presented since the influence of array flexibility upon dynamic interactions can be shown with the rollup array structure.

As part of the evaluation of modal data and its influence upon dynamic interactions, the artificial "G" array configuration is also analyzed for various spin rates. The array configuration considered only includes four array membrane strips

per wing and the finite element model utilized is presented in Figure 29. The digital program used for this vibration analysis is presented in Reference 6. The programmed method requires the input of the mass, coriolis force, and stiffness matrices, the latter containing the effects of the steady spin rate. Complete matrix derivations for the spinning structure are provided in Reference 7. Eigenvalues and eigenvectors producing the orthogonalization are complex quantities and occur in complex conjugate pairs. Resulting modal frequencies from the application of this digital method are presented in Table 7 for a variation in spin rates about an axis paralleled to the "Z" axis and displaced along the "Y" axis, 44 feet from the root of the array. A complete set of modal results from this analysis is given in Reference 2. A comparison is also presented for results obtained by the "GIVENS" eigenvalue-eigenvector operational method in NASTRAN at zero rate of spin. The comparison indicates good frequency correlation except for the fundamental frequency. The separation noted in the lower mode frequency might be explained by the numerical roundoff occurring in the matrix manipulations required by NASTRAN prior to the use of the "GIVENS" routine. The frequency variation with spin rate in Table 7 shows the independence of the out-of-plane modes upon spin. This is expected since coriolis and centrifugal forces do couple with the out-of-plane inertial degrees-of-freedom. In contrast, the inplane modal frequencies are seen to decrease with increasing spin rate and this is of significance for the fundamental inplane mode. This frequency decrease is also exhibited for the case of the spinning beam presented in Reference 7. It may be concluded from the results of this array configuration that the effects of spin rate upon the structural mode properties can be of significance and should be considered in structural dynamic analyses.

Simulations

Simulations are performed with several space station and array structural configurations fixed in inertial space. Results from these simulations are described and interpreted in the following paragraphs. The configurations utilized in the simulations consist of the Zero "G" space station shown in Figure 20, the core module and power boom combination, a cantilever space station module, a cantilever solar array and a cantilever uniform beam representing basic solar array modal properties. In all simulations the plane of the solar array is positioned in the space station "X-Z" plane and the axis of symmetry is normal to the space station X axis. The uniform beam structure is utilized to perform response analysis with NASTRAN and to provide comparisons with simulation results. A symmetrical triangular force pulse shape is used as an externally applied force history to excite structural motions and this shape was chosen to be representative of a docking force. The direction of force application is designated by the "X", "Y" or "Z" subscript and is referenced to space station axes.

Several simulation solutions were obtained with the space station configuration consisting of the core and power boom with the two attached uniform beams, and inoperative control systems. Solutions for the same condition were also obtained by the "Direct Transient Response Method" of NASTRAN. The beam fundamental mode and mass distribution properties were chosen so as to approximately represent the corresponding properties of the rollup array. Figure 30 presents simulation and NASTRAN interaction load solutions for this structural combination forced by the triangular pulse. Each of the appendage and core boom structures was discretized into ten masses for NASTRAN analysis purposes. It is observed that a high frequency transient, representing the core boom frequency, exists in the simulation solution, but not in the NASTRAN solution. The reasons for this difference in wave form is attributed to the finite number of core-power boom and beam modes used in the simulation analysis. The NASTRAN solution, which is performed in discrete coordinates, does not represent modal truncation,

as is employed in the simulation's methodology. The truncation process guarantees less than 100% modal participation and therefore a rigid mass is apparent and exactly follows the perturbing motion, such as the accelerated motion of the central body. The rigid mass effect is also inherent to the results given in Table 3.

The effect on response wave form when using a truncated set of appendage modes, which represent only a portion of the total appendage rigid mass, is better seen from the results provided in Figure 31. A pulse having a period of 1 second is used to perturb a rigid core-power boom with attached rollup arrays and the number of array modes is varied (Table 6, in-plane-antisymmetric modes). The shape of the pulse is obvious in the wave form for those solutions corrresponding to the one and two array mode analysis. The rigid mass effect is therefore more pronounced with the smaller number of modes used and correspondingly, the smaller amount flexible mode participation. The period of the highest frequency mode in the two mode analysis is 5.2 seconds as compared to 3.1 seconds in the four mode analysis. It is also apparent that the waveform is affected by those modes with periods closer to the period of the forcing pulse -- even though the modal participation for those array modes is comparatively small. It may be concluded from these results that the interaction load solution is very dependent upon the number of modes utilized to define the flexibility parameters of the structural system. An automated plot of the four mode analysis solution of interaction "X" direction force and interaction "Y" direction torque is given in Figure 32 for 3 minutes of simulation time. A structural damping coefficient of 0.1% (g) has been used for this solution and is evident from the observable slowing decay peak load amplitude in time.

Interesting solutions from NASTRAN and the simulation are also provided in Figure 33 in which the basic waveforms are comparable and the "high frequency" pulse shape is not observed in the simulation load history. Here the core-power boom structure is taken to be rigid in the simulation and flexible for the NASTRAN solution. It is to be noted that the perturbation pulse is in the "X" direction and bending modes of the appendage are not excited by rotational base motion, but by

translational motions. This is also the case in the forcing condition producing the comparative results shown in Figure 18. In contrast, bending modes of the central body are excited in the simulation results of Figure 30. The magnitude of the higher frequency content of the simulation solution in Figure 30 would therefore be predominant due to the appendage beam base rotational acceleration resulting from the central body modal slopes at the interface point. It can be concluded from the presented solutions that a criterion must be established from known parameters which are to be used in the interactions simulation. This criterion must include considerations of the perturbing force frequency content and its relation with the primary structural mode frequencies and modal properties being simulated. In addition, it would be expected that a sufficient number of modes would be required to encompass the expected frequency content of the interaction load solution. For example, if a triangular pulse is used to excite the central body and has a period of one second, appendage modes with modal frequencies representing periods up to and beyond one second should be utilized unless corresponding modal participation factors are very small. Also the frequency range of appendage modes should encompass the frequency range of central body modes if the latter modal coordinates are expected to be significantly excited by the applied forces.

The variation of interaction load with rigid and flexible space station considerations can be identified by the results presented in Figures 34 and 35. In both sets of solutions with the core-power boom flexibility consideration the fundamental frequency of this body is predominant. Significant response from this mode is expected due to the period of the forcing pulse. Dynamic motion with the rigid core-power boom consideration is only represented by the lower frequency solar array modes. Again the pulse shape is noted in the response history and is due to that portion of the total array mass which is not represented by the modal load participation. Interaction load descriptions by the modal displacement method of load calculation would obviate this inherent high frequency shape, but is not considered as accurate of a method in analysis for the same number of modes.

Modal displacements, such as shown in the simulation solutions presented in Figures 36 and 37 for the indicated pulse forces, do not identify the pulse shape in the initial solution time. These displacement histories are graphically presented by the automated graphical provisions contained in the simulation.

Several simulations with the rollup array and core-power boom structures were performed with considered variations in forcing pulse magnitude and period. Corresponding interaction load solutions are presented in Figures 38 and 39. As expected, the interaction load magnitudes vary linearly with applied force magnitude. The solutions given in Figure 39 also are representative of the classical response solutions; i.e., higher responses occur as the ratio of the pulse period to modal period become closer to 1.0. The interaction load magnitude for the same force pulse is also reduced with an increased central body mass, as is indicated by the interaction load solution history for the zero "G" space station configuration presented in Figure 40. A large reduction in magnitude is noted when comparing this history with that presented in Figure 34 in which rigid body accelerations at the interface are greater. Figure 41 presents the variation of maximum interaction load with space station mass and forcing pulse magnitude. These results can be considered an example of using the simulation for the prediction of solar array design loads when structural system parameters and external perturbation force definitions are known.

Waveform differences in interaction load solution histories for the inplane and out-of-plane array responses are exhibited by the results presented in Figures 42 and 43. Solutions in Figure 42 represent the inplane response of the array and those given in Figure 43 represent array out-of-plane response. For both conditions a higher coupled system frequency produced by the fundamental core-power boom bending mode is predominate. The lower frequency solar array modes are also evident by the low frequency modulation.

The effect of increased space station or central body mass upon the solar array interaction load is seen by the solutions given in Figure 44. Here two

modules have been attached to the space station as flexible appendages in the "X-Z" plane at node point 21. The longitudinal axis of one module is in the "Z" direction and the other in the "-Z" direction. Comparison of maximum solution magnitudes with that given in Figure 33 shows the effect of the reduced inertial acceleration. The high frequency content in the interaction history is due to the high frequency mode of the attached modules. Again the representation of module flexibility by one mode does not produce 100% modal load participation and the pulse shape is predominate in the initial solution time. Interaction load feedback through the central body in terms of accelerated motion at the array frequency is low as evidenced by the absence of low frequency content in the module interaction load history. Figure 45 presents selected interaction load histories for the structural configuration of four attached flexible module appendages, solar arrays and the core-power boom. The consideration of a total of six appendages is the limitation of the simulation. The four modules are all positioned in the "X-Z" plane and normal to the space station or central body "X" axis, and at nodes 21 and 31 depicted in Figure 23.

A simulation is also performed using the zero "G" space station rigid inertial properties with the reaction jet control system. The structural system is given an initial attitude error of 1^{o} and the control system is chosen to be operative for equivalent angular errors above 0.5 degrees as defined by Equation 26. Two thrusters of 200 lbs. magnitude have been positioned along the "X" axis of the space station to produce a maximum of 6000 ft. lbs. of controlling torque. Figure 46 presents the histories of rigid body attitude error, attitude rate and controlling torque. Solar arrays have been arbitrarily omitted as part of the structural system in this condition. These solution histories show the proper operation of the contained reaction jet control system. Solutions of motion and interaction load histories are also obtained by the simulation for the initial array attitude conditions given in Figures 47 and 48. The non-linear orientation control is operative as the array controlling system and the simplified CMG system is considered to be both nonoperative (Figure 47) and operative (Figure 48).

per wing and the finite element model utilized is presented in Figure 29. The digital program used for this vibration analysis is presented in Reference 6. The programmed method requires the input of the mass, coriolis force, and stiffness matrices, the latter containing the effects of the steady spin rate. Complete matrix derivations for the spinning structure are provided in Reference 7. Eigenvalues and eigenvectors producing the orthogonalization are complex quantities and occur in complex conjugate pairs. Resulting modal frequencies from the application of this digital method are presented in Table 7 for a variation in spin rates about an axis paralleled to the "Z" axis and displaced along the "Y" axis, 44 feet from the root of the array. A complete set of modal results from this analysis is given in Reference 2. A comparison is also presented for results obtained by the "GIVENS" eigenvalue-eigenvector operational method in NASTRAN at zero rate of spin. The comparison indicates good frequency correlation except for the fundamental frequency. The separation noted in the lower mode frequency might be explained by the numerical roundoff occurring in the matrix manipulations required by NASTRAN prior to the use of the "GIVENS" routine. The frequency variation with spin rate in Table 7 shows the independence of the out-of-plane modes upon spin. This is expected since coriolis and centrifugal forces do couple with the out-of-plane inertial degrees-of-freedom. In contrast, the inplane modal frequencies are seen to decrease with increasing spin rate and this is of significance for the fundamental inplane mode. This frequency decrease is also exhibited for the case of the spinning beam presented in Reference 7. It may be concluded from the results of this array configuration that the effects of spin rate upon the structural mode properties can be of significance and should be considered in structural dynamic analyses.

Simulations

Simulations are performed with several space station and array structural configurations fixed in inertial space. Results from these simulations are described and interpreted in the following paragraphs. The configurations utilized in the simulations consist of the Zero "G" space station shown in Figure 20, the core module and power boom combination, a cantilever space station module, a cantilever solar array and a cantilever uniform beam representing basic solar array modal properties. In all simulations the plane of the solar array is positioned in the space station "X-Z" plane and the axis of symmetry is normal to the space station X axis. The uniform beam structure is utilized to perform response analysis with NASTRAN and to provide comparisons with simulation results. A symmetrical triangular force pulse shape is used as an externally applied force history to excite structural motions and this shape was chosen to be representative of a docking force. The direction of force application is designated by the "X", "Y" or "Z" subscript and is referenced to space station axes.

Several simulation solutions were obtained with the space station configuration consisting of the core and power boom with the two attached uniform beams, and inoperative control systems. Solutions for the same condition were also obtained by the "Direct Transient Response Method" of NASTRAN. The beam fundamental mode and mass distribution properties were chosen so as to approximately represent the corresponding properties of the rollup array. Figure 30 presents simulation and NASTRAN interaction load solutions for this structural combination forced by the triangular pulse. Each of the appendage and core boom structures was discretized into ten masses for NASTRAN analysis purposes. It is observed that a high frequency transient, representing the core boom frequency, exists in the simulation solution, but not in the NASTRAN solution. The reasons for this difference in wave form is attributed to the finite number of core-power boom and beam modes used in the simulation analysis. The NASTRAN solution, which is performed in discrete coordinates, does not represent modal truncation,

as is employed in the simulation's methodology. The truncation process guarantees less than 100% modal participation and therefore a rigid mass is apparent and exactly follows the perturbing motion, such as the accelerated motion of the central body. The rigid mass effect is also inherent to the results given in Table 3.

The effect on response wave form when using a truncated set of appendage modes, which represent only a portion of the total appendage rigid mass, is better seen from the results provided in Figure 31. A pulse having a period of 1 second is used to perturb a rigid core-power boom with attached rollup arrays and the number of array modes is varied (Table 6, in-plane-antisymmetric modes). The shape of the pulse is obvious in the wave form for those solutions corrresponding to the one and two array mode analysis. The rigid mass effect is therefore more pronounced with the smaller number of modes used and correspondingly, the smaller amount flexible mode participation. The period of the highest frequency mode in the two mode analysis is 5.2 seconds as compared to 3.1 seconds in the four mode analysis. It is also apparent that the waveform is affected by those modes with periods closer to the period of the forcing pulse -- even though the modal participation for those array modes is comparatively small. It may be concluded from these results that the interaction load solution is very dependent upon the number of modes utilized to define the flexibility parameters of the structural system. An automated plot of the four mode analysis solution of interaction "X" direction force and interaction "Y" direction torque is given in Figure 32 for 3 minutes of simulation time. A structural damping coefficient of 0.1% (g) has been used for this solution and is evident from the observable slowing decay peak load amplitude in time.

Interesting solutions from NASTRAN and the simulation are also provided in Figure 33 in which the basic waveforms are comparable and the "high frequency" pulse shape is not observed in the simulation load history. Here the core-power boom structure is taken to be rigid in the simulation and flexible for the NASTRAN solution. It is to be noted that the perturbation pulse is in the "X" direction and bending modes of the appendage are not excited by rotational base motion, but by

translational motions. This is also the case in the forcing condition producing the comparative results shown in Figure 18. In contrast, bending modes of the central body are excited in the simulation results of Figure 30. The magnitude of the higher frequency content of the simulation solution in Figure 30 would therefore be predominant due to the appendage beam base rotational acceleration resulting from the central body modal slopes at the interface point. It can be concluded from the presented solutions that a criterion must be established from known parameters which are to be used in the interactions simulation. This criterion must include considerations of the perturbing force frequency content and its relation with the primary structural mode frequencies and modal properties being simulated. In addition, it would be expected that a sufficient number of modes would be required to encompass the expected frequency content of the interaction load solution. For example, if a triangular pulse is used to excite the central body and has a period of one second, appendage modes with modal frequencies representing periods up to and beyond one second should be utilized unless corresponding modal participation factors are very small. Also the frequency range of appendage modes should encompass the frequency range of central body modes if the latter modal coordinates are expected to be significantly excited by the applied forces.

The variation of interaction load with rigid and flexible space station considerations can be identified by the results presented in Figures 34 and 35. In both sets of solutions with the core-power boom flexibility consideration the fundamental frequency of this body is predominant. Significant response from this mode is expected due to the period of the forcing pulse. Dynamic motion with the rigid core-power boom consideration is only represented by the lower frequency solar array modes. Again the pulse shape is noted in the response history and is due to that portion of the total array mass which is not represented by the modal load participation. Interaction load descriptions by the modal displacement method of load calculation would obviate this inherent high frequency shape, but is not considered as accurate of a method in analysis for the same number of modes.

Modal displacements, such as shown in the simulation solutions presented in Figures 36 and 37 for the indicated pulse forces, do not identify the pulse shape in the initial solution time. These displacement histories are graphically presented by the automated graphical provisions contained in the simulation.

Several simulations with the rollup array and core-power boom structures were performed with considered variations in forcing pulse magnitude and period. Corresponding interaction load solutions are presented in Figures 38 and 39. As expected, the interaction load magnitudes vary linearly with applied force magnitude. The solutions given in Figure 39 also are representative of the classical response solutions; i.e., higher responses occur as the ratio of the pulse period to modal period become closer to 1.0. The interaction load magnitude for the same force pulse is also reduced with an increased central body mass, as is indicated by the interaction load solution history for the zero "G" space station configuration presented in Figure 40. A large reduction in magnitude is noted when comparing this history with that presented in Figure 34 in which rigid body accelerations at the interface are greater. Figure 41 presents the variation of maximum interaction load with space station mass and forcing pulse magnitude. These results can be considered an example of using the simulation for the prediction of solar array design loads when structural system parameters and external perturbation force definitions are known.

Waveform differences in interaction load solution histories for the inplane and out-of-plane array responses are exhibited by the results presented in Figures 42 and 43. Solutions in Figure 42 represent the inplane response of the array and those given in Figure 43 represent array out-of-plane response. For both conditions a higher coupled system frequency produced by the fundamental core-power boom bending mode is predominate. The lower frequency solar array modes are also evident by the low frequency modulation.

The effect of increased space station or central body mass upon the solar array interaction load is seen by the solutions given in Figure 44. Here two

modules have been attached to the space station as flexible appendages in the "X-Z" plane at node point 21. The longitudinal axis of one module is in the "Z" direction and the other in the "-Z" direction. Comparison of maximum solution magnitudes with that given in Figure 33 shows the effect of the reduced inertial acceleration. The high frequency content in the interaction history is due to the high frequency mode of the attached modules. Again the representation of module flexibility by one mode does not produce 100% modal load participation and the pulse shape is predominate in the initial solution time. Interaction load feedback through the central body in terms of accelerated motion at the array frequency is low as evidenced by the absence of low frequency content in the module interaction load history. Figure 45 presents selected interaction load histories for the structural configuration of four attached flexible module appendages, solar arrays and the core-power boom. The consideration of a total of six appendages is the limitation of the simulation. The four modules are all positioned in the "X-Z" plane and normal to the space station or central body "X" axis, and at nodes 21 and 31 depicted in Figure 23.

A simulation is also performed using the zero "G" space station rigid inertial properties with the reaction jet control system. The structural system is given an initial attitude error of 1^{o} and the control system is chosen to be operative for equivalent angular errors above 0.5 degrees as defined by Equation 26. Two thrusters of 200 lbs. magnitude have been positioned along the "X" axis of the space station to produce a maximum of 6000 ft. lbs. of controlling torque. Figure 46 presents the histories of rigid body attitude error, attitude rate and controlling torque. Solar arrays have been arbitrarily omitted as part of the structural system in this condition. These solution histories show the proper operation of the contained reaction jet control system. Solutions of motion and interaction load histories are also obtained by the simulation for the initial array attitude conditions given in Figures 47 and 48. The non-linear orientation control is operative as the array controlling system and the simplified CMG system is considered to be both nonoperative (Figure 47) and operative (Figure 48).

A limiting CMG controlling torque is arbitrarily chosen to be 1000 ft lbs when simulated, and the solar array is given an initial attitude error about the space station "X" axis. The resulting history of attitude error and error rate is similar to that presented in Reference 15. The change in slope of the attitude error history at zero degrees is due to the loss of controlling torque and the application of friction torque. The error history of the space station in Figure 47 appears to be divergent, but is only the result of the reactive torque. The application of the array control torque produces the interaction torque history shown. In addition, the coupling of the transient array response is evident in the array and space station rigid body motions. The control of space station attitude with the simplified CMG system produces the attitude oscillations shown in Figure 48 and this is attributed to the system coupling with the flexible dynamics of the solar array. The oscillation becomes relatively large when the array controlling torque is removed and friction torque begins reducing the array angular rate. A simulation in which only the rigid body properties of the array and space station are considered, show the flexibility effects cause a 40% increase in interaction torque. A variation of one control system parameter, K (Figure 9), was made for this simulated condition and results are presented in Figure 49 in terms of the maximum interaction torque and space station attitide error experienced in a 100 second period. Parameter variations of this type, demonstrate the reduction in response that can be obtained and also the sensitivity of the maximum response to these parameters. No attempt was made in simulating this condition with other attitude or orientation control parameters which are user input. These parameters are those coefficients listed in Figure 8 and 9.

The results for the structural configurations and controlling systems show the analytical flexibility of the simulation and its use as a design tool. It is concluded from the interpretation of solutions that care must be taken in the formulation of the response condition with the modal synthesis technique. Sufficient and important structural modes must be utilized for the adequate description of the interactive dynamics and its effect upon system response and interactions.

CONCLUSIONS AND RECOMMENDATIONS

An integrated dynamic analysis method has been developed and implemented in a digital computer program for simulating structural dynamic interactions between a space station and controllable solar arrays. The methodology in the simulation has been verified through the performance of simple response problems and comparison with other solution methods, and the performance of simulations with space station and array structural configurations.

The modal synthesis technique employed in the simulation provides an accurate method of coupling structural components into one integrated system. Care must be taken, however, in the choice and number of structural component modes utilized in the coupling technique.

The use of the modal acceleration method of computing interaction loads and the inherent "rigid mass" which remains after modal truncation can result in appreciable loading magnitudes. This is due to the coupling with transient inertial forces at frequencies higher than the frequency range of modes considered for representing appendage flexibility. This result would not occur with the use of the modal displacement method of load calculation.

Modal frequency comparisons of an array in a non-spinning and spinning environment indicate a decrease in frequency with increase in spin rate; this therefore warrants the consideration of the effect of spin rate upon modal properties in structural dynamic analyses.

From the demonstrated application of the simulation it is recommended that this simulation be utilized as a design tool for use in future spacecraft design studies.

REFERENCES

1. P. W. Likins and H. K. Bouvier, "Attitude Control of Non-rigid Spacecraft," J. Astronautics and Aeronautics, May 1971/Vol. 9 No. 5, Pg. 64-71.

2. "Integrated Dynamic Analysis Simulation of Space Stations with Controllable Solar Arrays, Supplementary Data and Analyses," NASA CR-112145, June 1972.

3. Likins, P. W., "Dynamics and Control of Flexible Space Vehicles," Jet Propulsion Laboratory Technical Report 32-1329, Revision 1, January 1970.

4. "The NASTRAN Theoretical Manual," NASA SP-221, 1970, Office of Technology Utilization, NASA, Washington, D. C.

5. "NASTRAN: Users Experiences," NASA Technical Memorandum NASA TMX-2378, Article No. 25, September 1971.

6. K. K. Gupta, "Free Vibration Analysis of Spinning Structural Systems," International Journal for Numerical Methods in Engineering, to be published.

7. "The NASTRAN Users Manual," NASA SP-222, Sections 3.10 and 3.13, 1970, Office of Technology Utilization, NASA, Washington, D.C.

8. Rosen, R., "Stardyne User's Manual," Mechanical Research, Inc., Document, Los Angeles, California, January 1971.

9. R. L. Bisplinghoff and H. Ashley, Principles of Aeroelasticity, pp. 344-350. John Wiley and Sons, Inc., 1962.

10. R. H. Lyddane, "Small Eccentricities or Inclinations in the Browner Theory of the Artificial Satellite," Astronomical Journal, Vol. 68, No. 8, October 1963, pg. 555.

11. "Preliminary Synthesis and Simulation of the Selected CMG Attitude Control System," General Electric Report EL-506-D, 5 March 1970, General Electric Company, Binghamton, New York.

12. "Modular Space Station - Phase B Extension, First Quarterly Review," North American Rockwell, Space Division, PDS-71-2, May 1971.

13. J. A. Heinrichs, "Integrated Dynamic Analysis of a Space Station, with Controllable Solar Arrays," et al, paper presented at the 42nd Shock and Vibration Symposium.

14. D. Young and R. P. Felgar, Jr., "Tables of Characteristic Functions Representing Normal Modes of Vibration of A Beam," University of Texas Publication No. 4913, 1 July 1949.

15. "Space Station Solar Array Technology Evaluation Program-Design and Analysis," Second Topical Report LMSC-A995719, Lockheed Missile and Space Company, November 1971.

16. "Design and Development of a Thirty Watt per Pound-25 Square Foot Roll-up Subsolar Array," Final Report GE-SSO-71SD4239, General Electric Company, May 20, 1971.

17. "Third Quarterly Report-Large Area Solar Array," The Boeing Company Report No. D2-113355-3, July 1967.

Frequency Ratios: f_n/f_1 free-free

Reference Frequency Ratios (Ref. 14)			Coupled Mode Frequency Ratios				
Symmetric Mode No. n	Free-Free Beam	Uncoupled Cantilever Beam	1 Cantilever + Rigid Body Coordinates	2 Cantilever + Rigid Body Coordinates	3 Cantilever + Rigid Body Coordinates	4 Cantilever + Rigid Body Coordinates	5 Cantilever + Rigid Body Coordinates
1	1.000	0.632	1.0101	1.0006	1.0003	1.0000	1.0000
2	5.404	3.958	-	5.548	5.420	5.408	5.405
3	13.344	11.074	-	-	13.749	13.410	13.367
4	24.814	21.652	-	-	-	25.584	24.965
5	39.812	35.861	-	-	-	-	41.030

TABLE 1. FREQUENCY COMPARISONS OF CANTILEVER + RIGID BODY MODE REPRESENTATIONS OF A FREE BEAM

Mode No. i	f_i (Hz)	V_i (Slugs)	Meq_i (Slugs)	$\frac{V_i^2}{Meq_i}$ (Slugs)	$MPF_i = \frac{V_i^2}{M_J Meq_i}$
1	2	1.957479	1.25	3.06538	0.6131
2	12.5338	-1.084840	1.25	0.941502	0.1883
3	35.0950	0.636063	1.25	0.323661	0.0647
4	68.7721	-0.454745	1.25	0.165434	0.0331
5	113.6852	0.353677	1.25	0.100070	0.0200
$\sum_{n=1}^{5}$	Q = 10 - 4.59605 =		5.40395	4.59605	0.919209
		Residual =		(0.40395)	(0.080191)
6	169.67	0.289373	1.25	0.066989	0.013398
$\sum_{n=1}^{6}$				4.66304	0.932607
		Residual =		(0.33696)	(0.067393)

Beam Properties - M_J = 5 Slugs, L = 10 Feet

$$\lim_{m \to \infty} \sum_{i=1}^{m} \frac{V_i^2}{Meq_i} = M_J = 5.0$$

$$\lim_{m \to \infty} \sum_{i=1}^{m} MPF_i = 1.0$$

TABLE 2 . CANTILEVER BEAM - NUMERICAL MODE DATA

PARAMETERS	FIRST 5 MODES	LIM $n \longrightarrow \infty$
$\ddot{\xi}_1(0)$ $Ft/_{Sec}$	-2.90	-3.13
$\ddot{\xi}_2(0)$	+1.62	+1.75
$\ddot{\xi}_3(0)$	-0.928	-1.00
$\ddot{\xi}_4(0)$	+0.679	+0.740
$\ddot{\xi}_5(0)$	-0.517	-0.560
$\ddot{\xi}_n(0)$	$-1.48\left(\frac{Vn}{\omega_n^2}\right)$	$-1.6\left(\frac{Vn}{\omega_n^2}\right)$
$\ddot{X}(0)$	1.85	2.00
$F_{FA}(0)$ LBS	0.736	0
$T_{FA}(0)$ Ft Lbs	0.215	0
First Mode Only		
$F_{FA}(0)$ Lbs	2.79	0
$T_{FA}(0)$ Ft Lbs	3.95	0

TABLE 3. TIME ZERO MODAL SOLUTIONS

MEMBER	AE (lbs.)	EI_X* (lb-in.^{2})	EI_Y* (lb.-in.^{2})	EI_Z* (lb.-in.^{2})	GJ (lb-in.^{2})	RUNNING WEIGHT (lbs/in.)
Extendible Boom (Full)	22.4×10^6		2.8×10^8	2.8×10^8		.212
Outer Support	10.4×10^6 (Y=0 to 72) 5.9×10^6 (Y=72 to 369)	9.3×10^8		3.32×10^8 (Y=0 to72) 1.87×10^8 (Y=72 to 369)	26.8×10^6	.130
Inner Support	5.9×10^6	9.3×10^8		1.87×10^8	26.8×10^6	.115
Membrane Strip	3.33 lb/in.					.2
Guy Wire	$.203 \times 10^6$					

* - For axis system, refer to Figure 21.

TABLE 4. STIFFNESS AND MASS PROPERTIES-ROLLUP SOLAR ARRAY

SPACE STATION CONFIGURATION (FIGURE 20)			
MODE NO.	FREQUENCY (Hz)	GENERALIZED MASS ($LB\text{-}SEC^2/IN.$)	MODAL DESCRIPTION
1	1.57	230	CORE TORSION
2	2.28	36.4	CORE MODULE "Y" AXIS BENDING
3	2.28	36.6	CORE MODULE "Z" AXIS BENDING
4	3.15	87.7	CORE MODULE "Z" AXIS BENDING
5	3.25	109	CORE MODULE "Y" AXIS BENDING
6	4.39	151	CORE MODULE "Y" AXIS BENDING
7	4.48	312	CORE MODULE "Z" AXIS BENDING
CANTILEVER SPACE STATION MODULE			
1	8.48	25.3	FUNDAMENTAL "Y" AXIS BENDING
2	8.48	25.3	FUNDAMENTAL "X" AXIS BENDING
3	34.27	$1.12(10^5)$*	TORSION
* units of $lb\text{-}in\text{-}sec^2$			
FREE-FREE CORE MODULE-POWER BOOM			
1	5.64	18.2	"Z" AXIS BENDING
2	5.64	18.2	"Y" AXIS BENDING
3	13.1	36.7	"Z" AXIS BENDING
4	13.1	36.7	"Y" AXIS BENDING

TABLE 5. SPACE STATION MODAL DATA SUMMARIES

DIRECTION	CONSTRAINT	MODE NO.	FREQUENCY (Hz)	GENERALIZED MASS (LB-SEC^2/IN.)	MODAL PARTICIPATION FACTOR		
					FORCE	BENDING MOMENT	TORQUE
OUT OF PLANE	SYMMETRIC	1	.0925	1.36	.681	.415	
		6	.087	1.30	.003	.044	
		22	.835	.158	.119	.001	
	ANTI-SYMMETRIC	1	.0640	.609			.779
		6	.167	.547			.074
		11	.241	.689			.078
IN PLANE	SYMMETRIC	26	1.35	.705	.520		
		27	3.28	.770	.165		
		28	3.49	.607	.058		
		31	6.07	.104	.062		
	ANTI-SYMMETRIC	1	.0974	1.35	.712	.514	
		6	.189	1.41	.001	.137	
		11	.265	1.46	.077	.105	
		16	.324	1.83	.055	.084	

TABLE 6. ROLLUP SOLAR ARRAY MODAL DATA

ELASTIC MODE NO.	NASTRAN RESULTS $\Omega = 0$	"GUPTA" PROGRAM RESULTS			
		$\Omega = 0$	$\Omega = 4$ RPM	$\Omega = 8$ RPM	$\Omega = 12$ RPM
1	0.1989	0.1786	0.1786	0.1787	0.1787
2	0.2032	0.1977	0.1977	0.1977	0.1977
3	0.3784	0.3768	0.3710	0.3524	0.3185
9	0.5037	0.5031	0.5025	0.5025	0.5025
10	0.5215	0.5142	0.5151	0.5151	0.5151
11	0.7045	0.7010	0.6969	0.6881	0.6716
17	0.7782	0.7774	0.7777	0.7777	0.7777
18	0.7941	0.7912	0.7911	0.7911	0.7911
19	0.9051	0.9047	0.9049	0.9049	0.9049
20	0.9349	0.9315	0.9291	0.9224	0.9090
28	1.0654	1.0544	1.0506	1.0454	1.0331
32	3.8422	3.8402	3.8413	3.8441	3.8462

OUT-OF-PLANE MODES 1, 2, 9, 10, 17, 18, 19

IN-PLANE MODES 3, 11, 20, 28, 32

TABLE 7. ART "G" SOLAR ARRAY CONFIGURATION LIST OF EIGENVALUES IN HERTZ

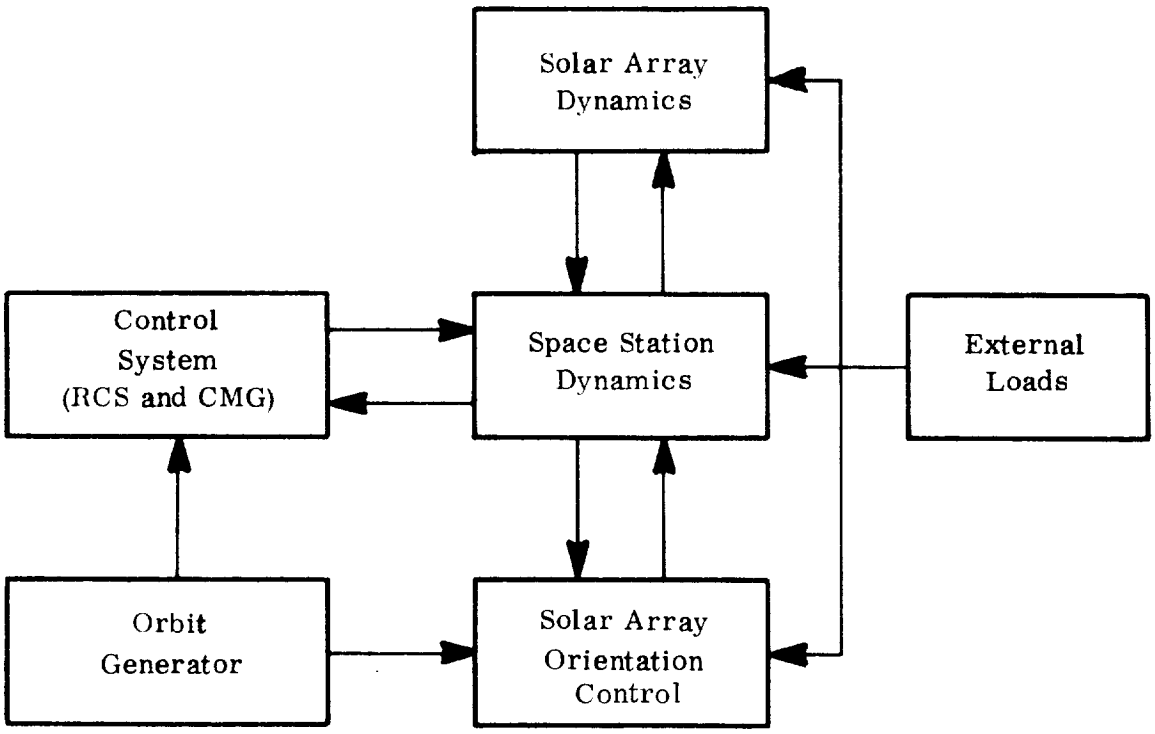

FIGURE 1. ANALYSIS CONSIDERATIONS

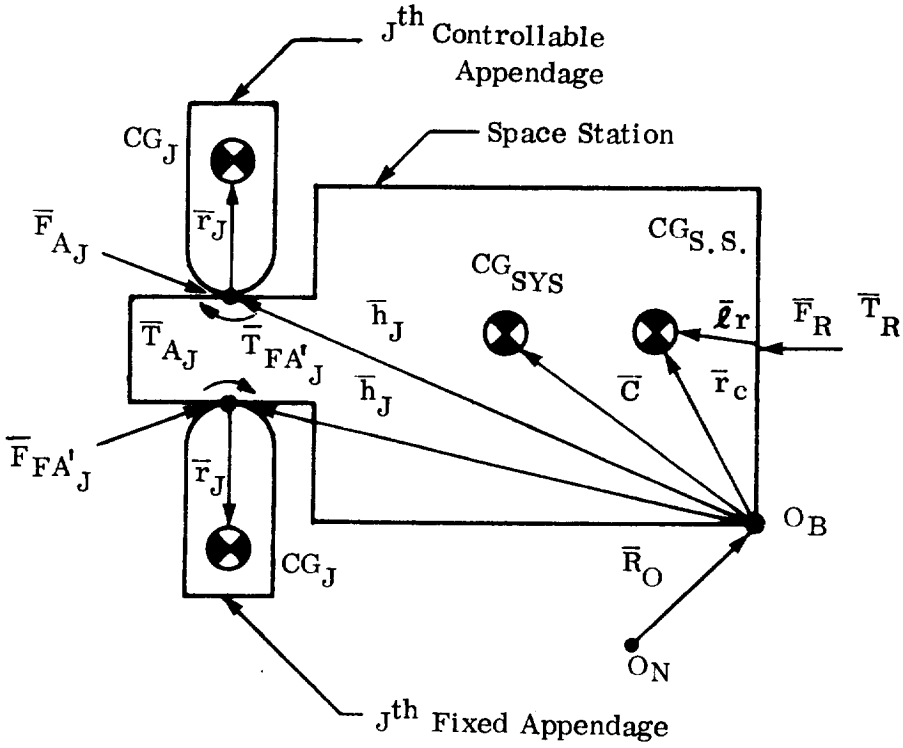

FIGURE 2. RIGID BODY COORDINATES

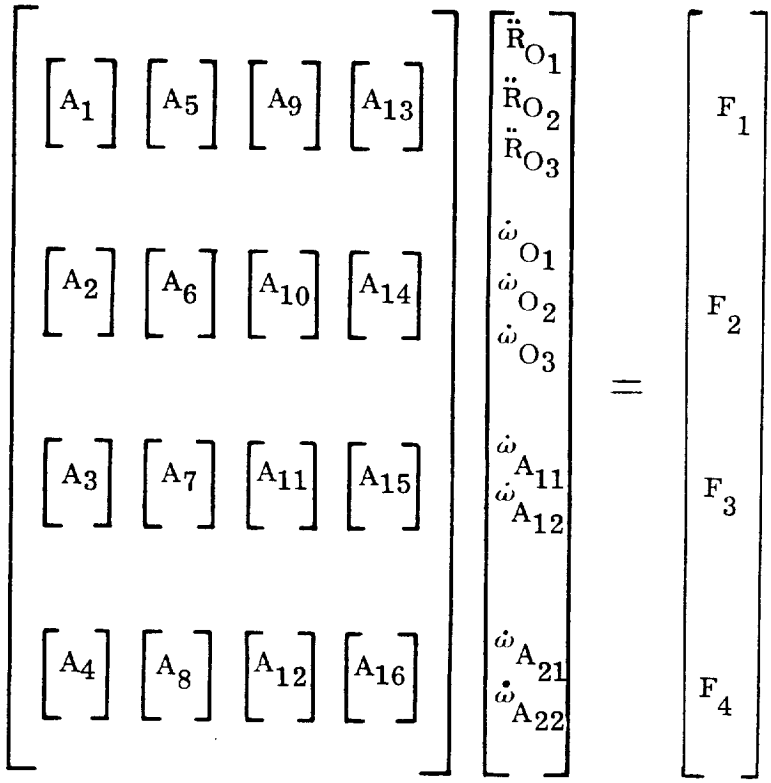

FIGURE 3. RIGID BODY MATRIX EQUATIONS

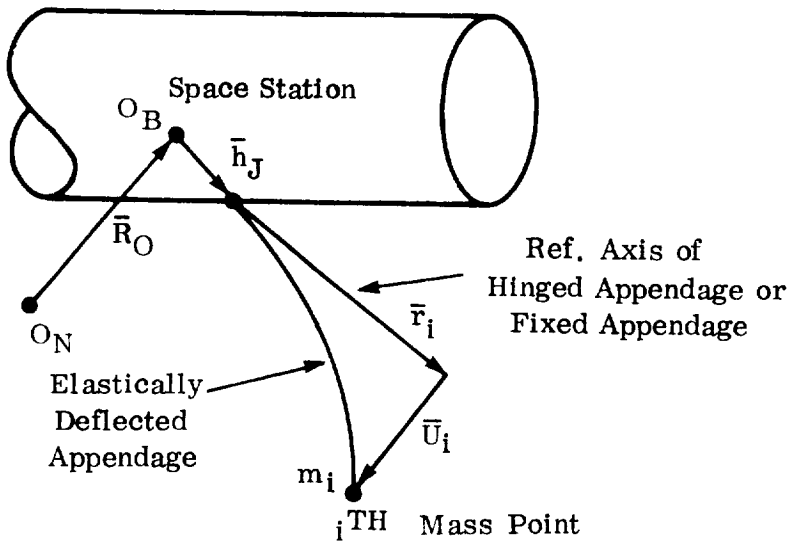

FIGURE 4. FLEXIBLE APPENDAGE COORDINATES

FORCE EQUATION

$$\bar{F}_{A_J} = -M_J \Big[\ddot{R}_o + 2\tilde{\omega}_o \dot{\bar{R}}_o + (\dot{\tilde{\omega}}_o + \tilde{\omega}_o \tilde{\omega}_o)(\bar{R}_o + \bar{h}_J + C_J \bar{r}_J)$$

$$+ 2\tilde{\omega}_o C_J \tilde{\omega}_J \bar{r}_J + C_J (\dot{\tilde{\omega}}_J + \tilde{\omega}_J \tilde{\omega}_J) \bar{r}_J \Big] \Bigg\} \bar{\bar{F}}'_{A_J}$$

$$-M_J \Big[\Phi_{S,J} - (C_J \tilde{r}_J) \Phi'_{S,J} \Big] \{\ddot{\xi}_s\}$$

$$-C_J \sum_E^T M_{iJ} \Phi_J \{\ddot{\xi}_c\}_J \Bigg\} \bar{\bar{F}}'_{A_J}$$

MOMENT EQUATION

$$\bar{T}_{A_J} = -C_J \Big[(C_J^T \widetilde{\omega_o + \omega_J}) \bar{I}_J (\bar{\omega}_J + C_J^T \bar{\omega}_o)$$

$$+ \bar{I}_J (\dot{\bar{\omega}}_J + C_J^T \dot{\bar{\omega}}_o + C_J^T \tilde{\omega}_o C_J \bar{\omega}_J) \Big]$$

$$+ (C_J \tilde{r}_J) \bar{\bar{F}}'_{A_J}$$

$$- C_J \bar{I}_J C_J^T \Phi'_{S,J} \{\ddot{\xi}_s\}$$

$$-C_J \sum_E^T \bar{r}_{iJ} M_{iJ} \Phi_J \{\ddot{\xi}_c\}_J$$

Note: $\omega_J = 0$ for fixed appendages.

FIGURE 5. ZERO "G" - INTERACTION FORCE AND MOMENT EQUATIONS

TIME= 40.0000 SECONDS

ATTITUDE INFORMATION

EULER ANGLE(DEGREES)

ROTATING ARRAY NO. 1	13.3264	0.	
ROTATING ARRAY NO. 2	-166.674	-180.000	
SPACECRAFT	-90.0000	1.663497E-13	2.302739E-02

ATTITUDE ERROR

1.30327	-2.107602E-13	
1.30327	2.107602E-13	
-2.302738E-02	-2.311546E-13	-1.664141E-13

BODY RATE(DEG/SEC)

ROTATING ARRAY NO. 1	-.145978	0.	
ROTATING ARRAY NO. 2	-.145978	0.	
SPACECRAFT	2.272544E-02	2.162777E-13	5.470554E-13

ACCELERATION(DEG/SEC/SEC)

1.145037E-02	0.	
1.145037E-02	0.	
1.654983E-03	1.526666E-13	8.651109E-13

MAIN BODY OF SPACECRAFT

	INERTIAL			ORBITAL		
POSITION(FEET)	-5.096060E-13	-6.018673E-11	-3.748842E-24	1.968500E+09	0.	0.
VELOCITY(FT/SEC)	-5.134645E-13	-4.448416E-12	-3.636276E-26	0.	8.202083E+07	0.
ACC(FT/SEC/SEC)	-5.288143E-15	-2.562311E-13	7.187178E-26			

MODAL RESPONSE

MODE SUMMARY = SS(0- 0),R1(1- 1),R2(2- 2),F1(0- 0),F2(0- 0),F3(0- 0),F4(0- 0)

MODE	ETA	ETADOT	ETADDOT	MODE	ETA	ETADOT	ETADDOT
1	-.717207	-2.527689E-02	.252047	2	.717207	2.527689E-02	-.252047

TORQUES AND FORCES

	SPACECRAFT BASIS			DRIVER BASIS		
CONTROL SYSTM TORQUE	-1000.00	-4.883380E-08	-5.034889E-08			
DSTURB FORCE/TORQUE 1	0.	0.	0.			
	0.	0.	0.			
DSTURB FORCE/TORQUE 2	0.	0.	0.			
	0.	0.	0.			
INTERACTION FORCES/TORQUES						
ROTATING ARRAY NO. 1	3.131461E-12	-8.29143	1.97975	3.131461E-12	-8.52449	1.527814E-02
	518.939	1.257630E-10	-3.948040E-10	518.939	2.133781E-10	-3.551847E-10
ROTATING ARRAY NO. 2	-3.131461E-12	8.29143	-1.97975	3.131461E-12	8.52449	1.527814E-02
	518.939	1.257630E-10	-3.948040E-10	-518.939	2.133781E-10	3.551847E-10
DRIVER CONTRL TORQUE						
ROTATING ARRAY NO. 1	15.0116	0.	0.	15.0116	0.	0.
ROTATING ARRAY NO. 2	15.0116	0.	0.	-15.0116	0.	0.

FIGURE 6. SOLAR ARRAY SPACE STATION DYNAMIC INTERACTION ANALYSIS (SUMMARY LISTING)

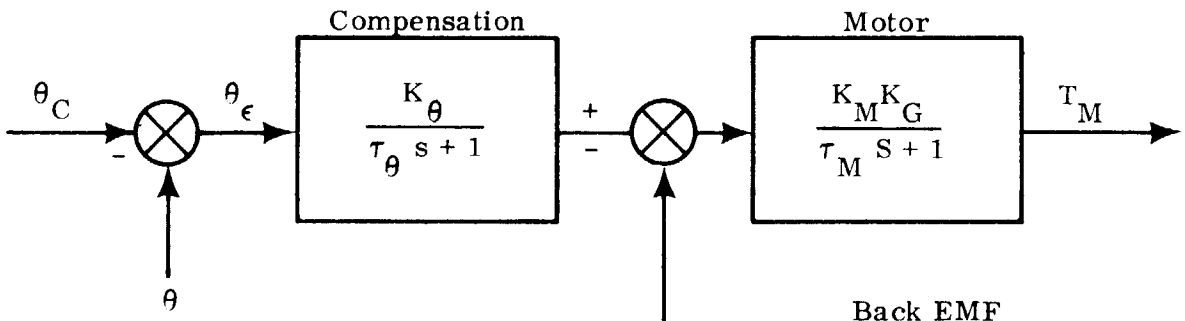

τ_M - motor time constant

K_B - back EMF coefficient

$K_{\theta,\tau\theta}$ - gain and time constant for loop compensation

K_G - system gear ratio

$\theta, \dot{\theta}$ - array attitude angle, attitude rate relative to space station

θ_C - array command angle relative to source station

T_M - torque to solar array

θ_ε - angular error

FIGURE 7. CONTINUOUS DRIVE ORIENTATION CONTROL SYSTEM MODEL

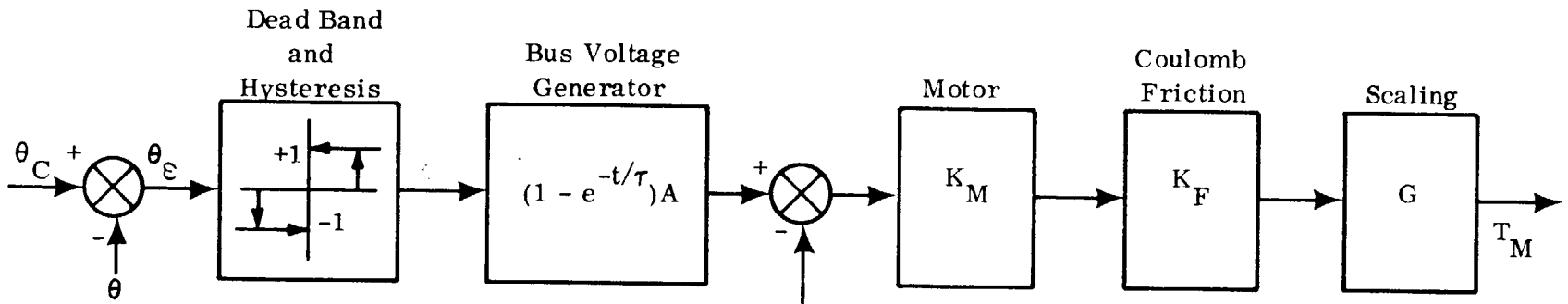

K_B - back EMF coefficient

K_G - system gear ratio

$\theta, \dot{\theta}$ - array attitude angle, attitude rate relative to space station

θ_C - array command angle relative to source station

K_F - Coulomb friction magnitude

A - bus voltage generator amplification constant

- bus voltage generator time constant

T_M - torque to solar array

K_M - motor coefficient

G - scale factor

θ_ε - attitude error

FIGURE 8. NON LINEAR ORIENTATION CONTROL SYSTEM MODEL

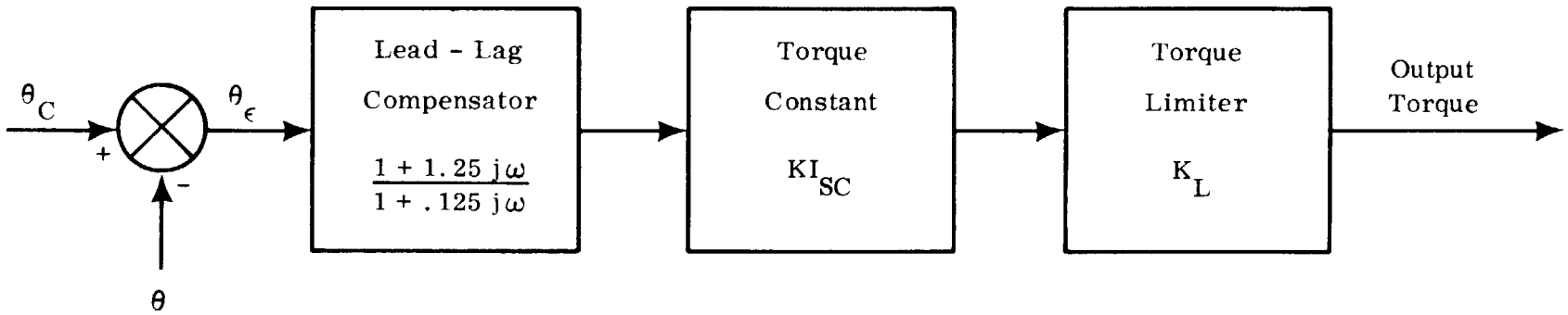

LEGEND

θ - Space Station Attitude Angle (Rigid + Flexible Body)

θ_C - Space Station Commanded Angle

K_L - Limiting Value of Torque

I_{SC} - Space Station Mass Moment of Inertia

ω - Circular Frequency

K - Constant

FIGURE 9. SIMPLIFIED CONTROL MOMENT GYRO CONTROL MODEL

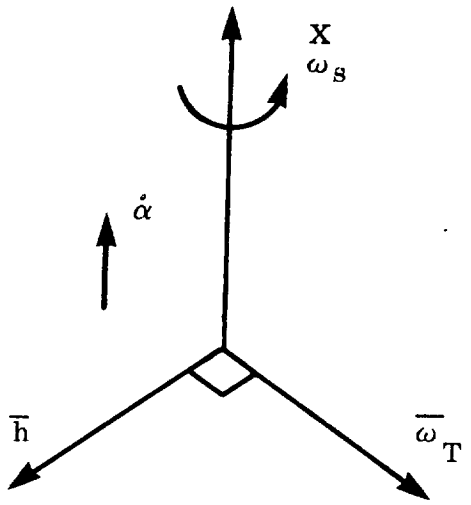

$\dot{\alpha}$ - Gimbal Rate of CMG

$\bar{h}$ - Momentum Vector

ω_s - Spin Axis Component of Spin Rate

ω_T - Transverse Component of Spin Rate

Applied Torques

$\bar{T}_c = -(\omega_s + \dot{\alpha}) \times \bar{h}$ (opposes $\bar{\omega}_T$)

$\bar{T}_s = -\bar{\omega}_T \times \bar{h}$ (increases spin rate)

FIGURE 10. WOBBLE DAMPER CONTROL TORQUES

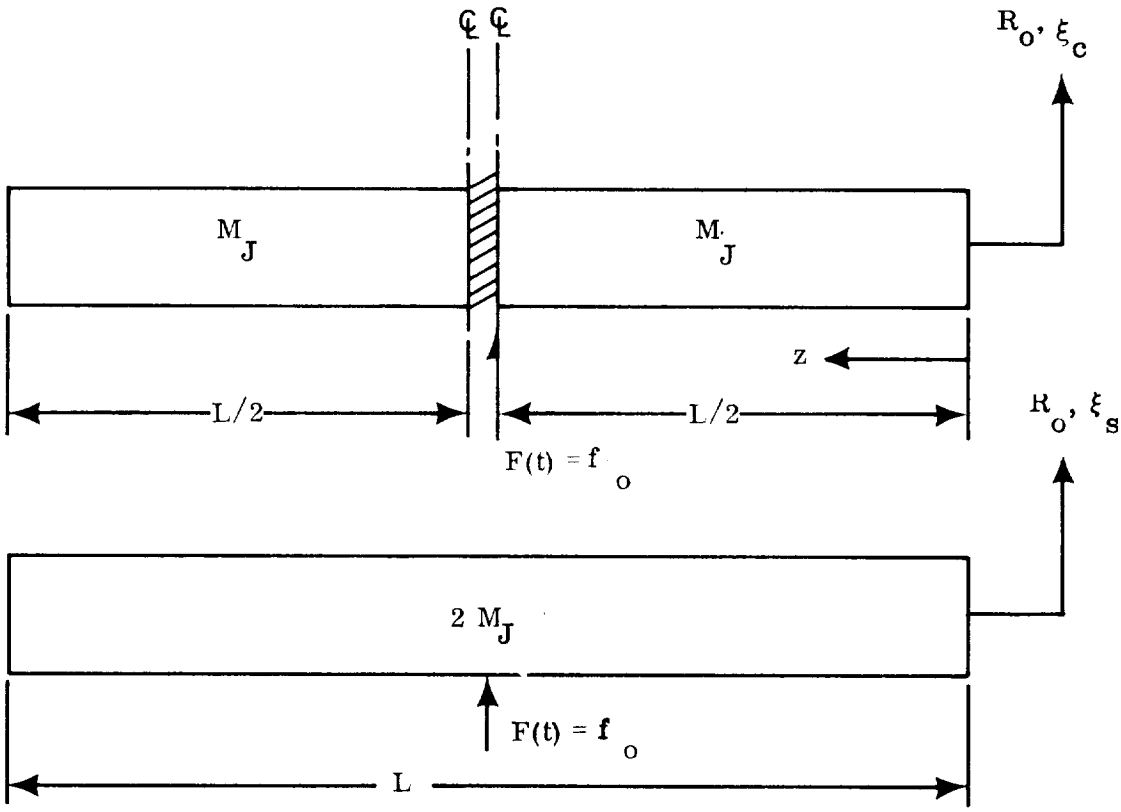

Free-Free Beam

R_o - Rigid Body Translation Coordinate

ξ_c - Generalized Coordinate of Cantilever Beam

ξ_s - Generalized Coordinate of Free-Free Beam

FIGURE 11. CANTILEVER BEAM SIMULATION OF A FREE-FREE BEAM

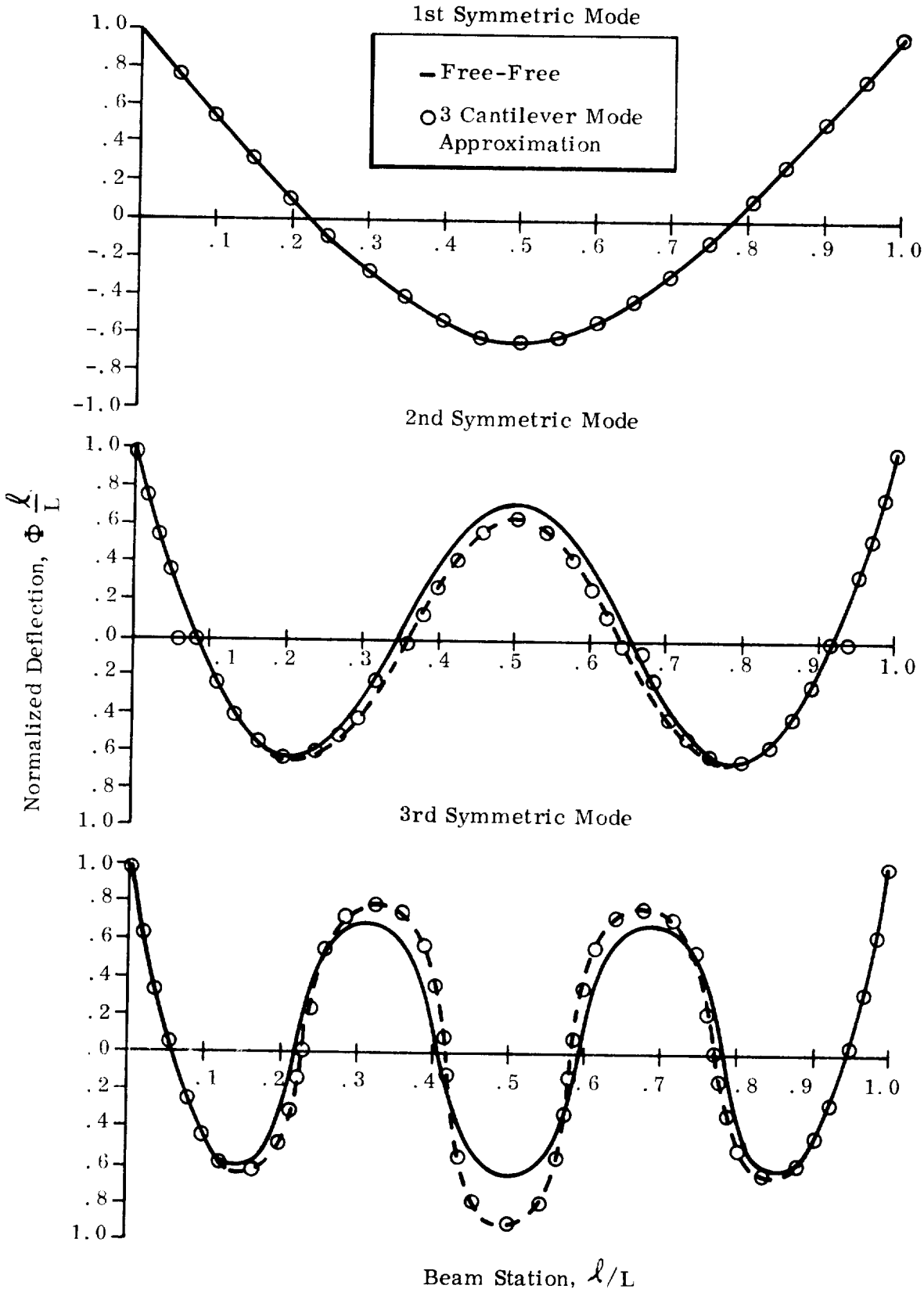

FIGURE 12. MODE SHAPE COMPARISONS

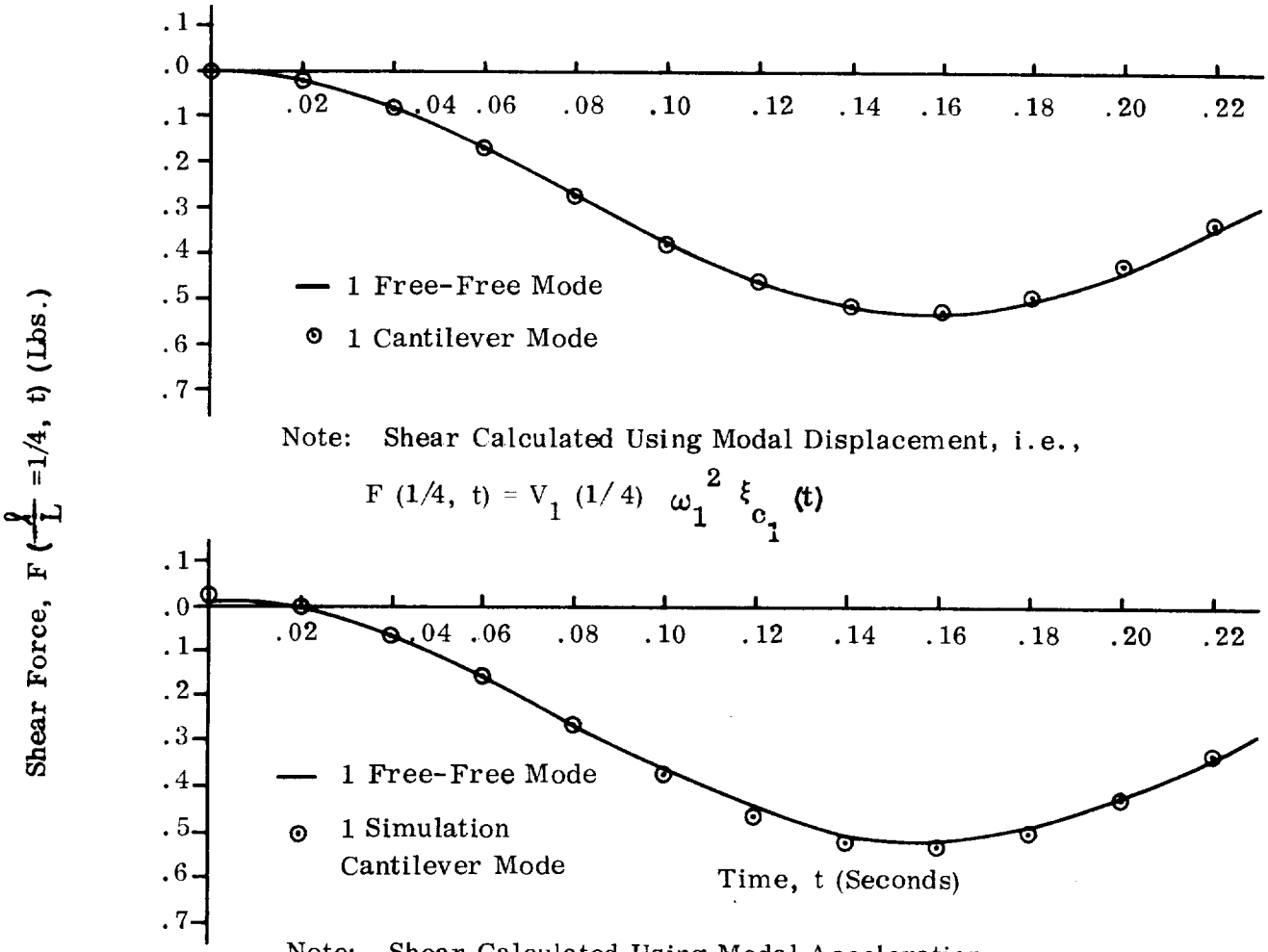

FIGURE 13. COMPARISON OF CANTILEVER & FREE-FREE BEAM SHEAR AT 1/4 SPAN VS TIME FOR A UNIT STEP FORCE APPLIED AT MID-SPAN.

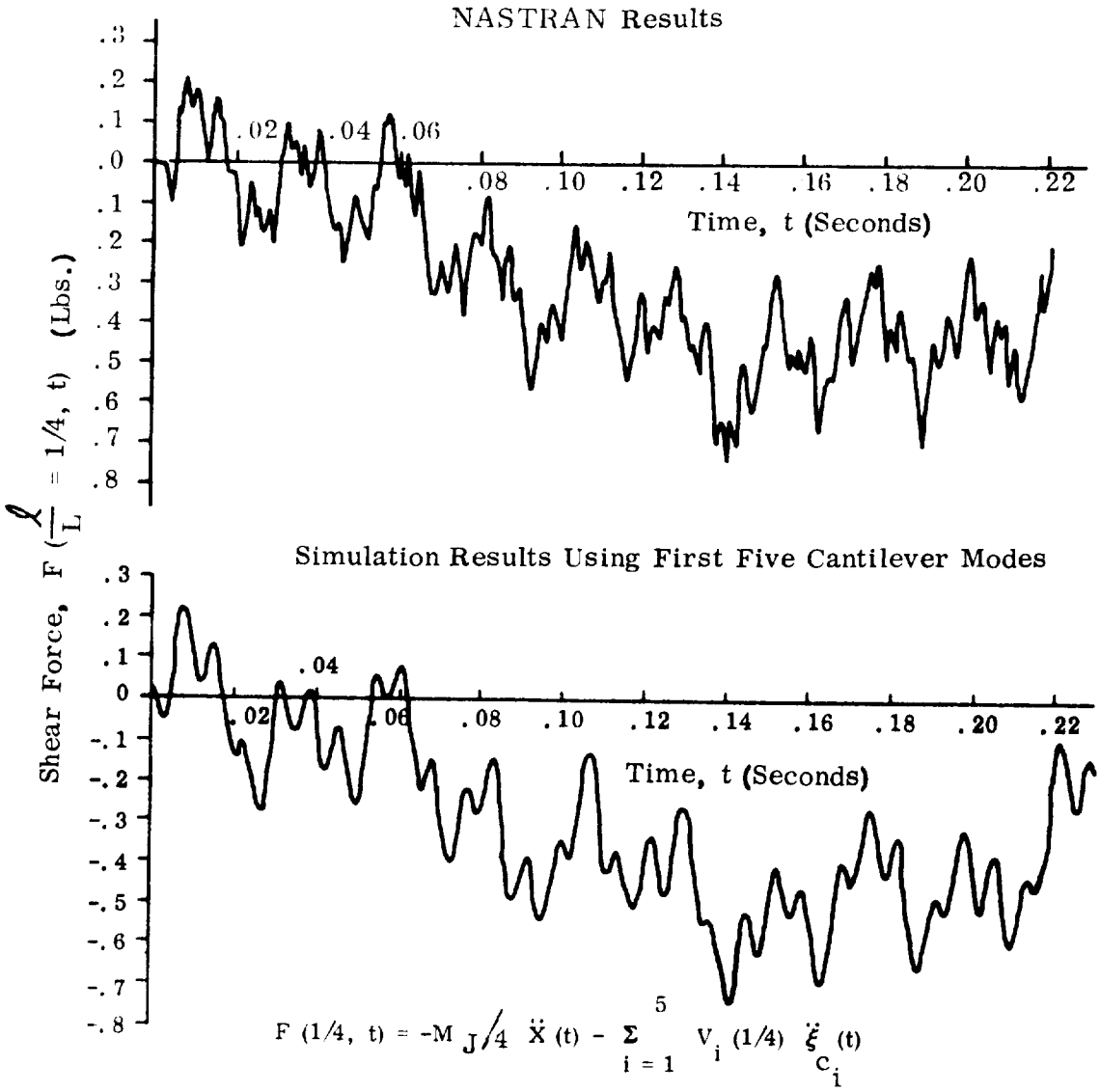

FIGURE 14. UNIFORM BEAM COMPARISONS OF SHEAR HISTORY AT 1/4 SPAN FOR A UNIT STEP FORCE APPLIED AT MID-SPAN

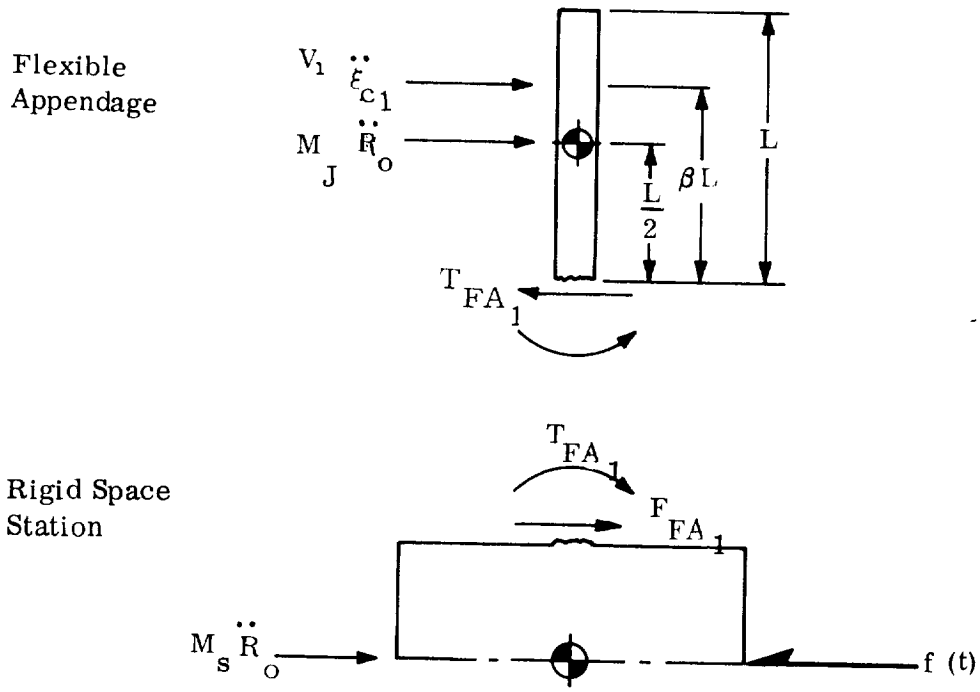

FIGURE 15. RIGID SPACE STATION-FLEXIBLE APPENDAGE FREE BODY DIAGRAM

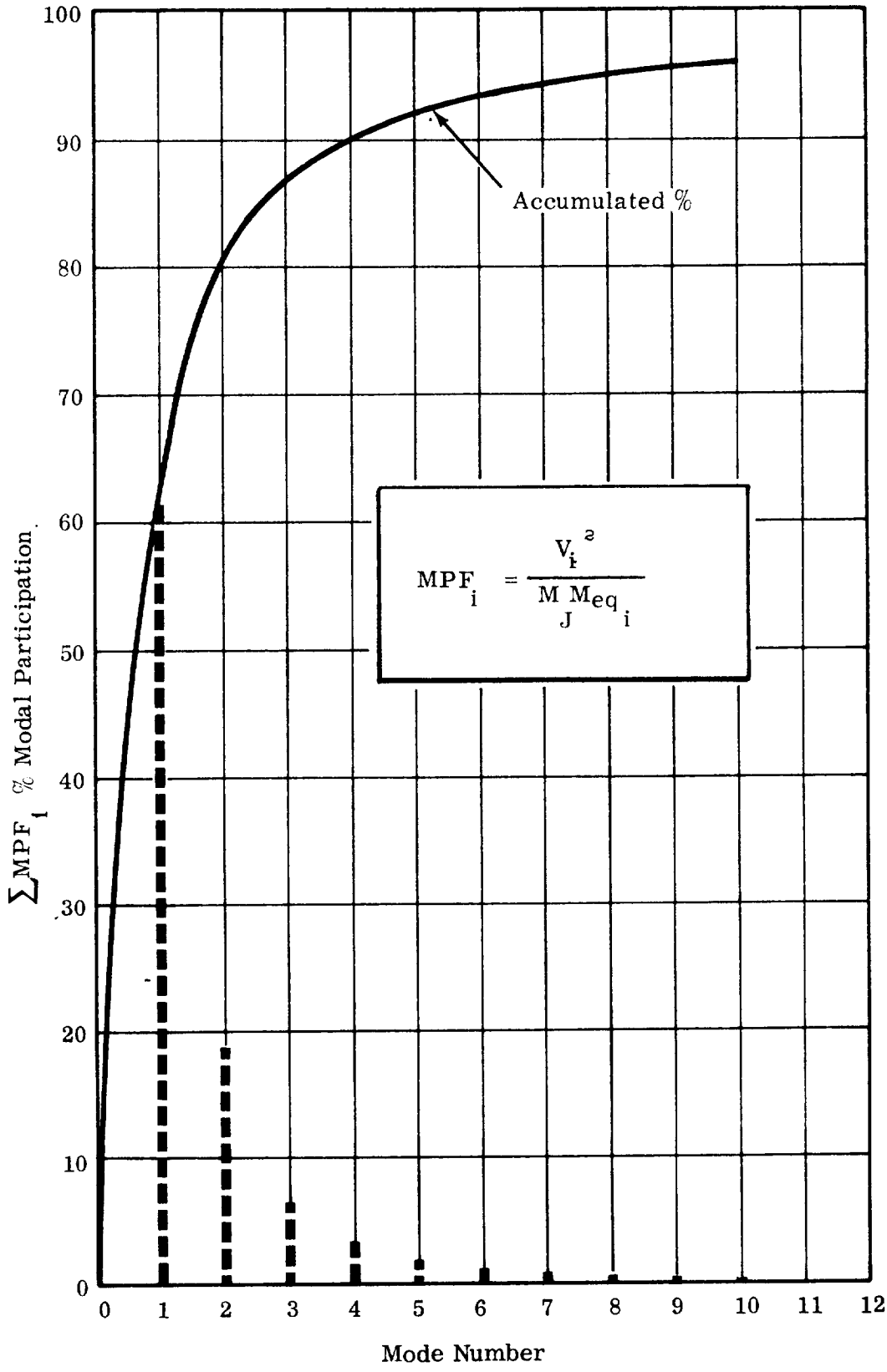

FIGURE 16. CANTILEVER BEAM MODAL PARTICIPATION FACTORS

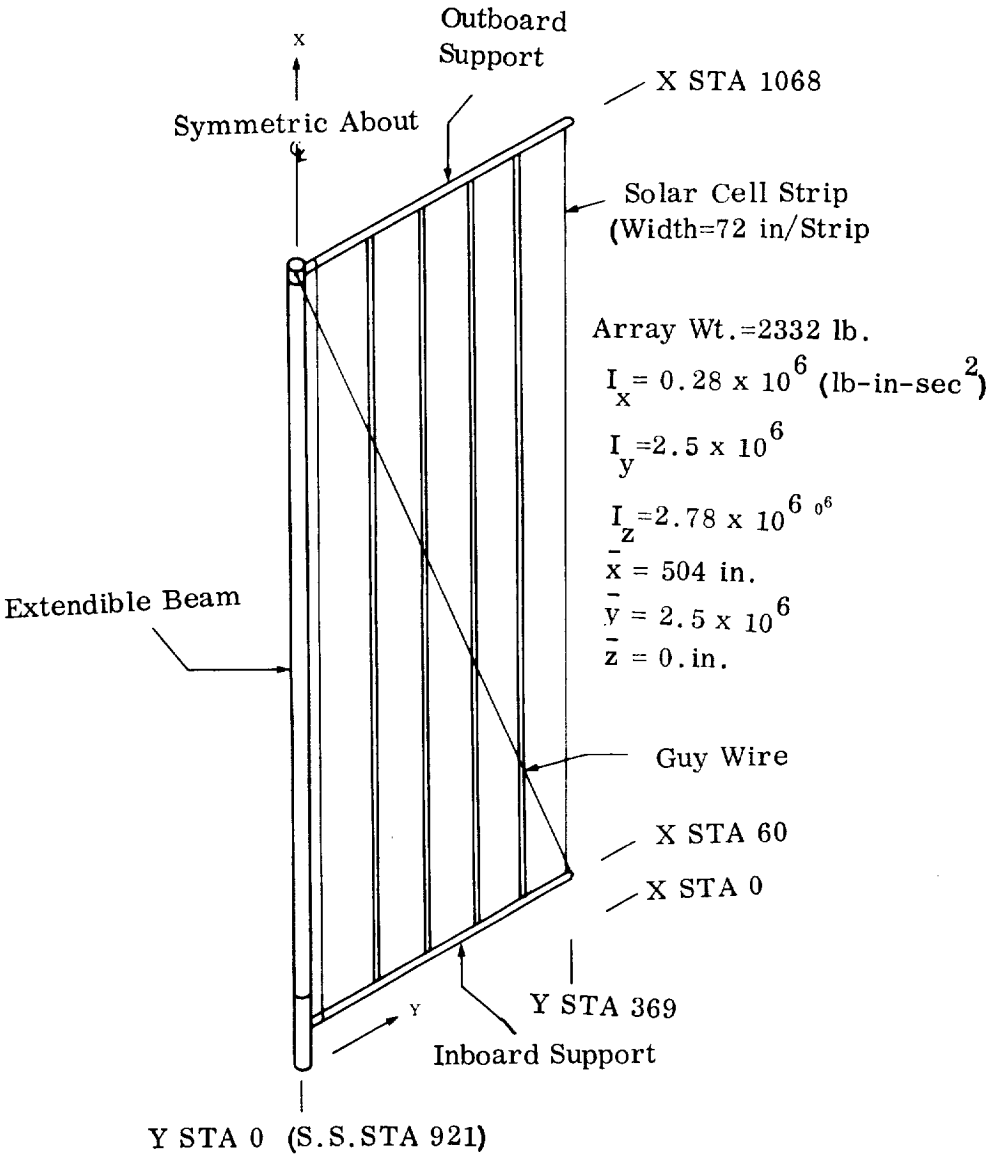

FIGURE 21. ZERO "G" ROLLUP SOLAR ARRAY

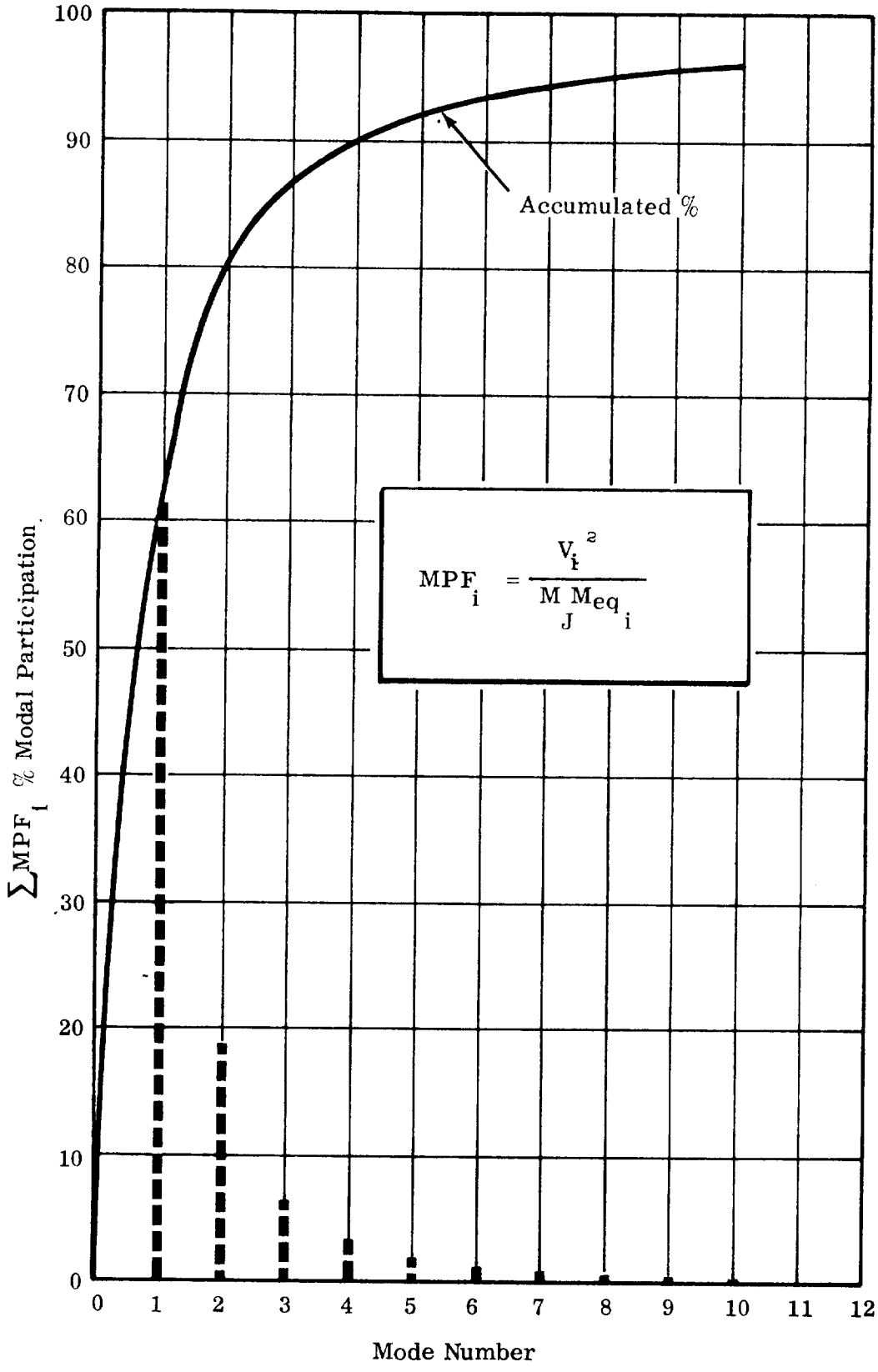

FIGURE 16. CANTILEVER BEAM MODAL PARTICIPATION FACTORS

Beam	Length (in)	No. of Nodes	EA (lbs.)	EI ($lb\text{-}in^2$)	Mass ($lb\text{-}sec^2/in$)	Mass/Node* ($lb\text{-}sec^2/in$)
I	12	27	2.	---	0.0416	.0016
II	6	26	—	28.4	0.0416	.0016

*nodes 1, 27, 53 have no mass

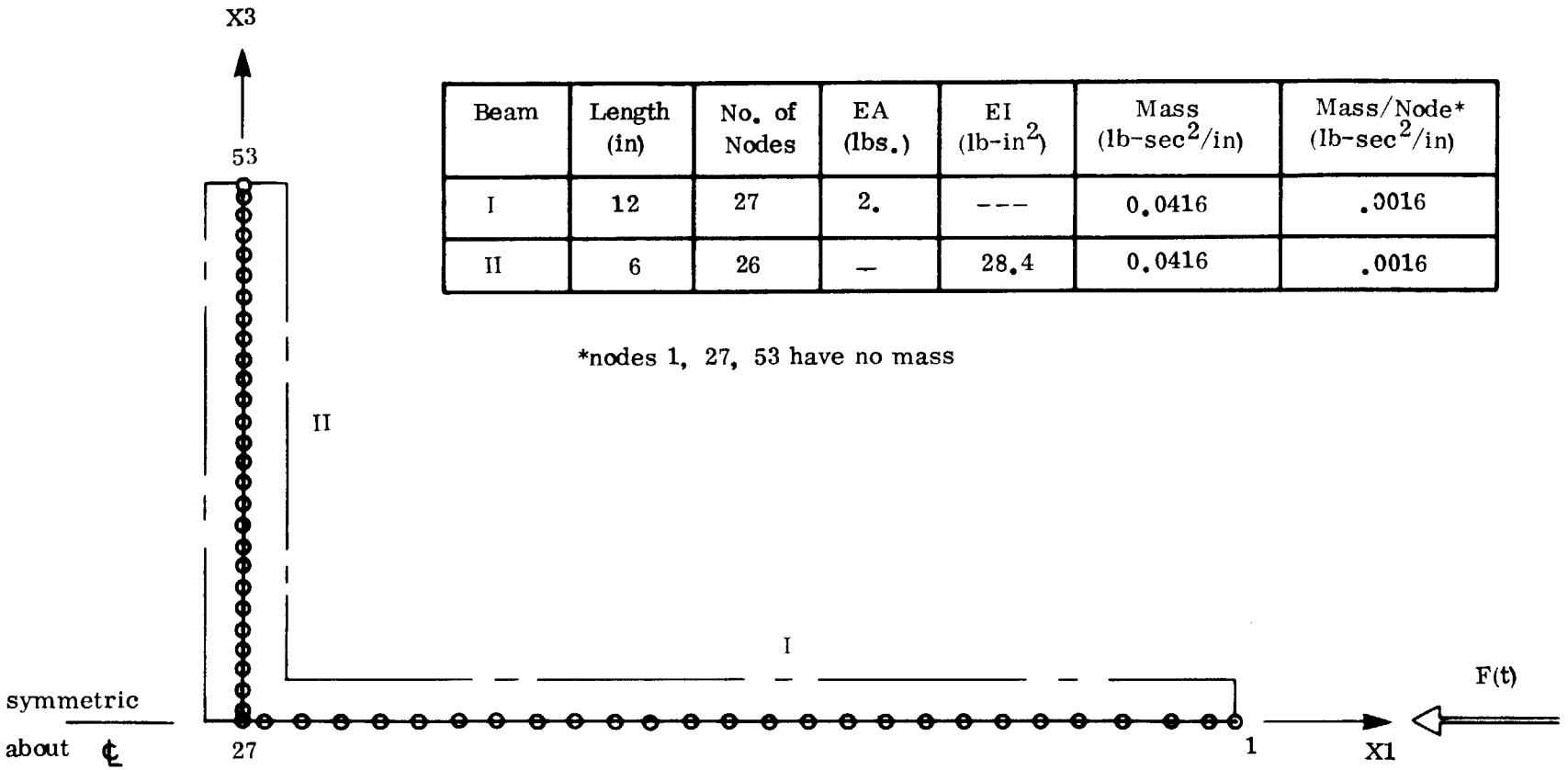

FIGURE 17. "T" BEAM STRUCTURAL MODEL

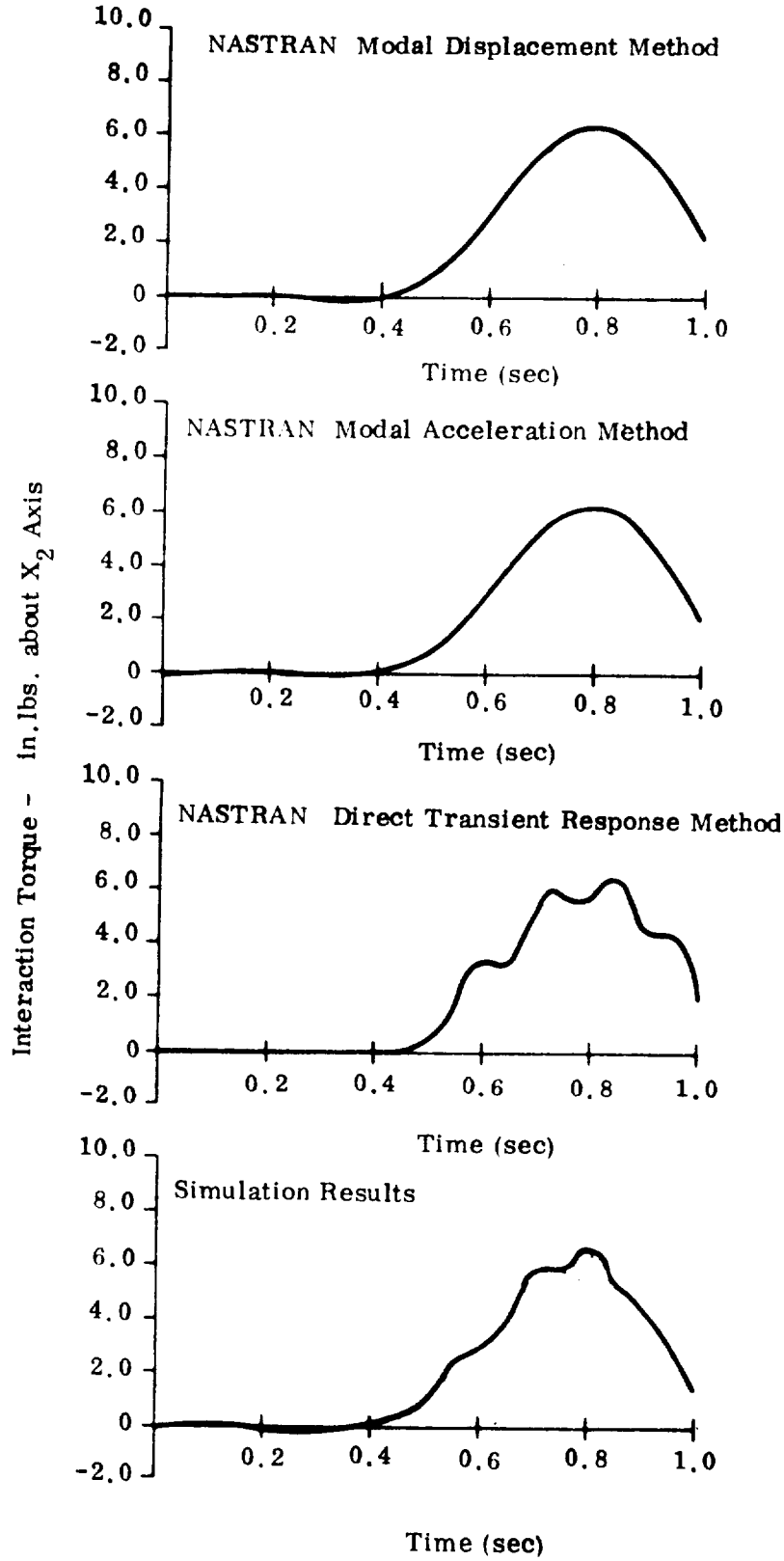

FIGURE 18. "T" BEAM INTERACTION TORQUE HISTORIES

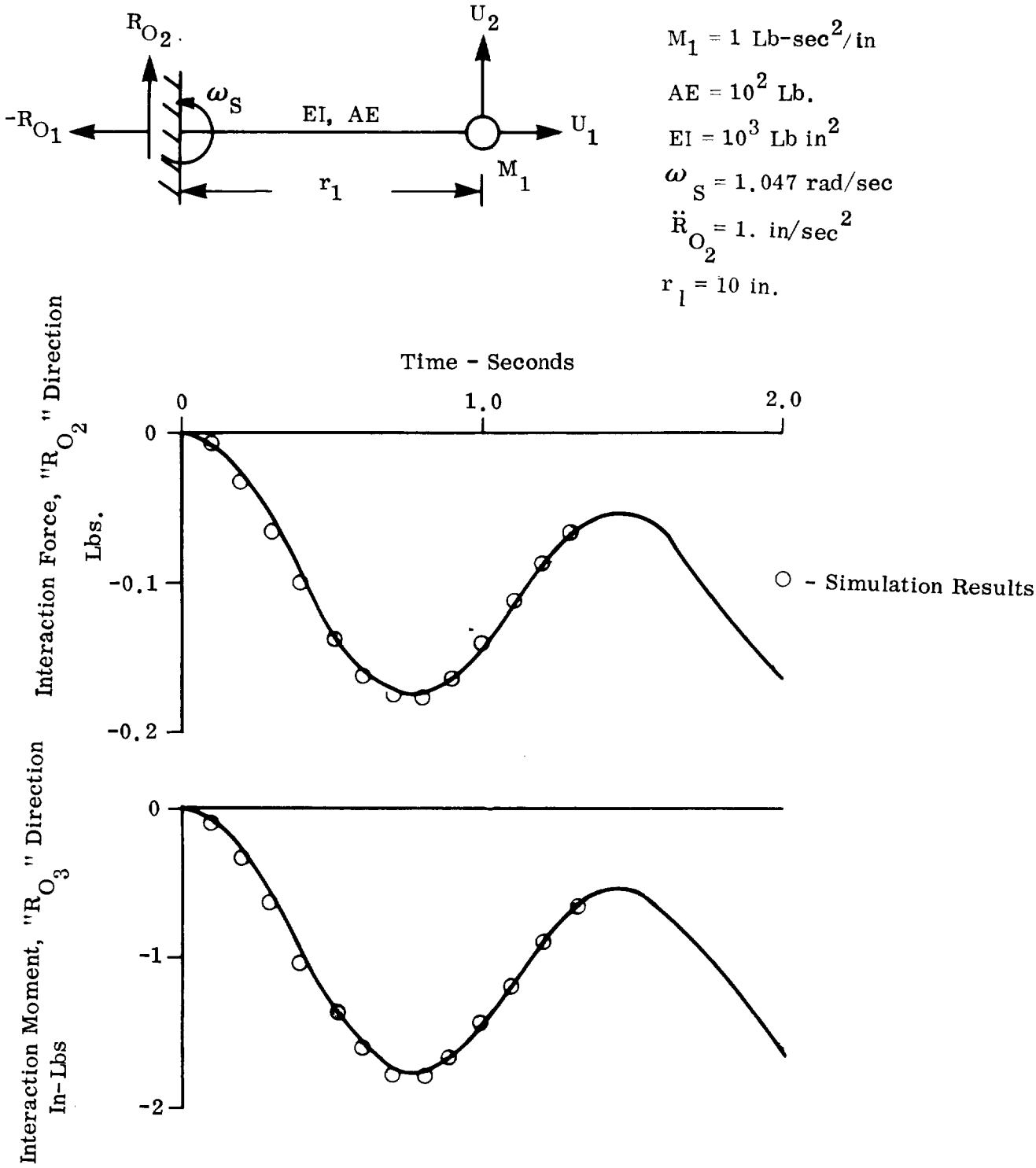

FIGURE - 19. INTERACTION LOAD SOLUTIONS FOR SPINNING MASS

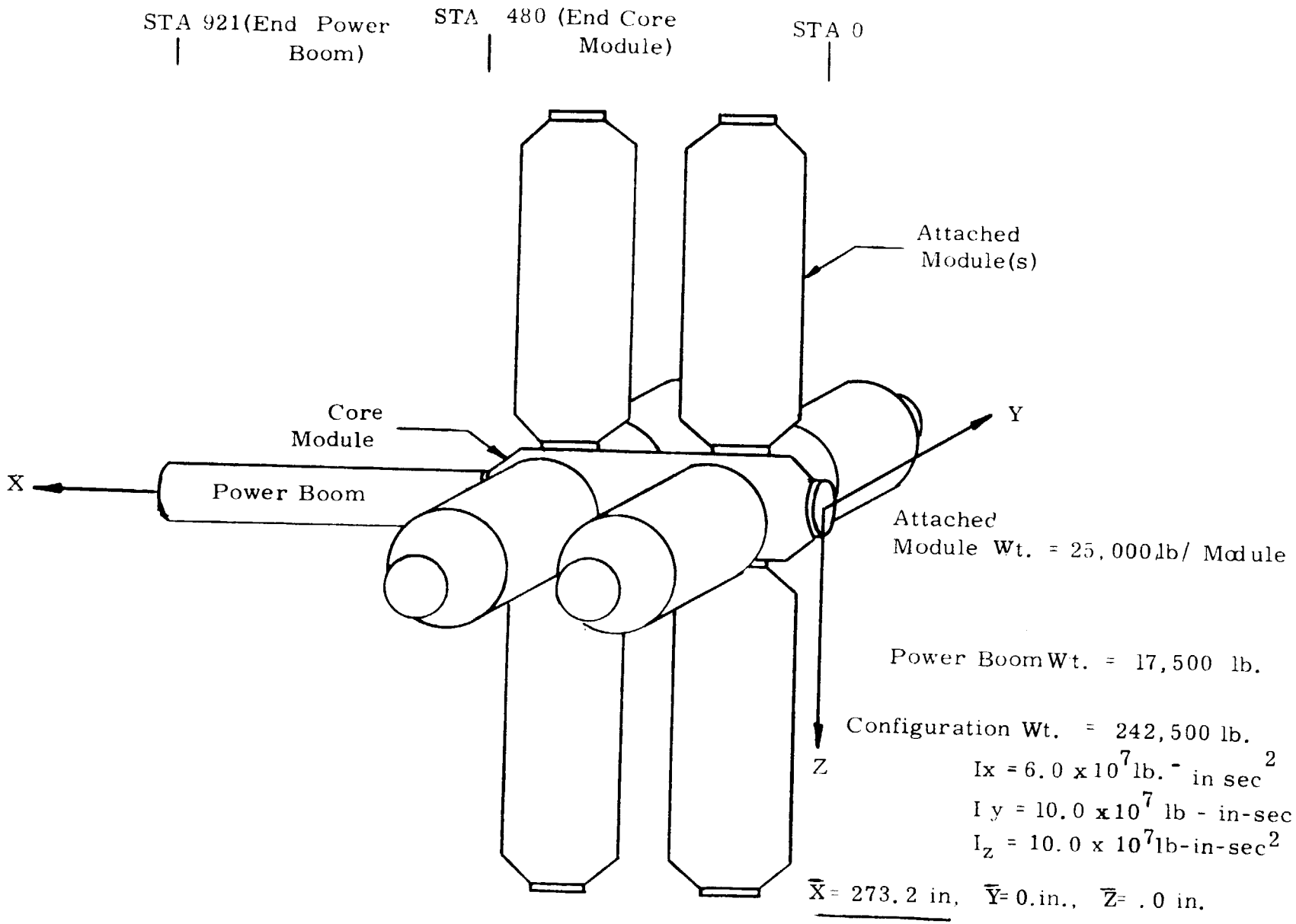

FIGURE 20. ZERO "G" SPACE STATION CONFIGURATION

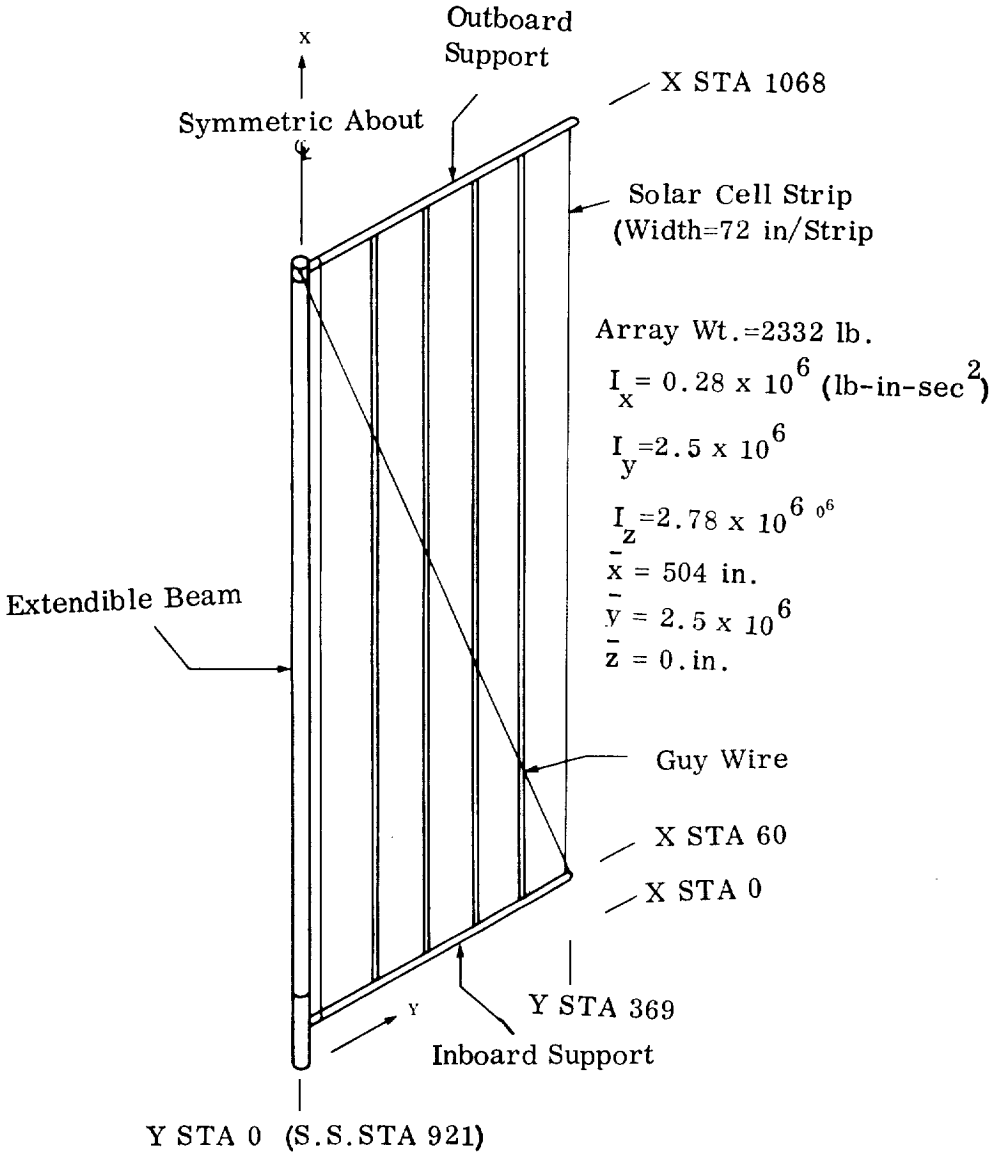

FIGURE 21. ZERO "G" ROLLUP SOLAR ARRAY

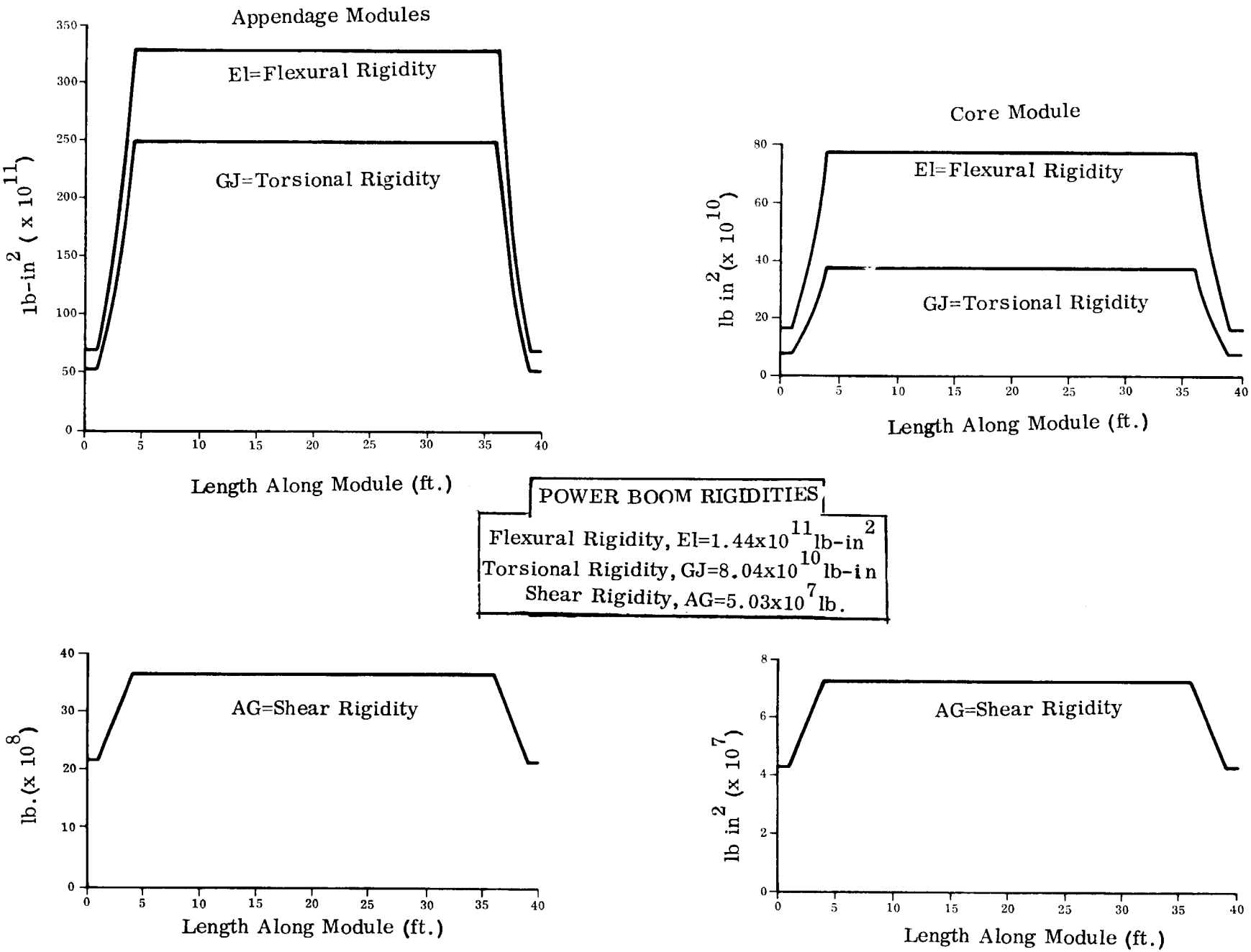

FIGURE 22. SPACE STATION STIFFNESS PROPERTIES

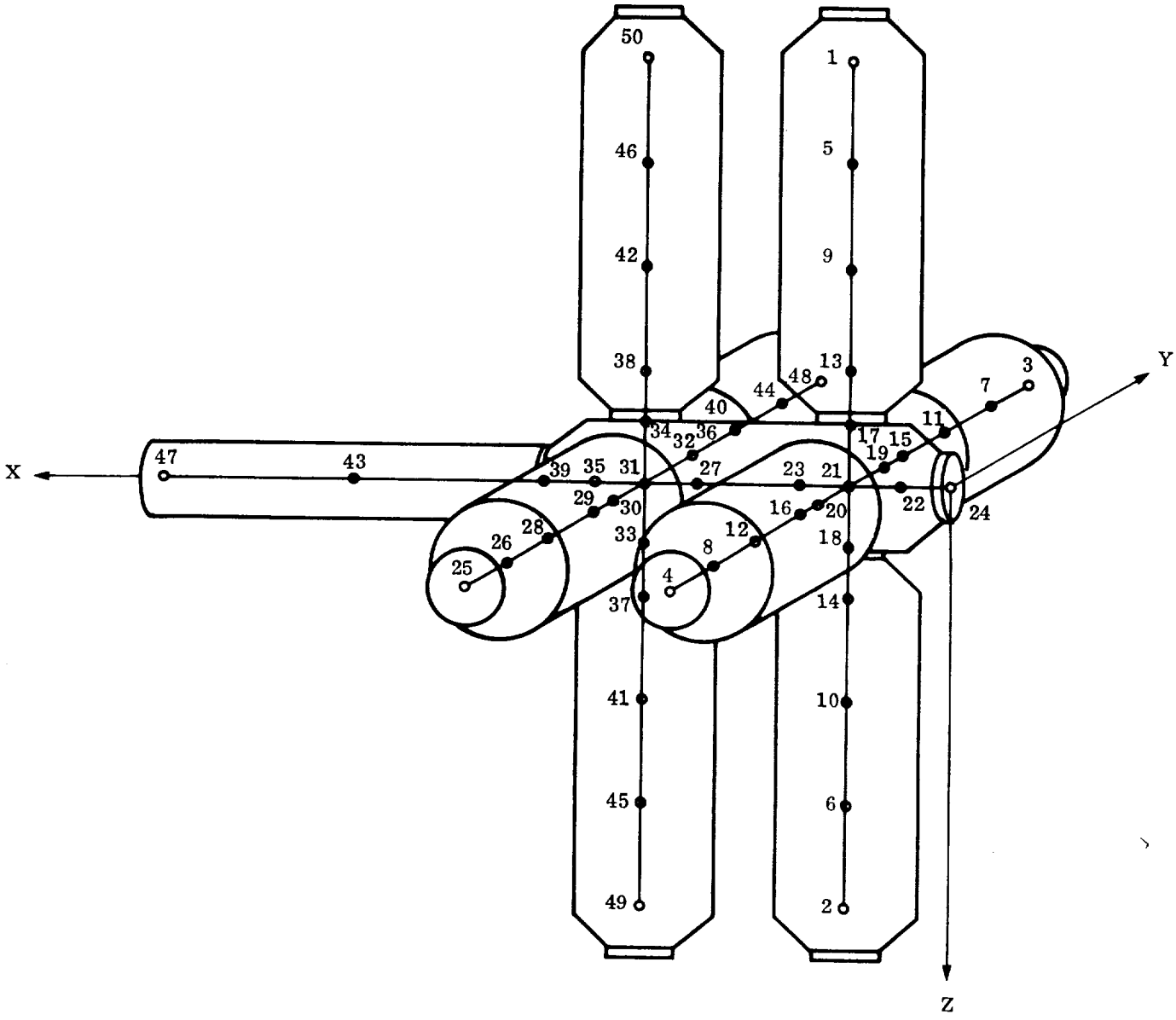

FIGURE 23. FINITE ELEMENT MODEL OF SPACE STATION

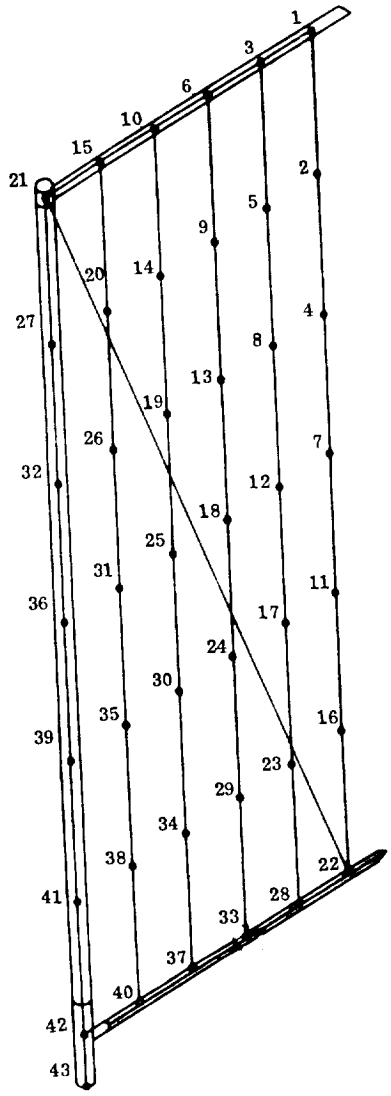

FIGURE 24. FINITE ELEMENT MODEL OF ROLLUP SOLAR ARRAY

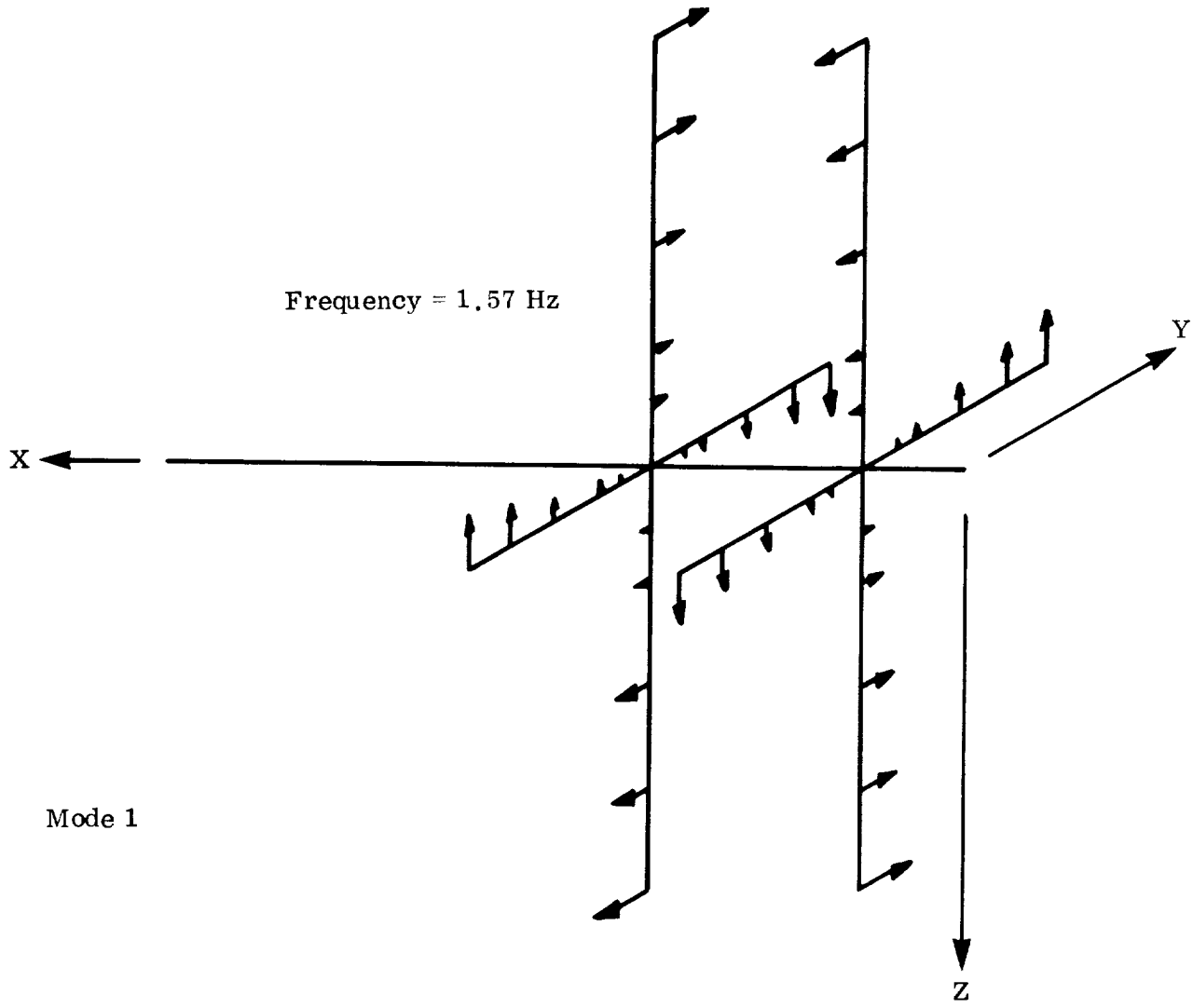

FIGURE 25. TRANSLATION VECTOR DISPLACEMENTS REPRESENTING FIRST SPACE STATION MODE

$$K = \frac{T}{6\ell_1}$$

	U_1	U_2	U_3	U_4
	2	-2	-1	1
	-2	2	1	-1
	-1	1	2	-2
	1	-1	-2	2

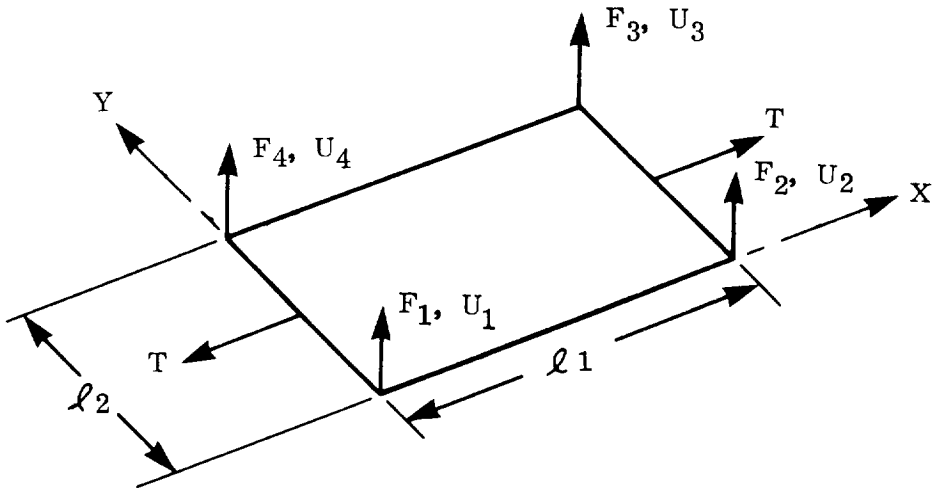

Rectangular Membrane Finite Element

$$K = \frac{2EI}{\ell 3}$$

$$\begin{bmatrix} 6 & & & \text{Sym.} \\ 3\ell & 2\ell^2 & & \\ -6 & -3\ell & 6 & \\ 3\ell & \ell^2 & -3\ell & 2\ell^2 \end{bmatrix} - T/5 \begin{bmatrix} 6/\ell & & & \text{Sym.} \\ 1/2 & 2\ell/3 & & \\ -6/\ell & -1/2 & 6/\ell & \\ 1/2 & -\ell/6 & -1/2 & 2\ell/3 \end{bmatrix}$$

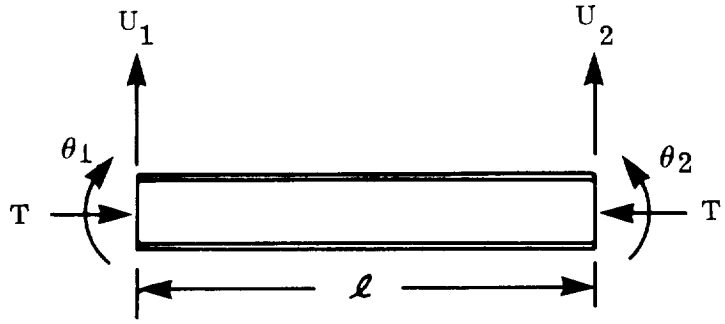

FIGURE 26. ARRAY ELEMENTAL STIFFNESS MATRICES

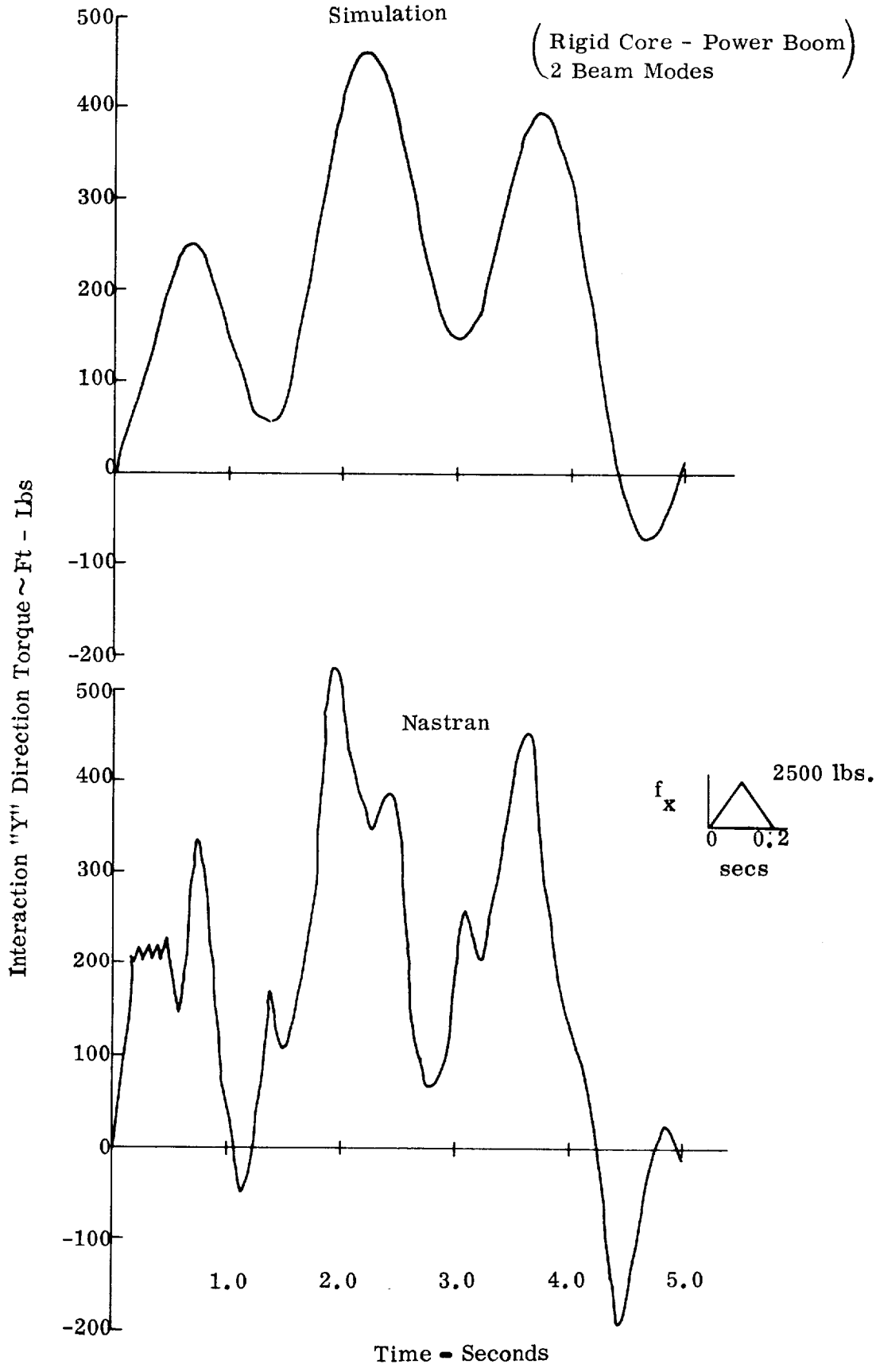

FIGURE 33. COMPARISON OF NASTRAN AND SIMULATION RESULTS

$$K = \frac{T}{6\ell_1}$$

	U_1	U_2	U_3	U_4
	2	-2	-1	1
	-2	2	1	-1
	-1	1	2	-2
	1	-1	-2	2

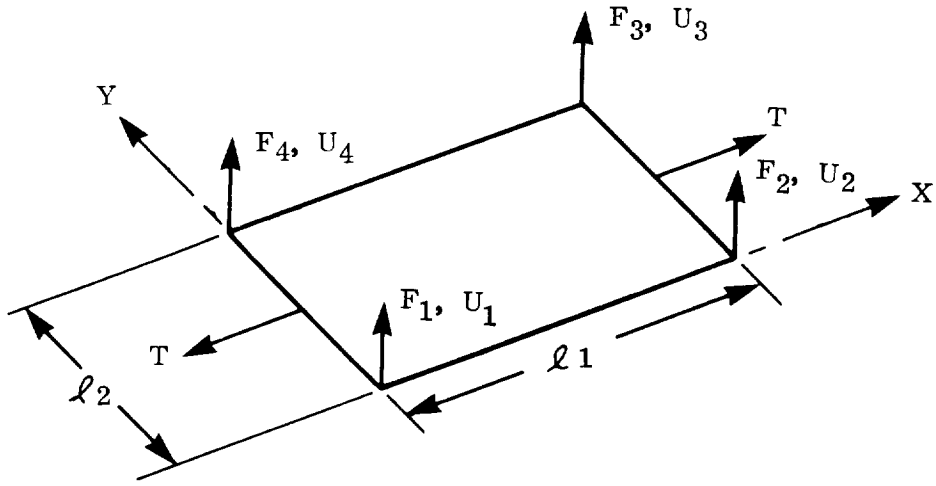

Rectangular Membrane Finite Element

$$K = \frac{2EI}{\ell 3}$$

$$\begin{bmatrix} 6 & & & \text{Sym.} \\ 3\ell & 2\ell^2 & & \\ -6 & -3\ell & 6 & \\ 3\ell & \ell^2 & -3\ell & 2\ell^2 \end{bmatrix} - T/5 \begin{bmatrix} 6/\ell & & & \text{Sym.} \\ 1/2 & 2\ell/3 & & \\ -6/\ell & -1/2 & 6/\ell & \\ 1/2 & -\ell/6 & -1/2 & 2\ell/3 \end{bmatrix}$$

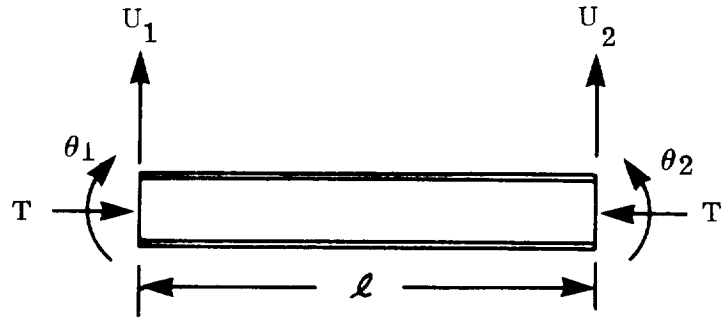

FIGURE 26. ARRAY ELEMENTAL STIFFNESS MATRICES

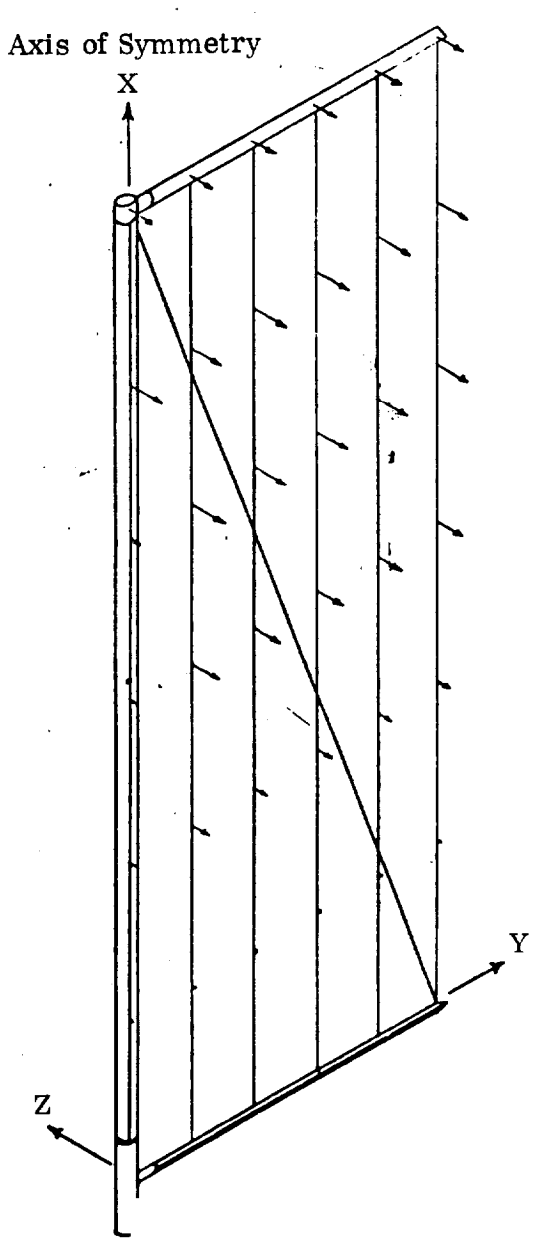

f = 0.092 Hz

"Z" Shear Modal Participation (68.1%)

"Y-Y" Moment Modal Participation (41.5%)

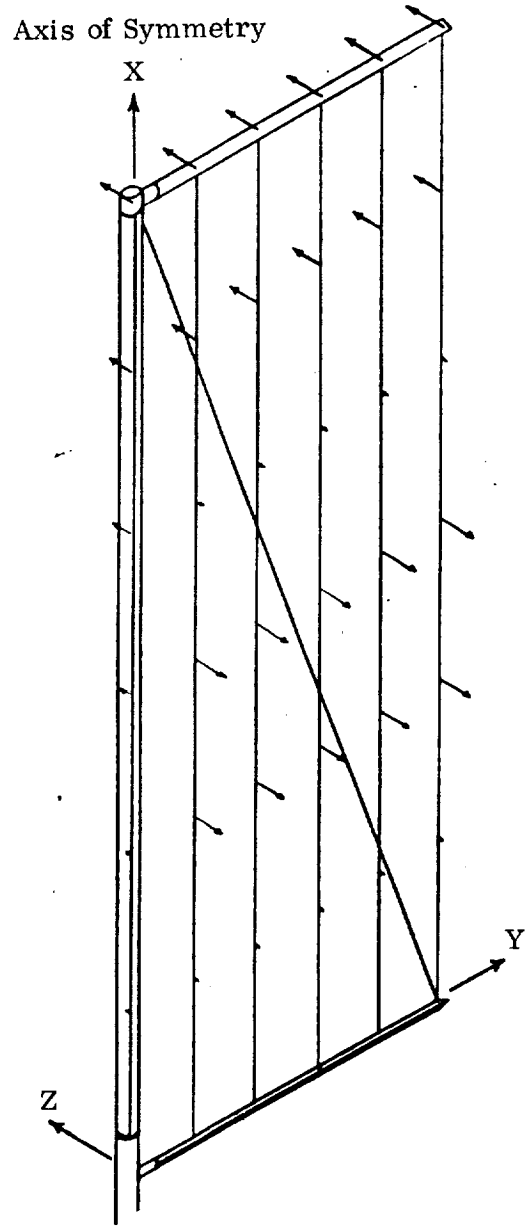

f = 0.187 Hz

"Z" Shear Modal Participation (0.3%)

"Y-Y" Moment Modal Participation (4.4%)

FIGURE 27. OUT-OF-PLANE SYMMETRIC MODAL DEFLECTIONS

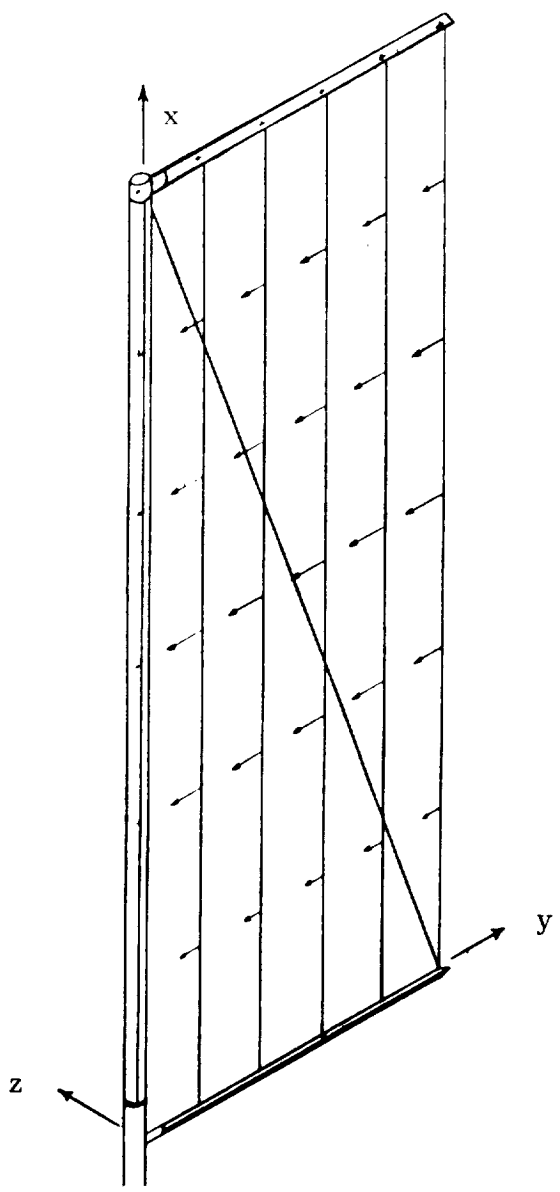

f_1 = 0.097 HZ
"Y" Shear Participation (71.2%)
"Z-Z" Moment Participation (51.4%)

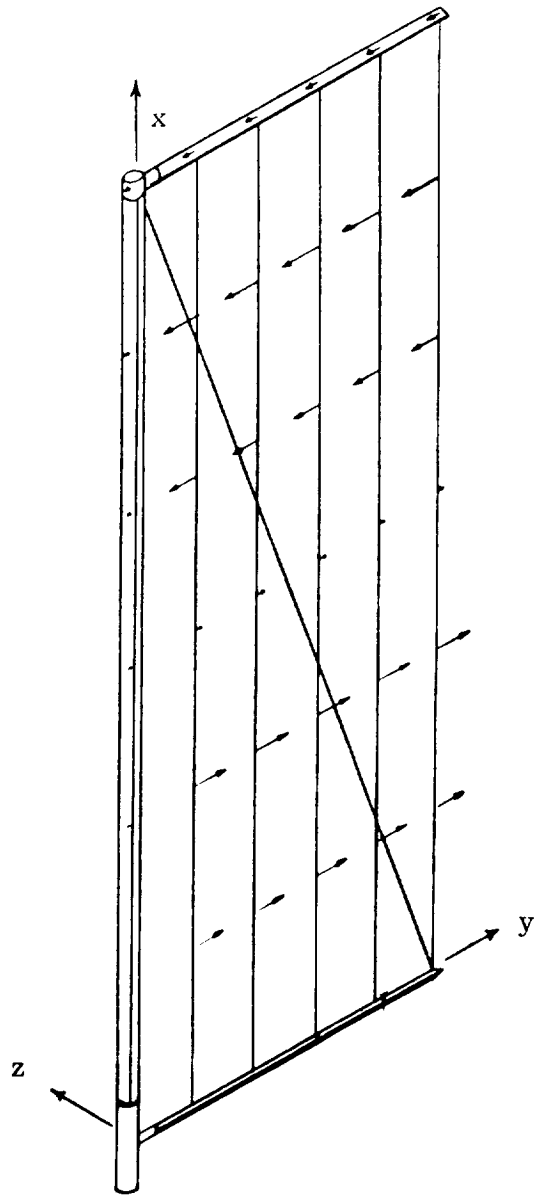

f_6 = 0.189 HZ
"Y" Shear Participation (0.1%)
"Z-Z" Moment Partcipation (13.7%)

FIGURE 28. IN-PLANE ANTISYMETRIC MODAL DEFLECTIONS

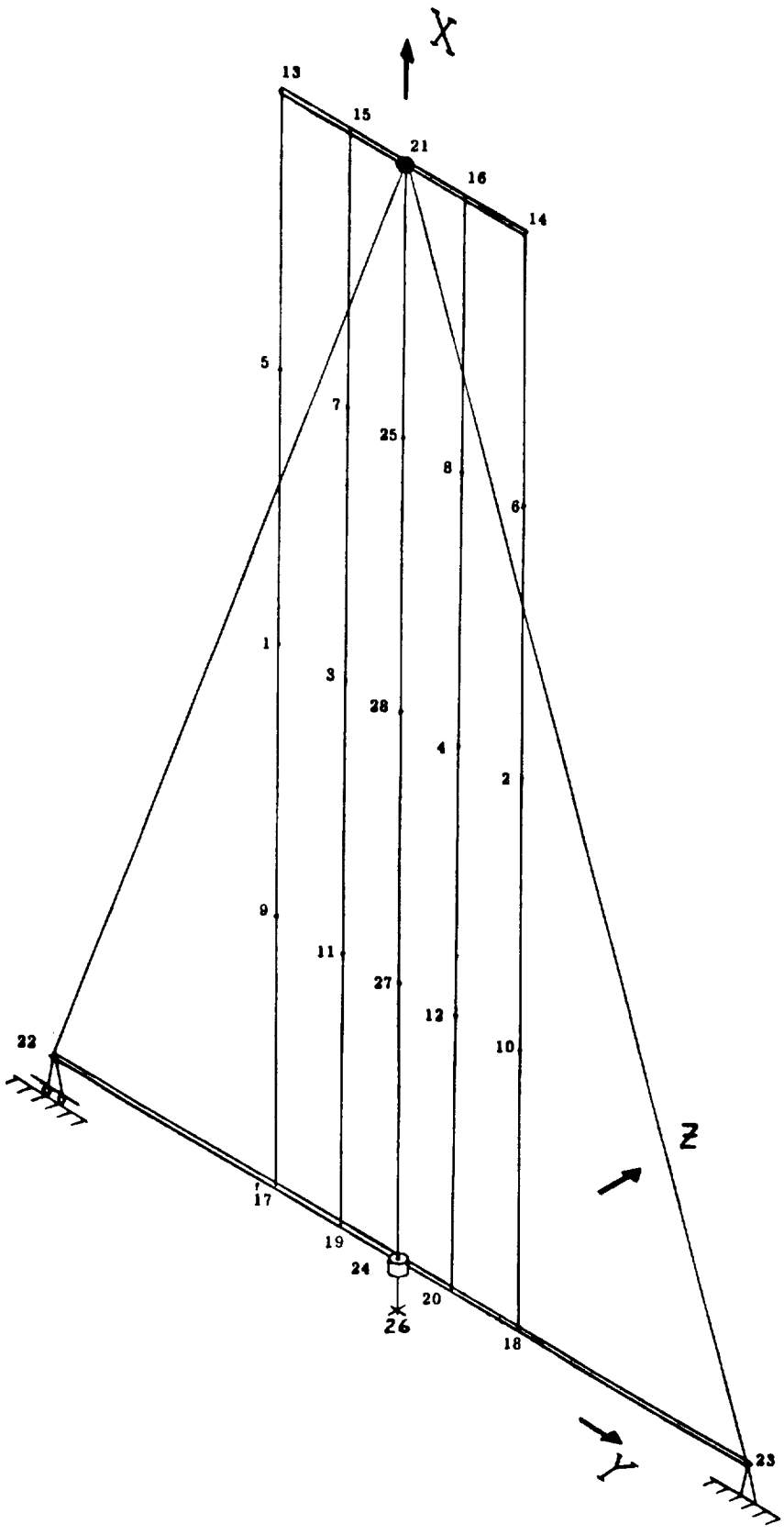

FIGURE 29. SOLAR ARRAY ARTIFICIAL "G" STRUCTURAL MODEL

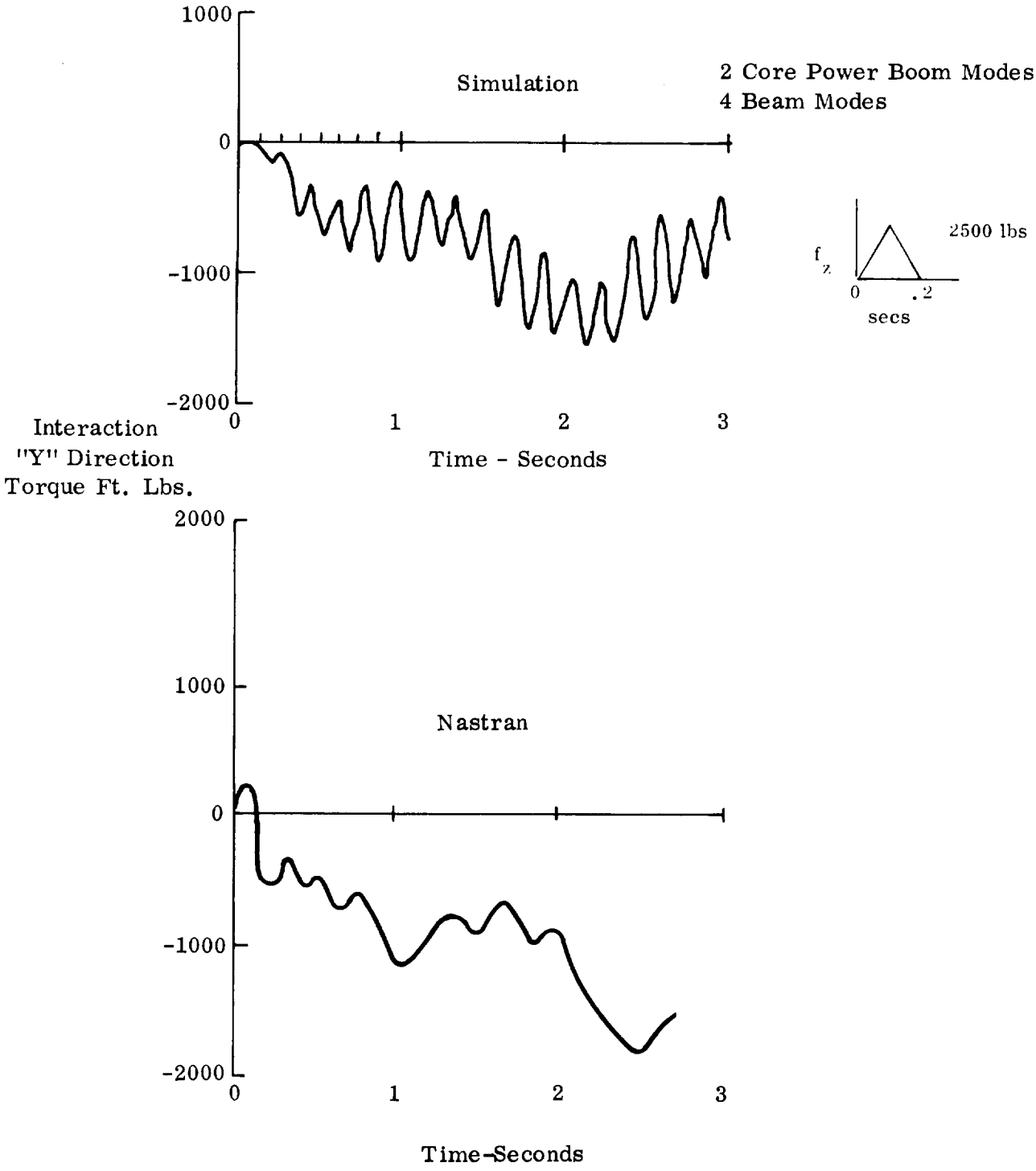

FIGURE 30. COMPARISON OF NASTRAN AND SIMULATION RESULTS

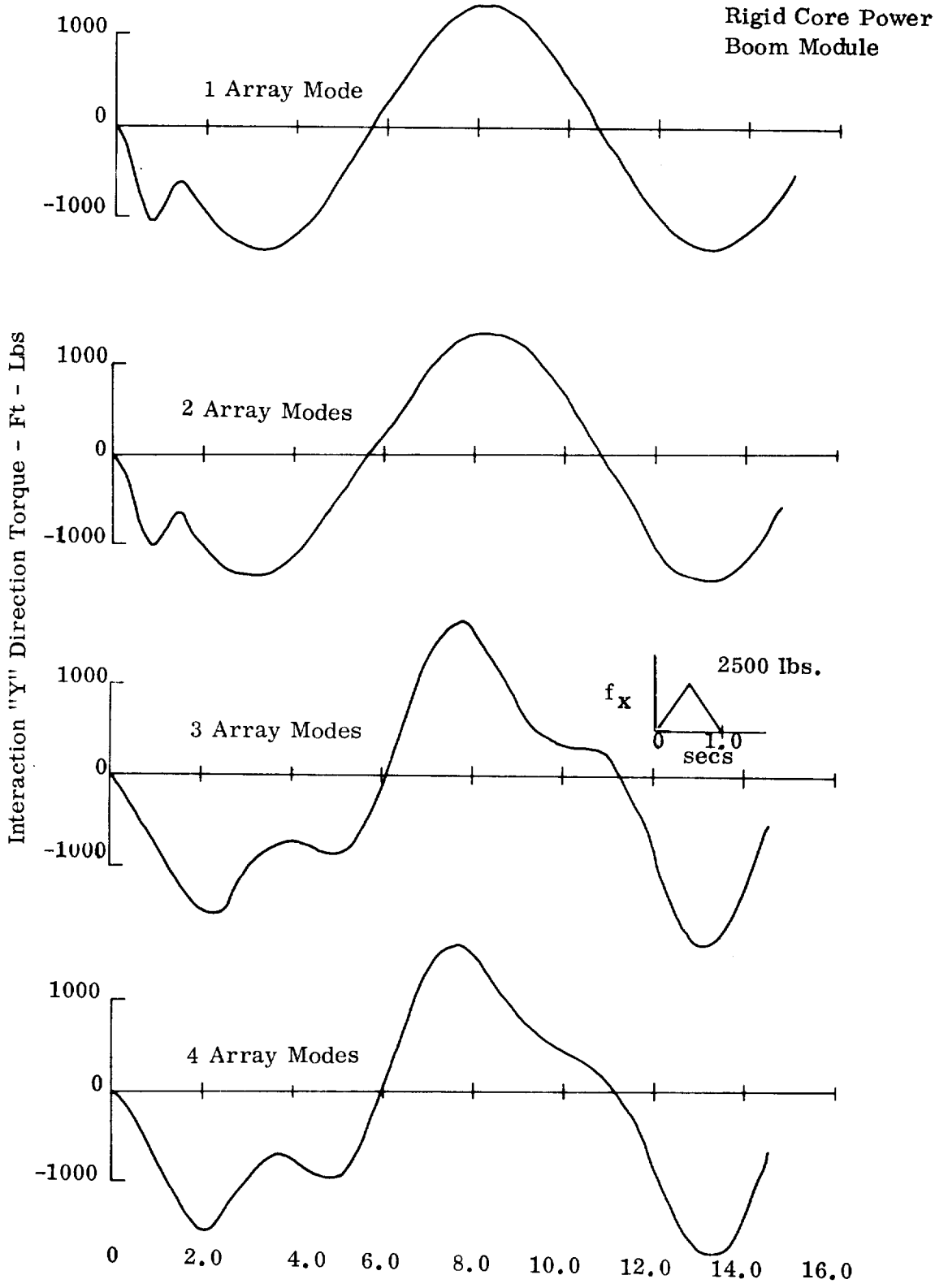

FIGURE 31. VARIATION OF INTERACTION LOAD WITH NUMBER OF ARRAY MODES

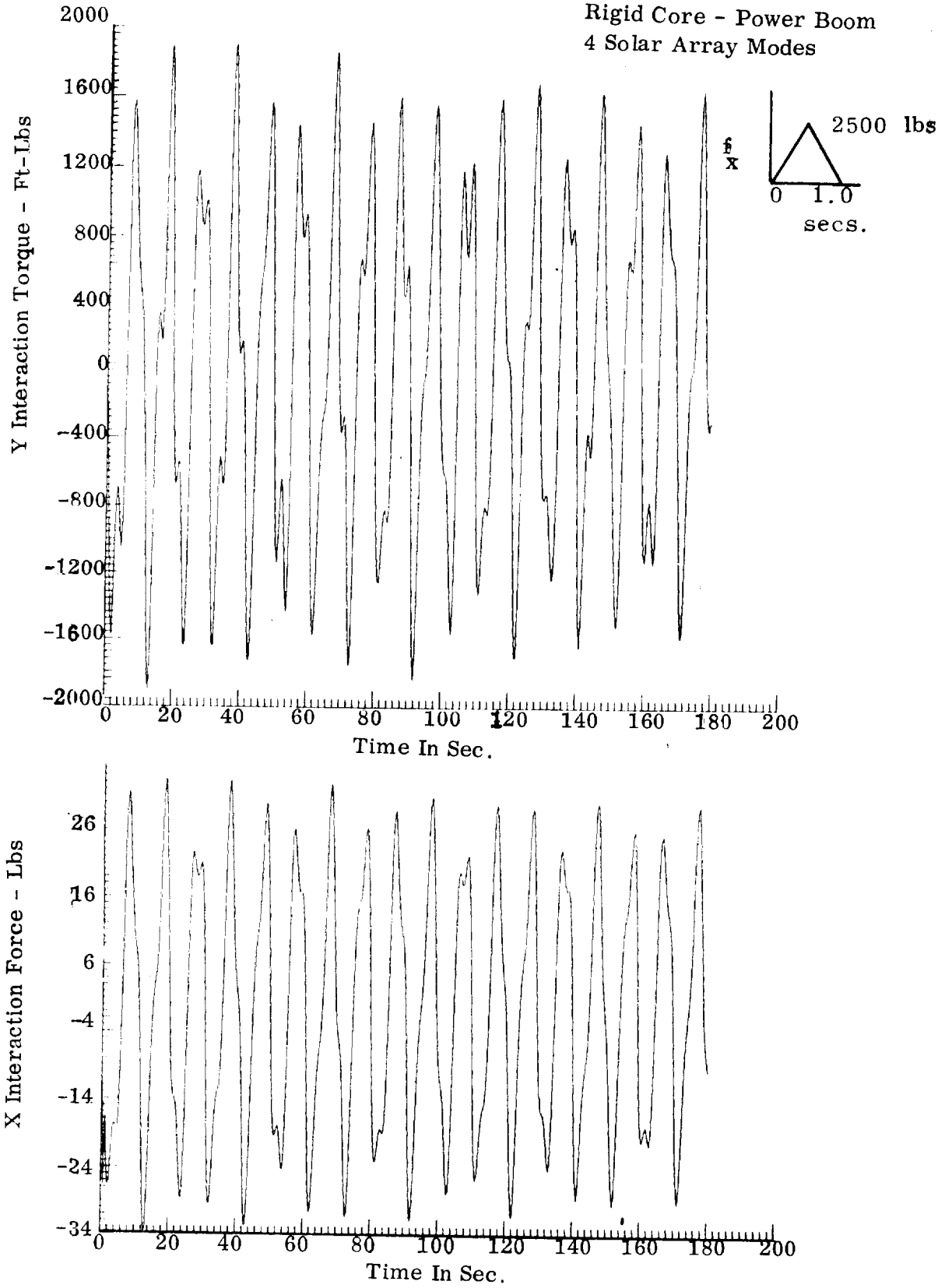

FIGURE 32. INTERACTION LOADS-SPACE STATION CONFIGURATION OF CORE-POWER BOOM AND SOLAR ARRAYS

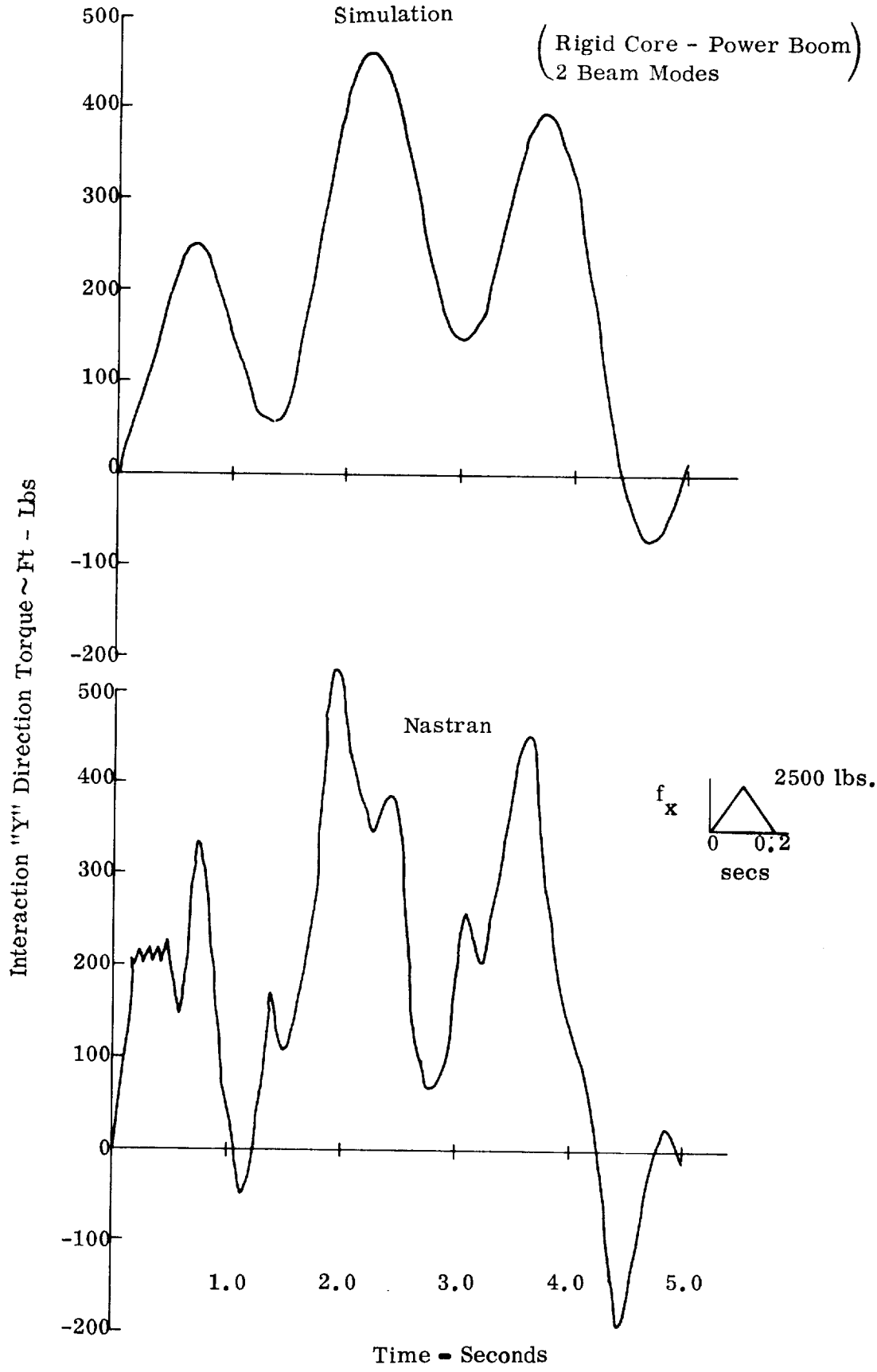

FIGURE 33. COMPARISON OF NASTRAN AND SIMULATION RESULTS

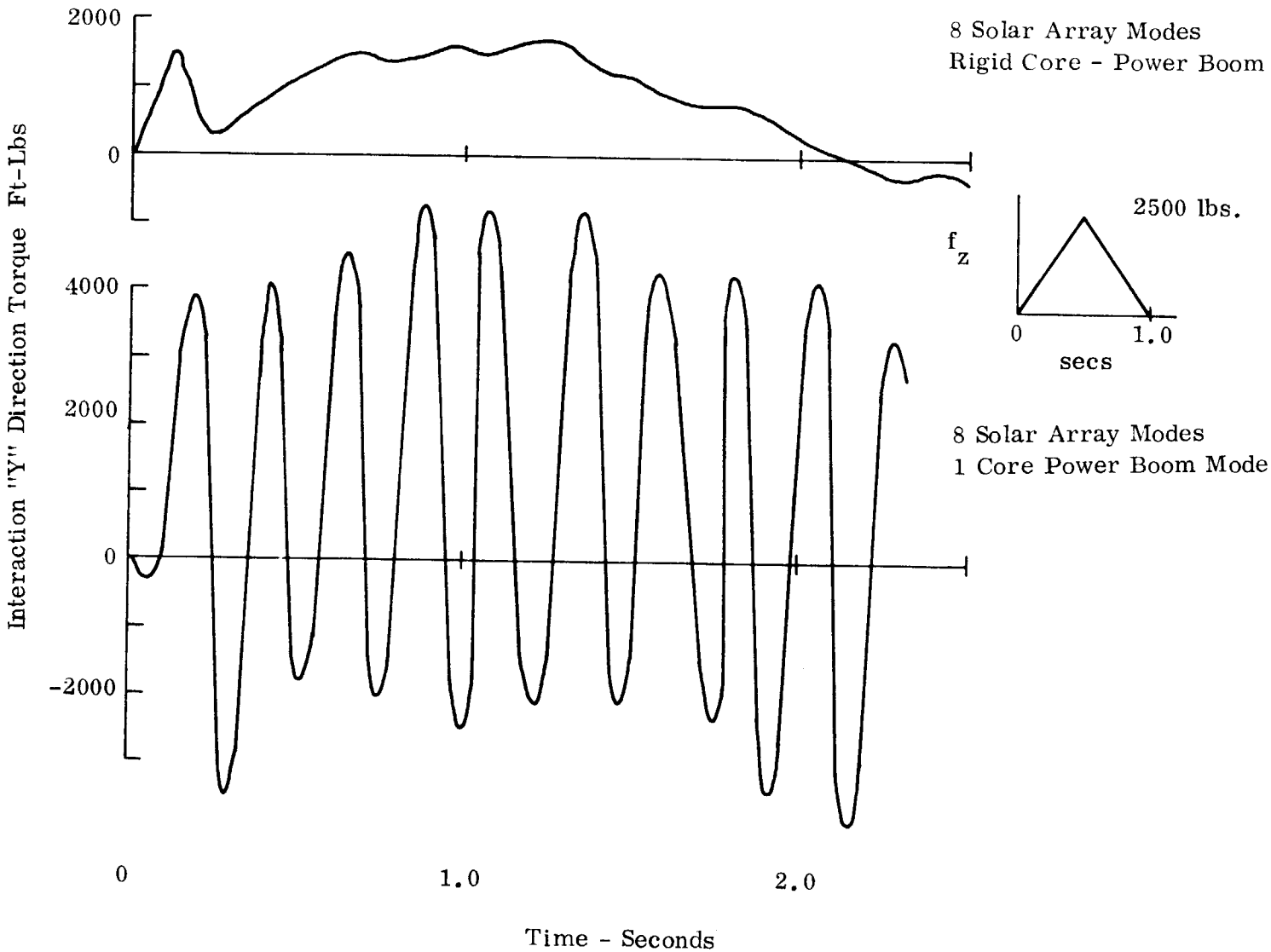

FIGURE 34. VARIATION OF INTERACTION LOAD WITH RIGID AND FLEXIBLE SPACE STATION CONFIGURATIONS

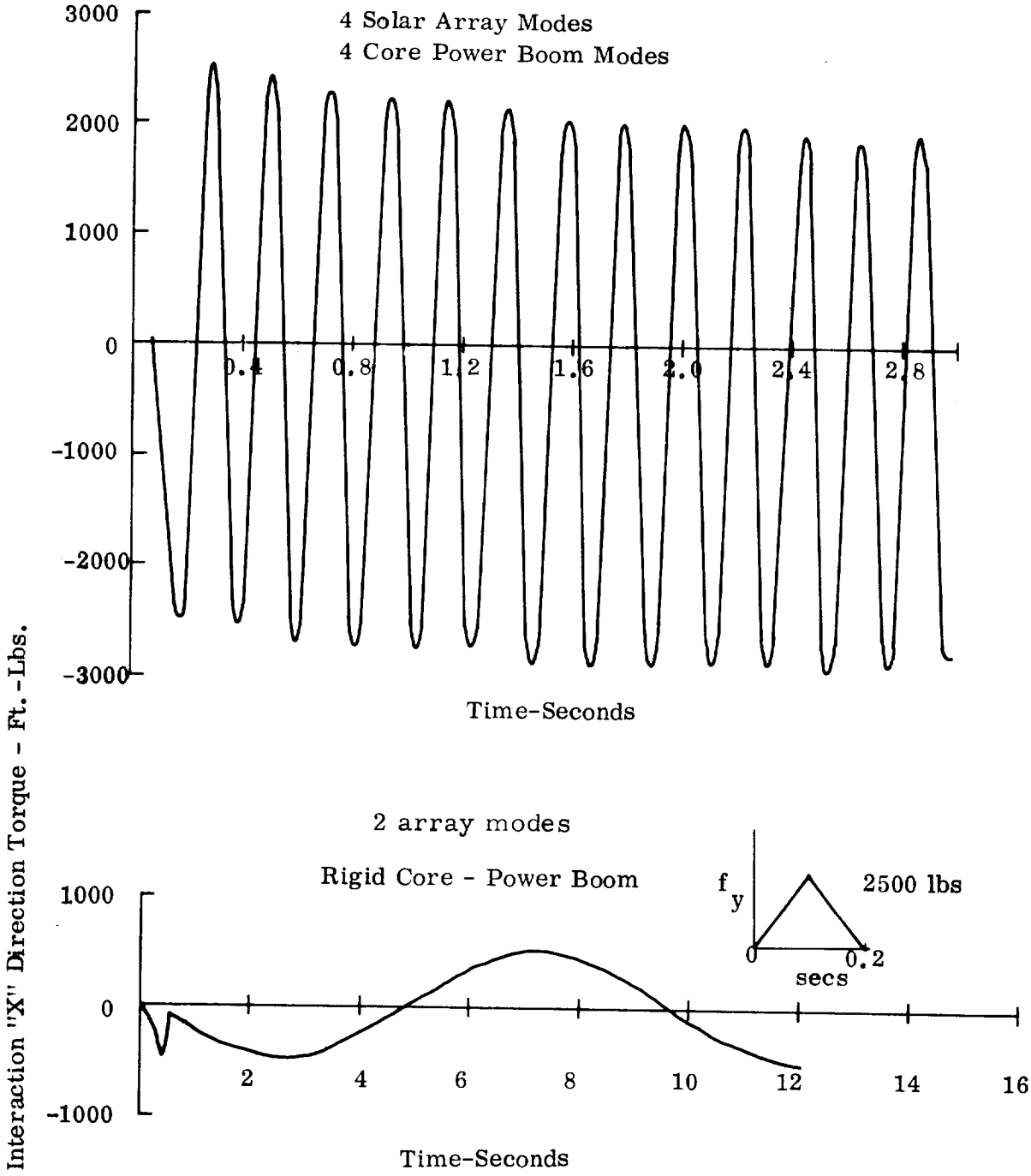

FIGURE 35. VARIATION OF INTERACTION LOAD WITH RIGID AND FLEXIBLE SPACE STATION CONSIDERATIONS

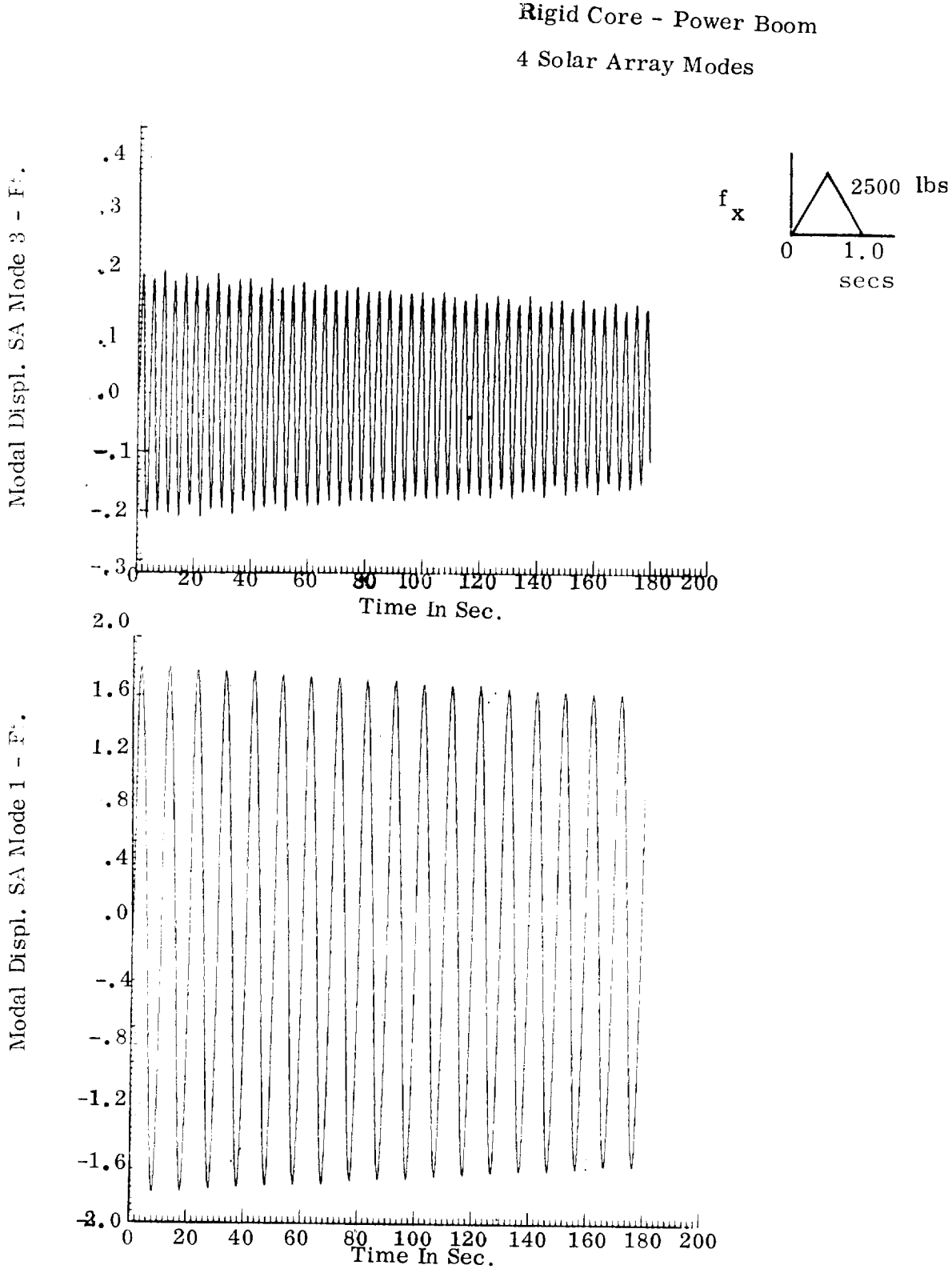

FIGURE 37. MODAL DISPLACEMENTS - SPACE STATION CONFIGURATION OF CORE-POWER BOOM AND SOLAR ARRAYS

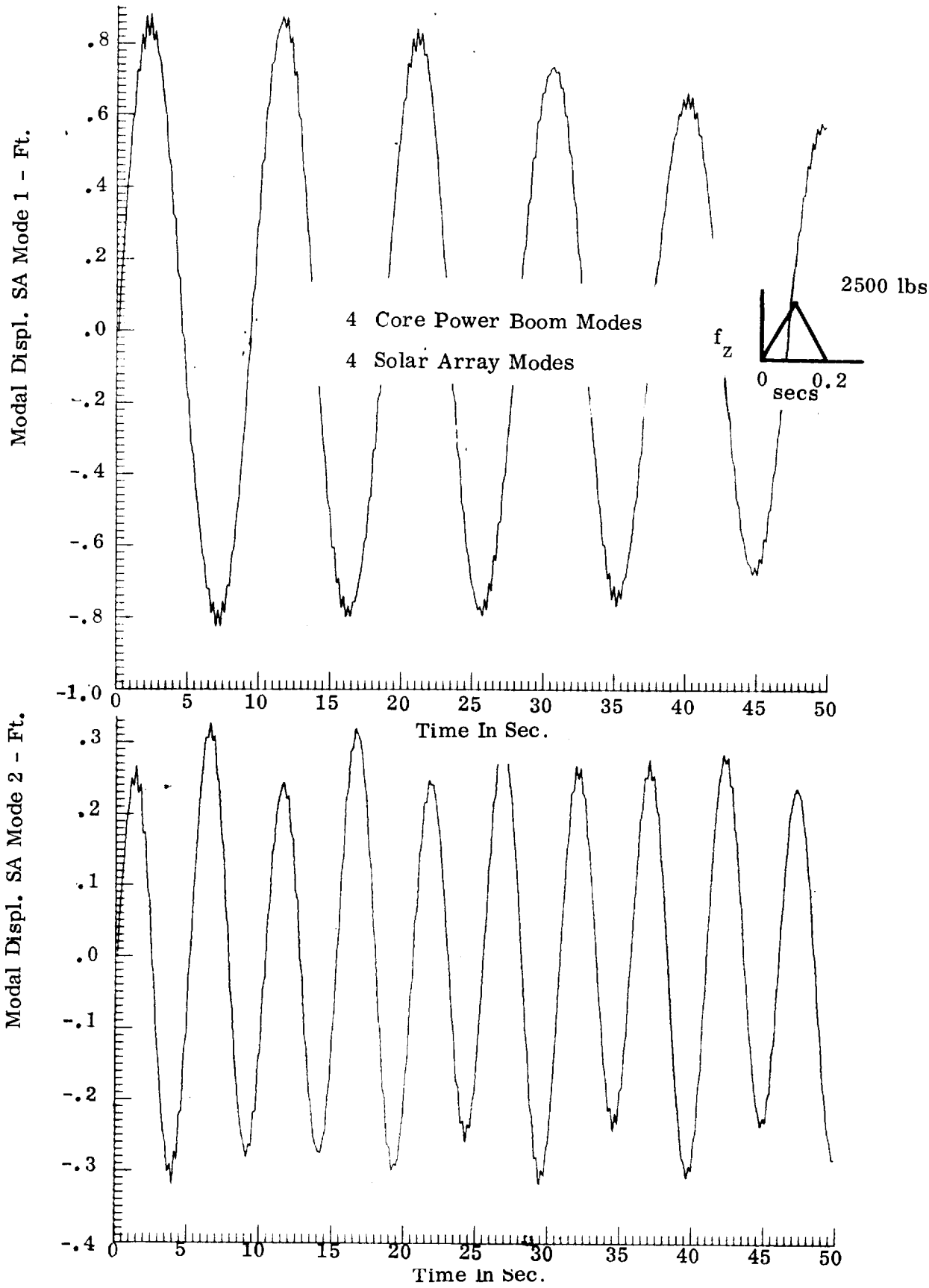

FIGURE 36. MODAL DISPLACEMENTS - SPACE STATION CONFIGURATION OF CORE-POWER BOOM, SOLAR ARRAYS

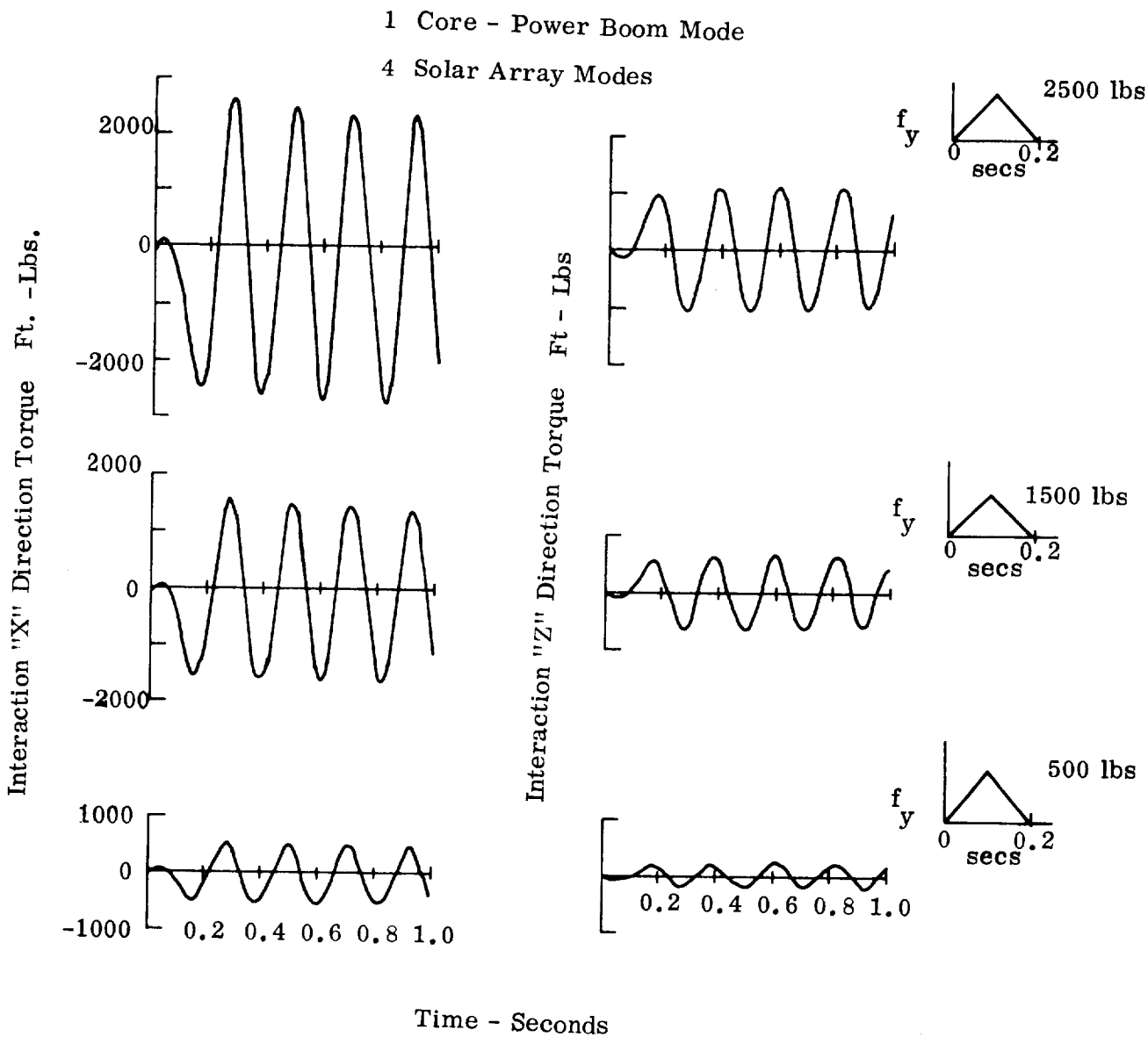

FIGURE 38. VARIATION OF INTERACTION LOADS WITH FORCE MAGNITUDE

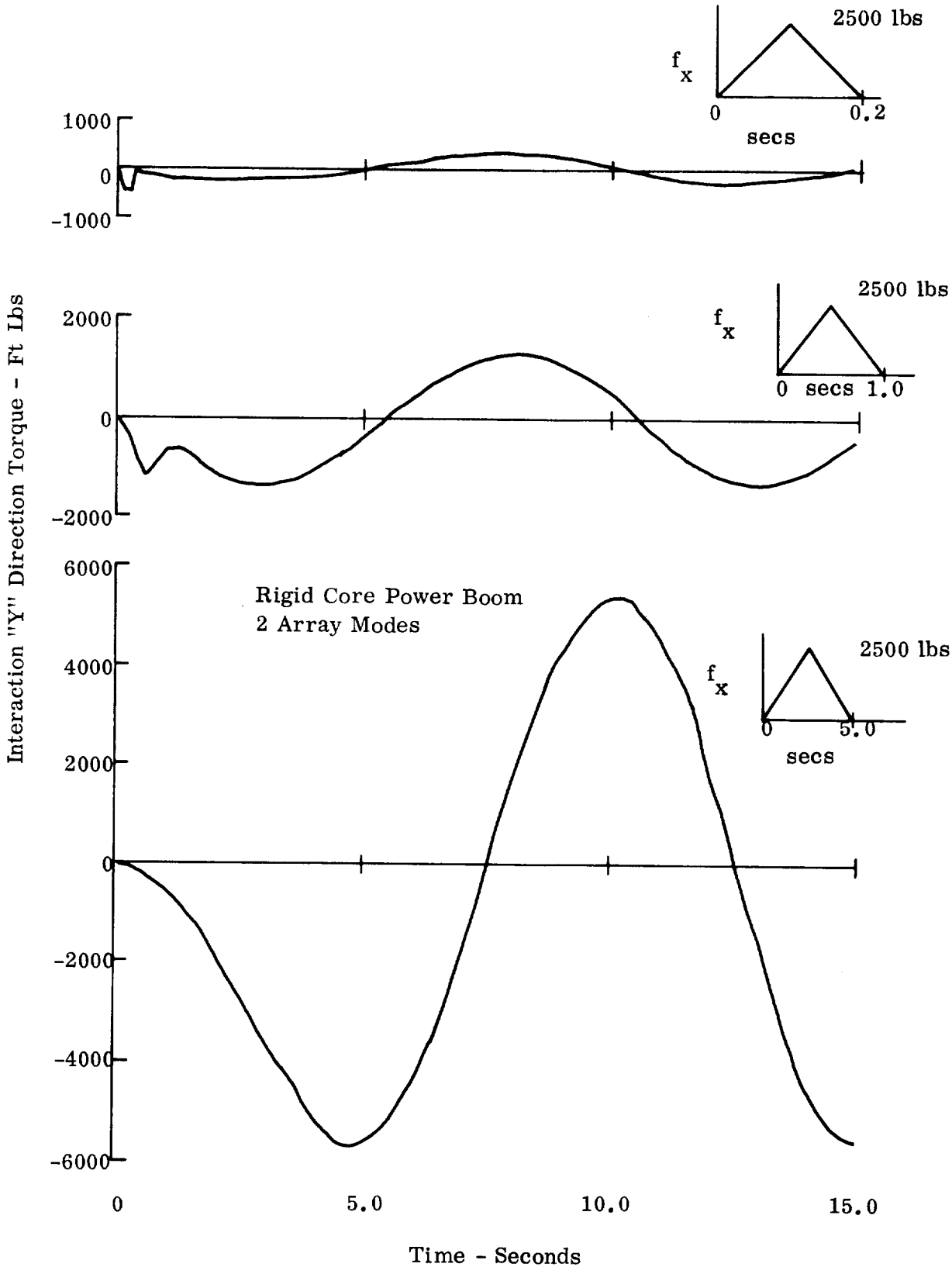

FIGURE 39. VARIATION OF INTERACTION LOAD WITH FORCE DURATION

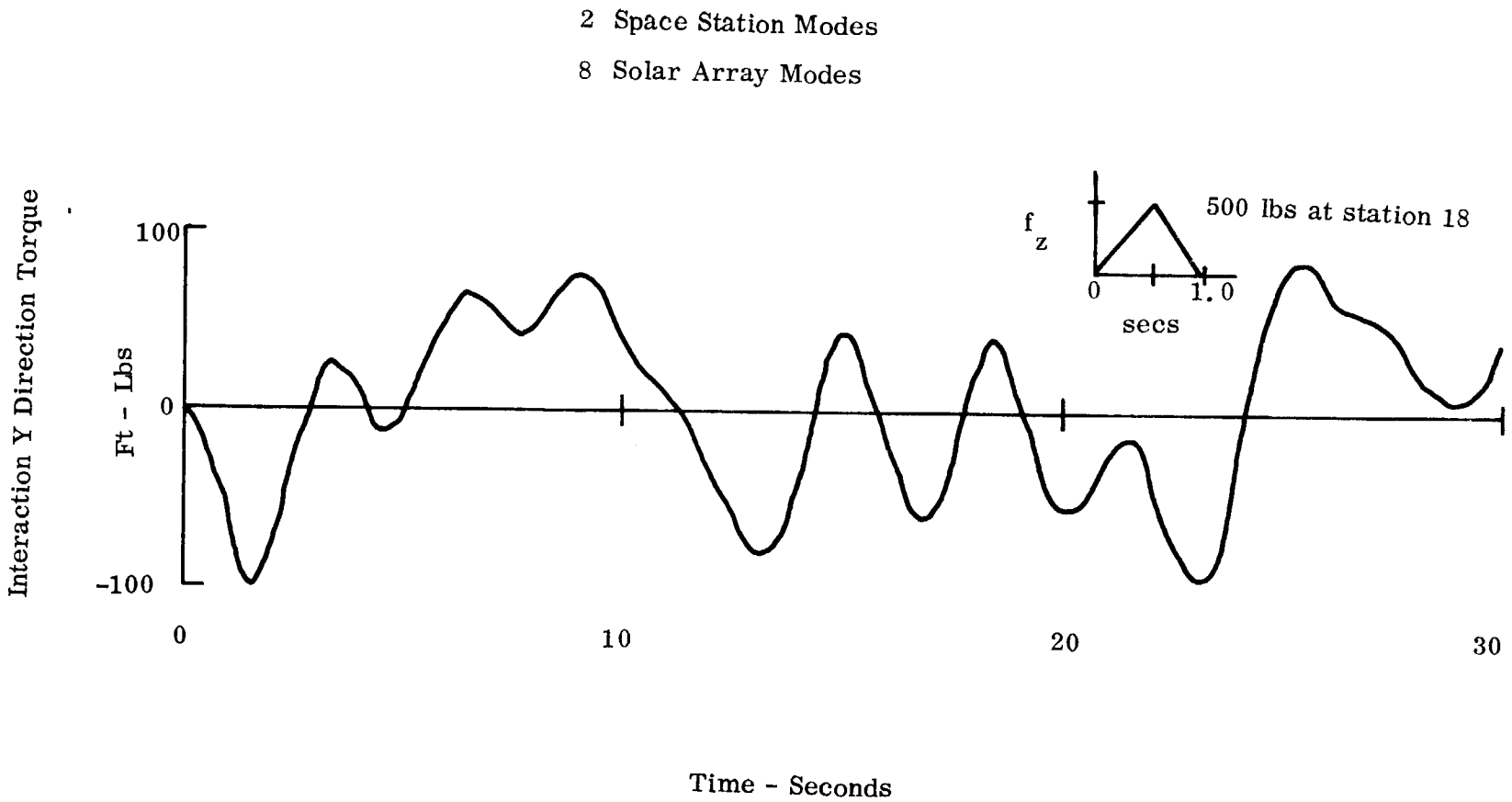

FIGURE 40. INTERACTION LOAD HISTORY - ZERO "G" SPACE STATION

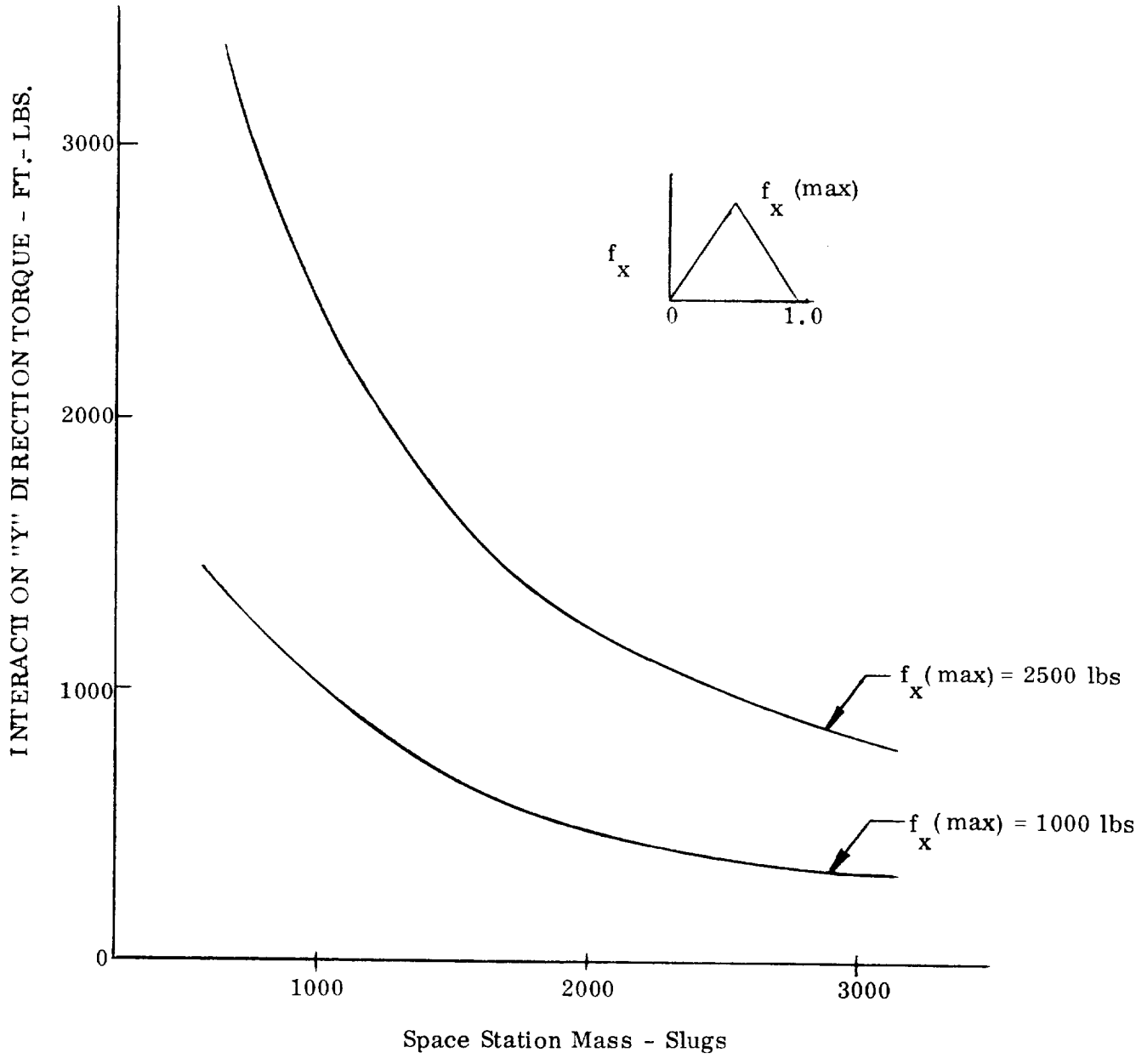

FIGURE 41. VARIATION OF MAXIMUM INTERACTION WITH SPACE STATION MASS AND FORCING PULSE MAGNITUDE

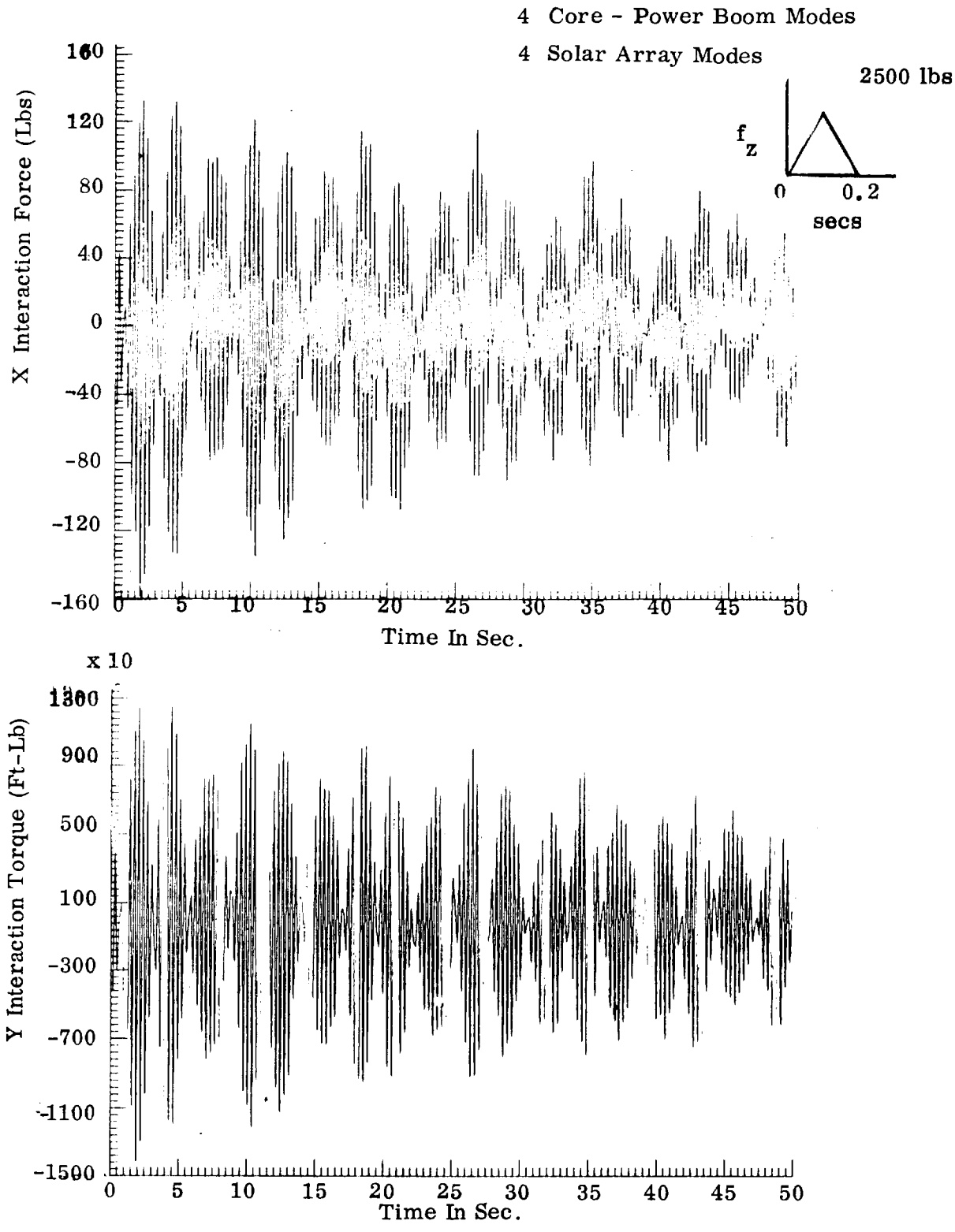

FIGURE 42. INTERACTION LOADS-SPACE STATION CONFIGURATION OF CORE-POWER BOOM AND SOLAR ARRAYS

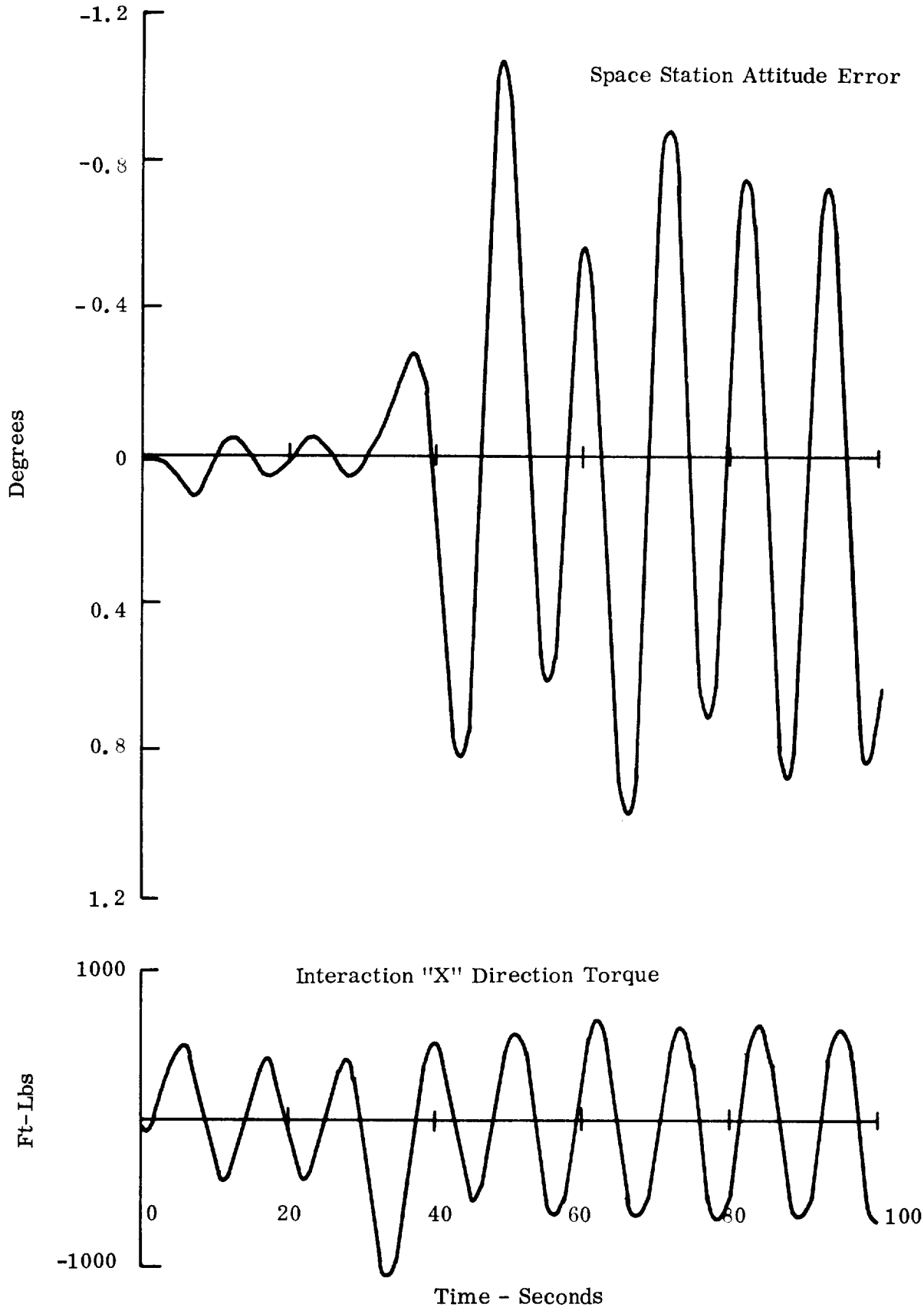

FIGURE 48. (CONTINUED)

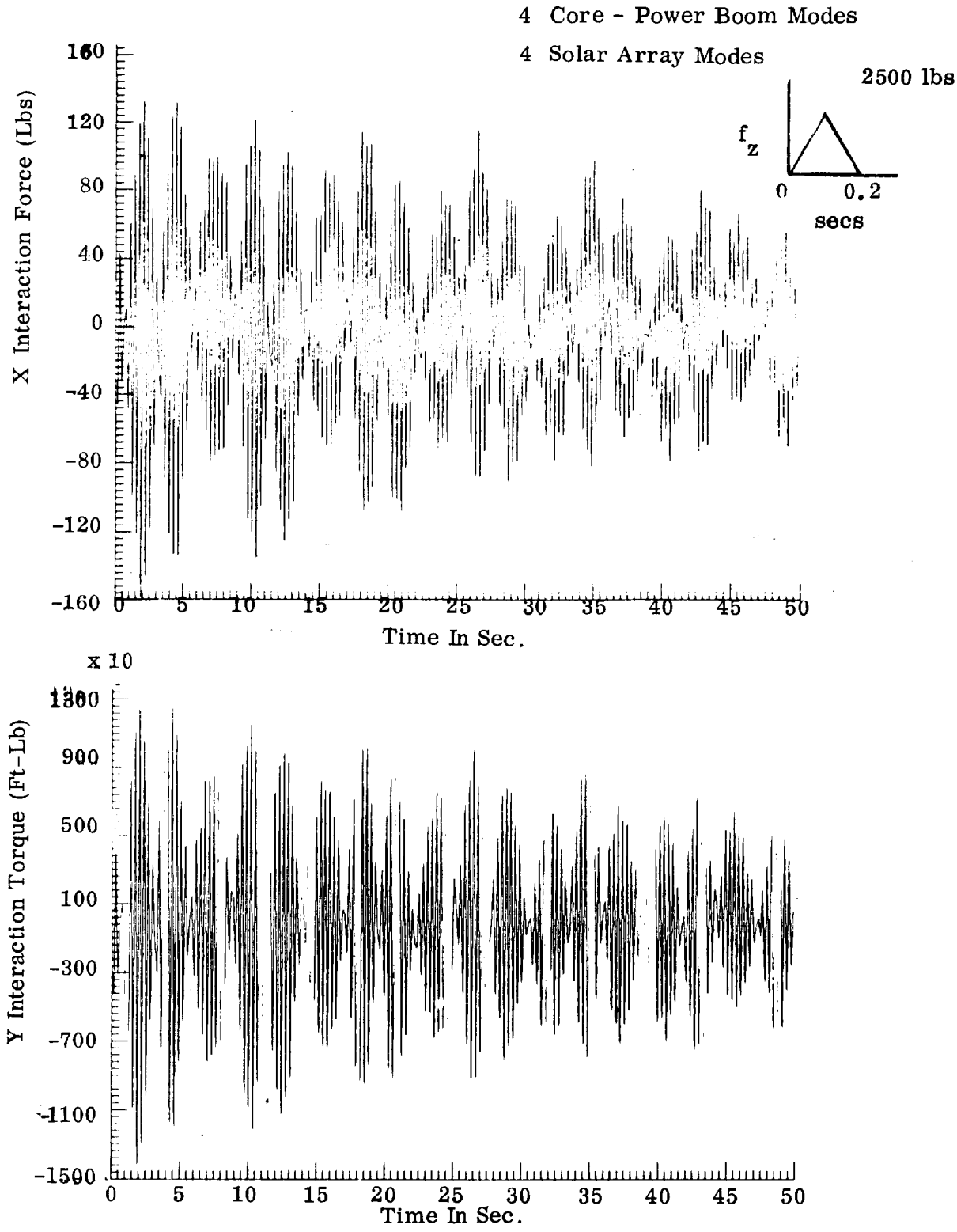

FIGURE 42. INTERACTION LOADS-SPACE STATION CONFIGURATION OF CORE-POWER BOOM AND SOLAR ARRAYS

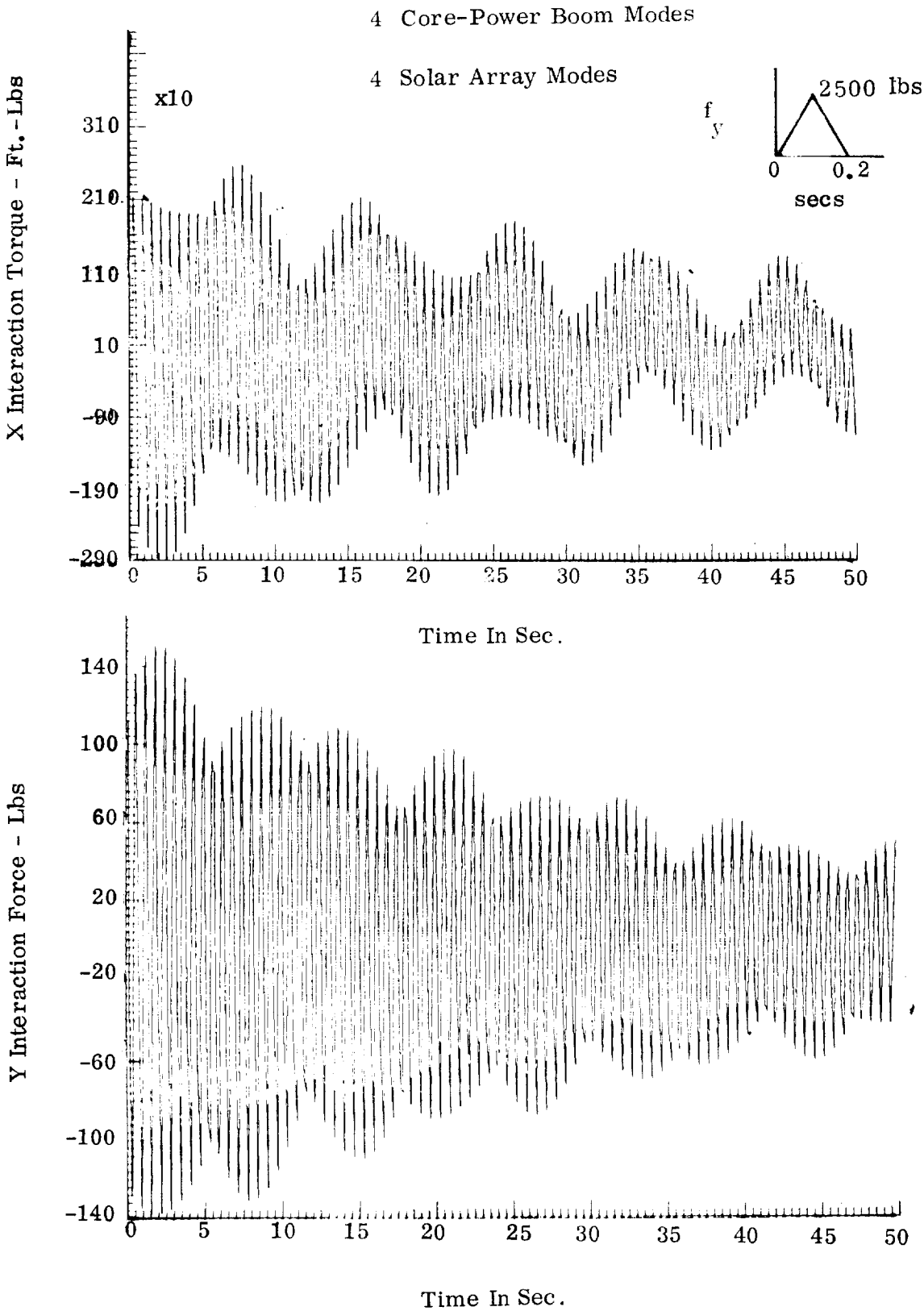

FIGURE 43. INTERACTION LOADS-SPACE STATION CONFIGURATION OF CORE-POWER BOOM, SOLAR ARRAYS

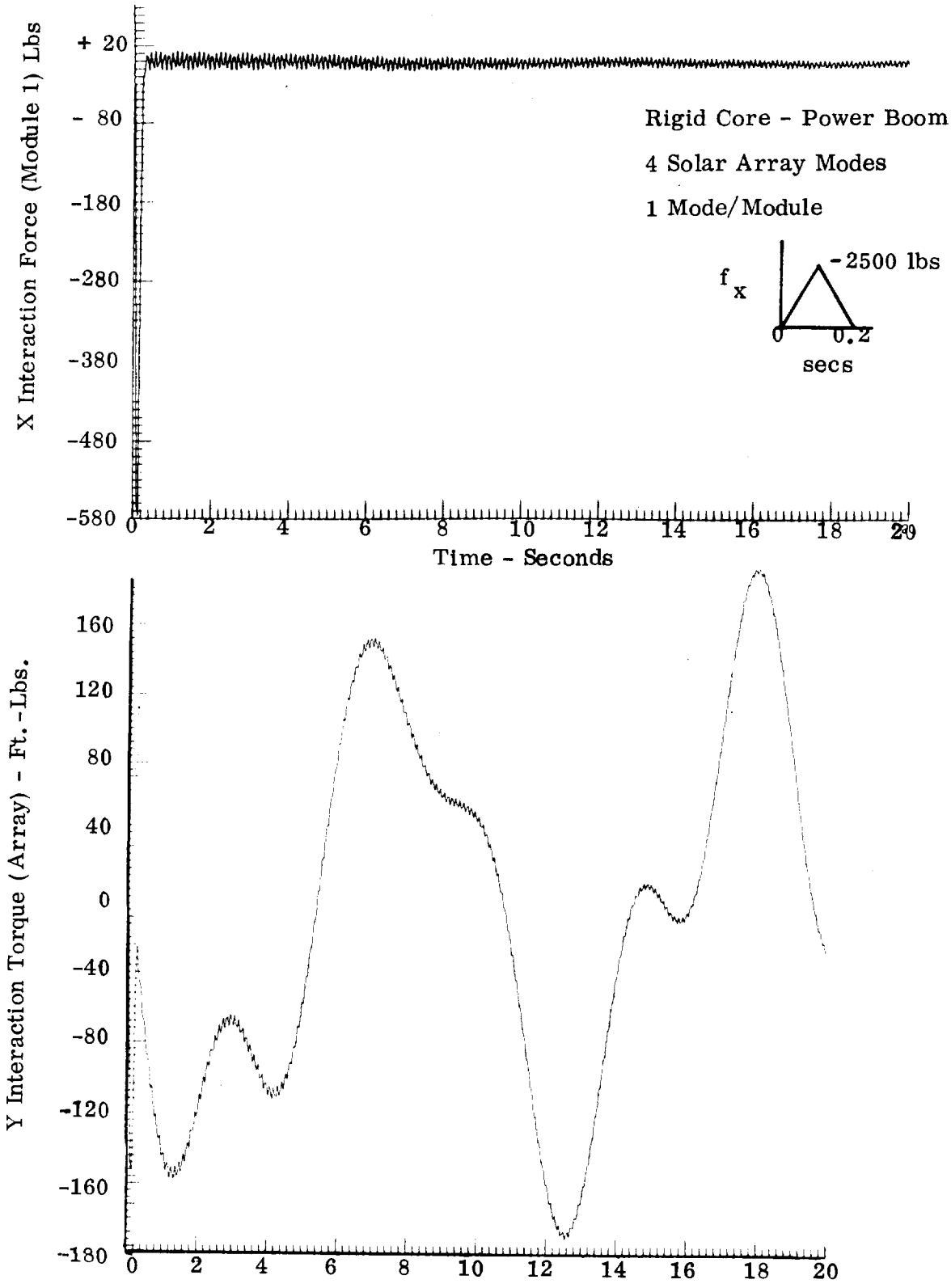

FIGURE 44 INTERACTION LOADS-SPACE STATION CONFIGURATION OF CORE-POWER BOOM, SOLAR ARRAYS, 2 MODULES

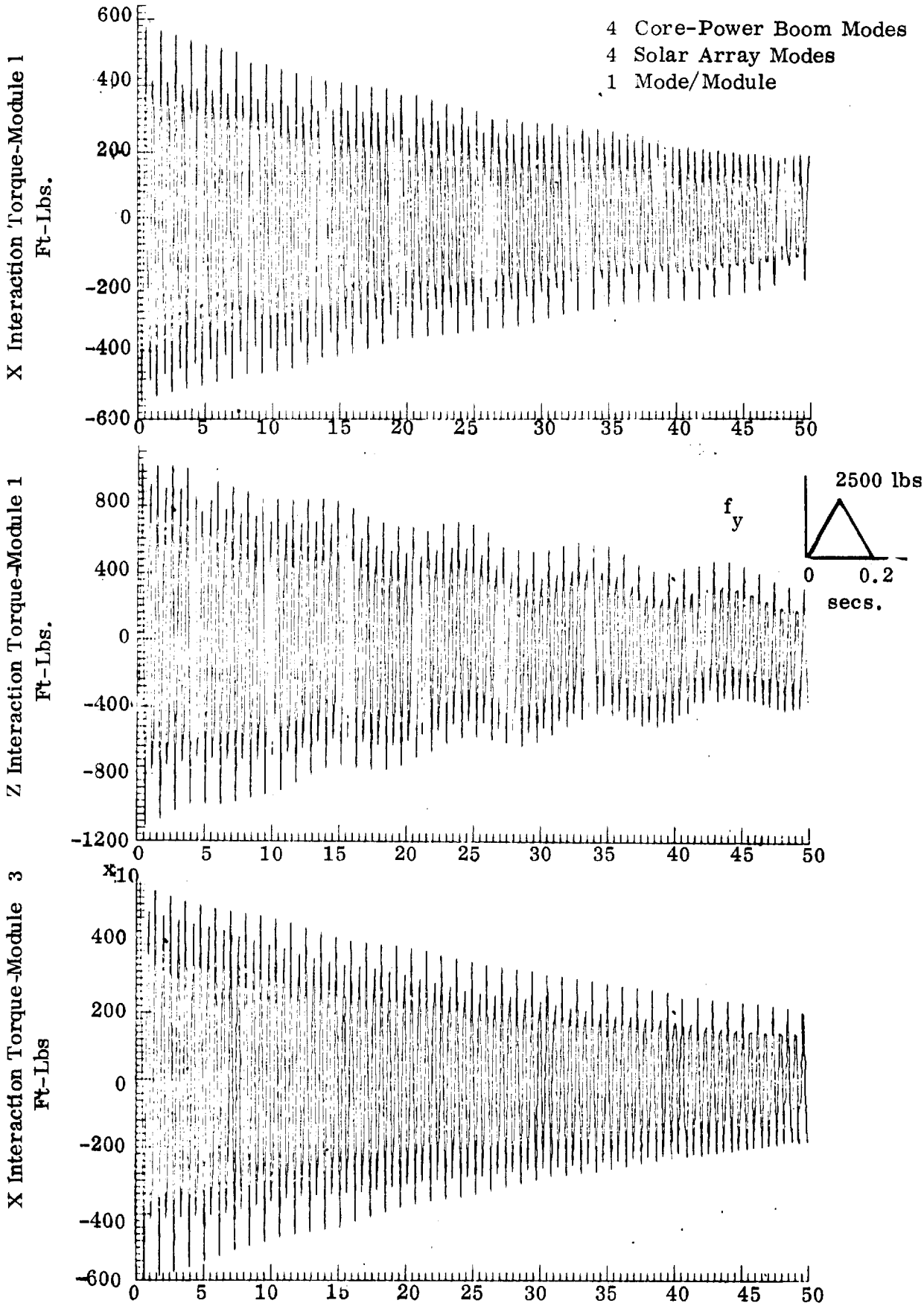

FIGURE 45. INTERACTION LOADS - SPACE STATION CONFIGURATION OF CORE-POWER BOOM, SOLAR ARRAYS, 4 MODULES

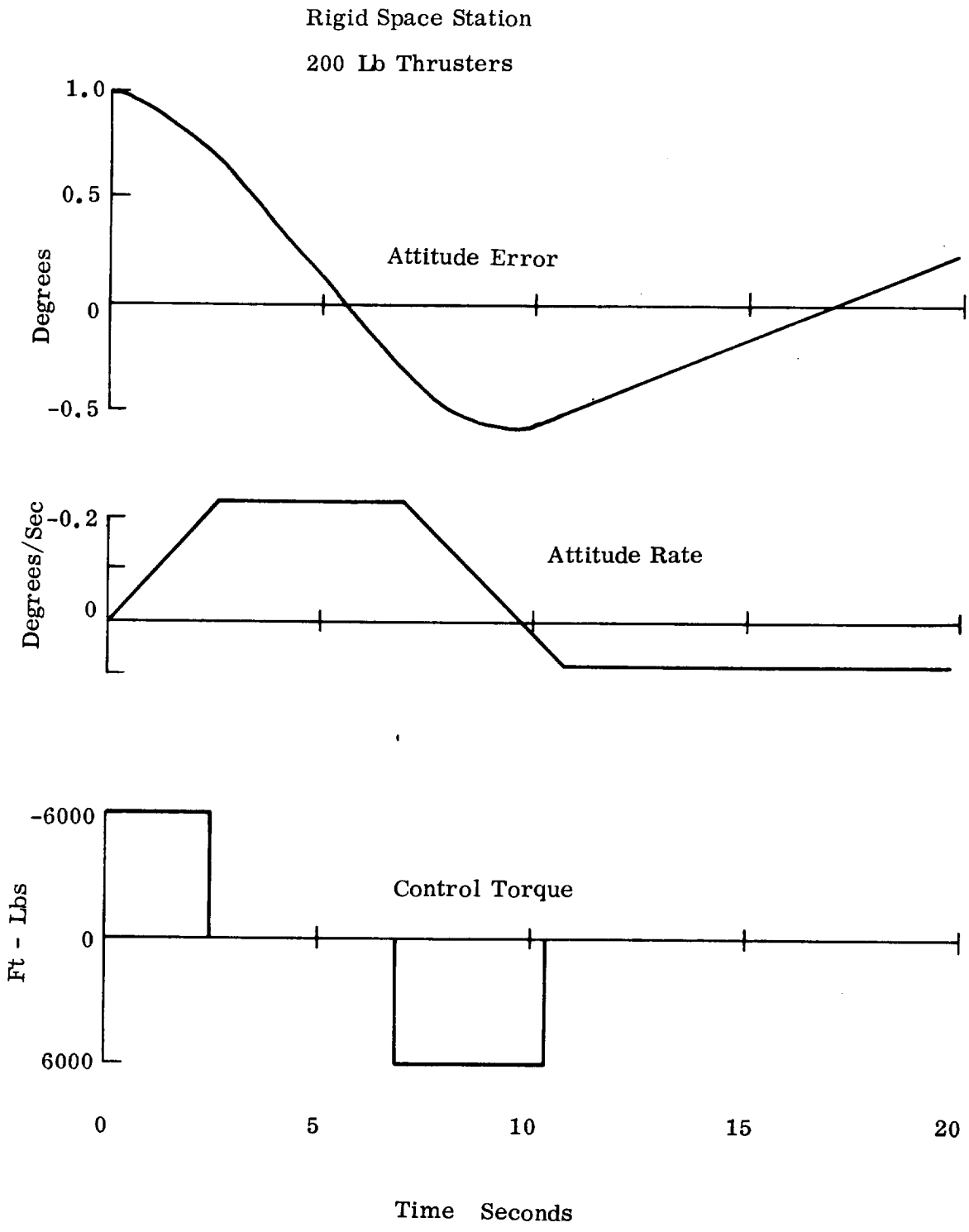

FIGURE 46. ZERO "G" SPACE STATION WITH INITIAL ATTITUDE ERROR - REACTION JET CONTROL

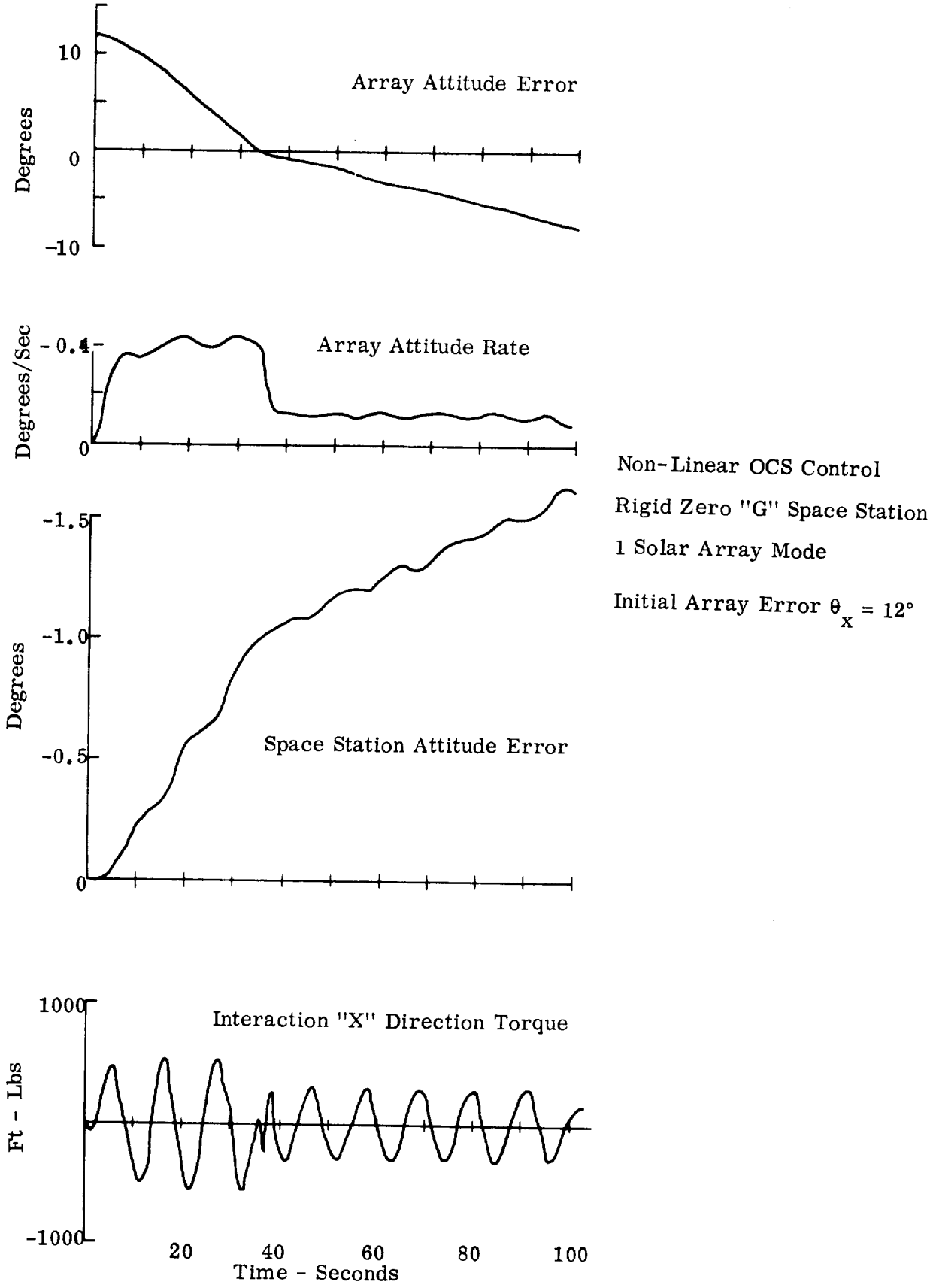

FIGURE 47. INTERACTIONS AND MOTIONS WITH OPERATIVE ORIENTATION CONTROL SYSTEM

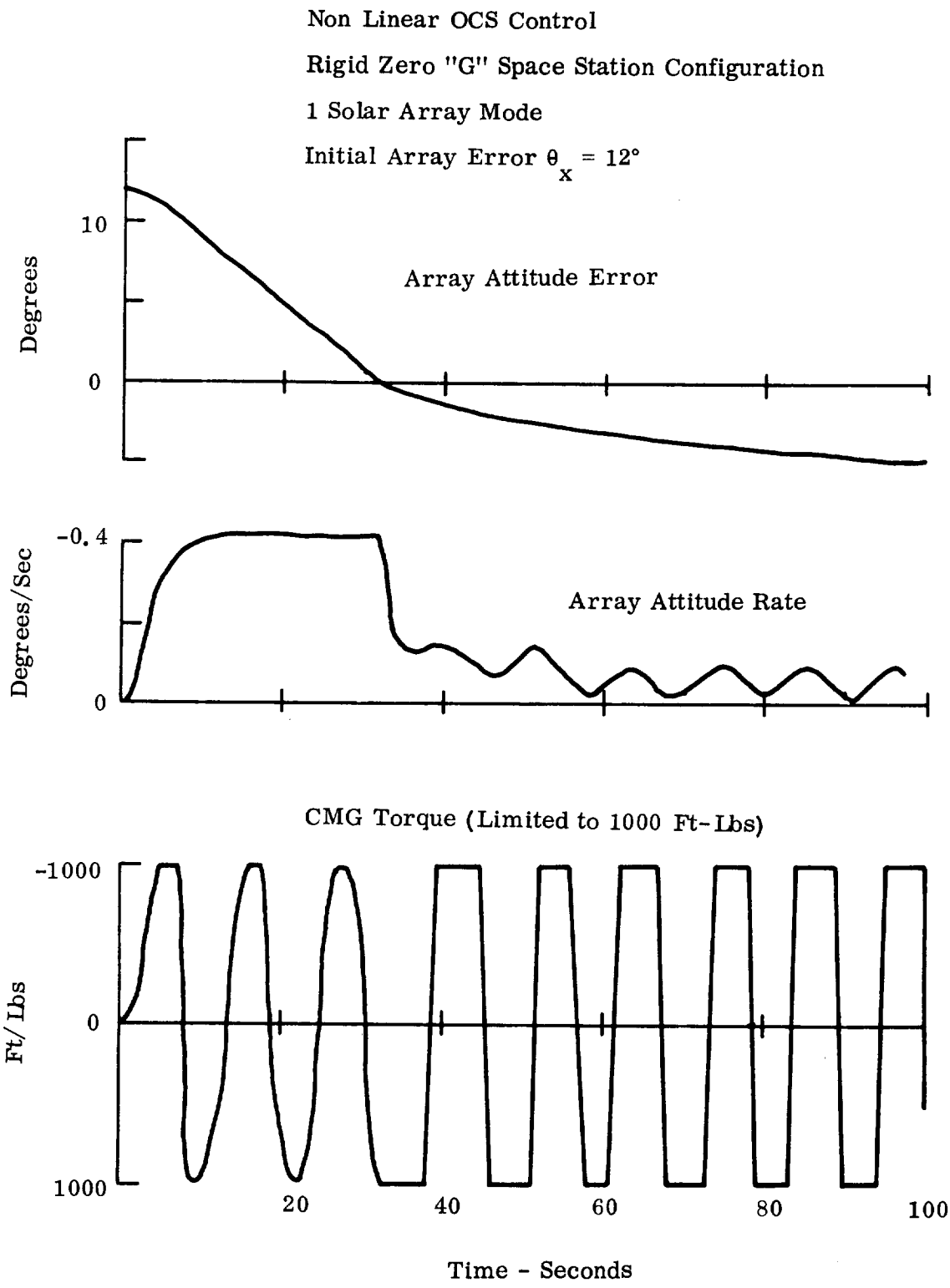

FIGURE 48. INTERACTIONS AND MOTIONS WITH OPERATIVE ORIENTATION CONTROL AND CONTROL MOMENT GYRO SYSTEMS

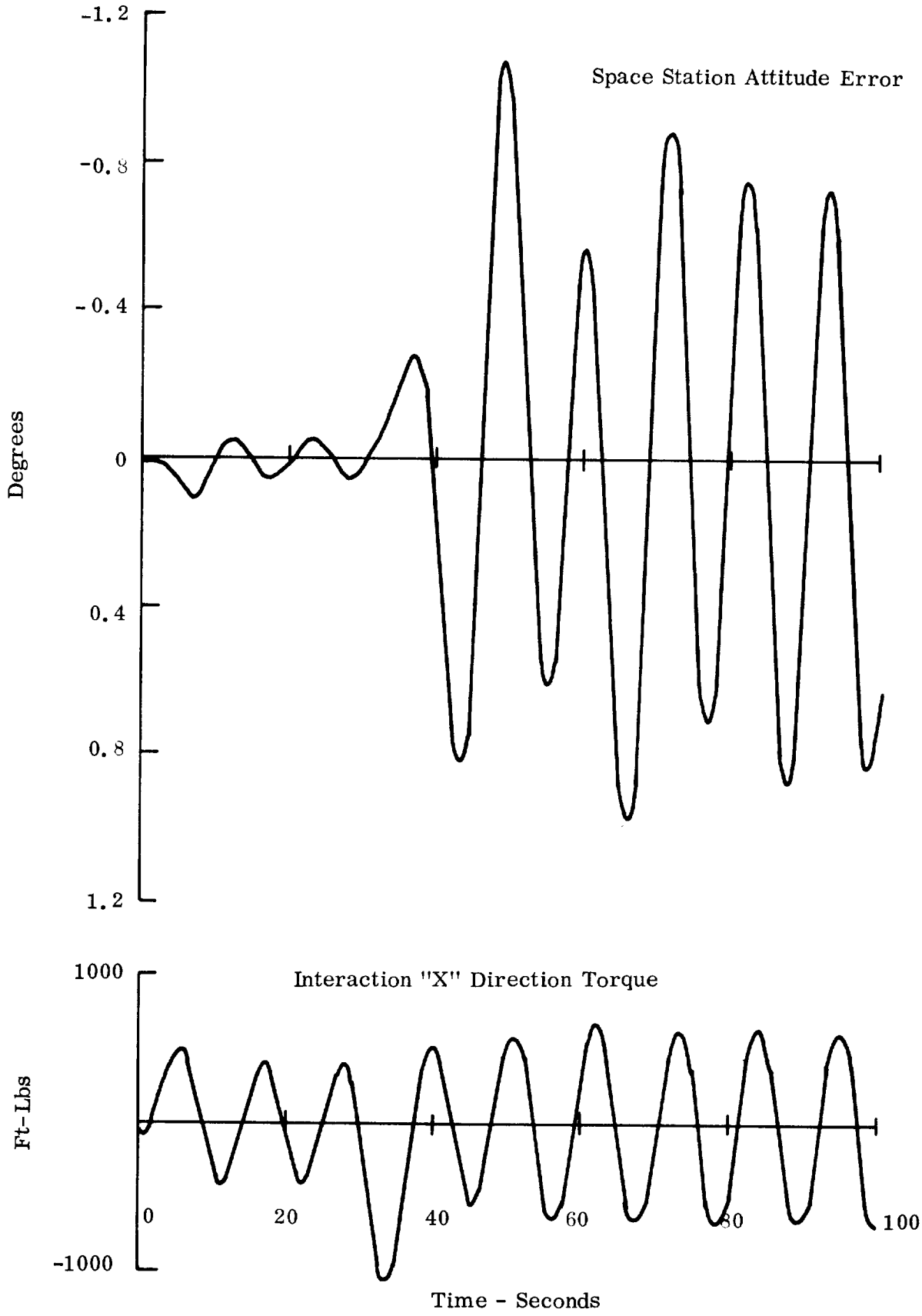

FIGURE 48. (CONTINUED)

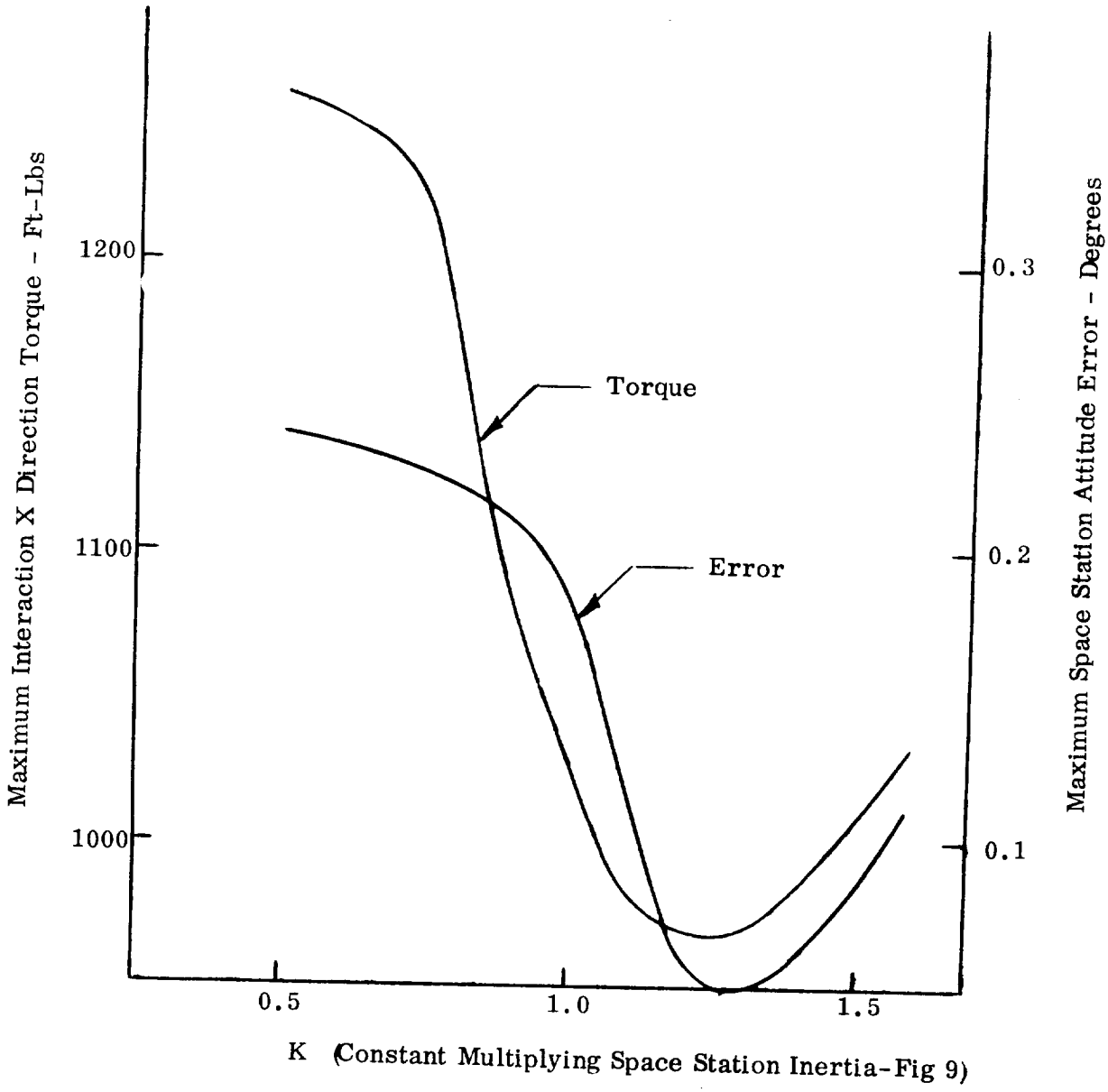

FIGURE 49. VARIATION OF MAXIMUM SPACE STATION ERROR AND INTERACTION TORQUE WITH CONTROL SYSTEM PARAMETER